AD-A081 240 RHODE ISLAND UNIV KINGSTON DEPT OF OCEAN ENGINEERING F/G 7/4
CHARACTERIZATION OF PASSIVE FILMS USING INFRARED AND RAMAN SPEC--ETC(U)
JAN 80 J KEISER, P FABIS, C BROWN N00014-76-C-0889
UNCLASSIFIED TR-8 NL

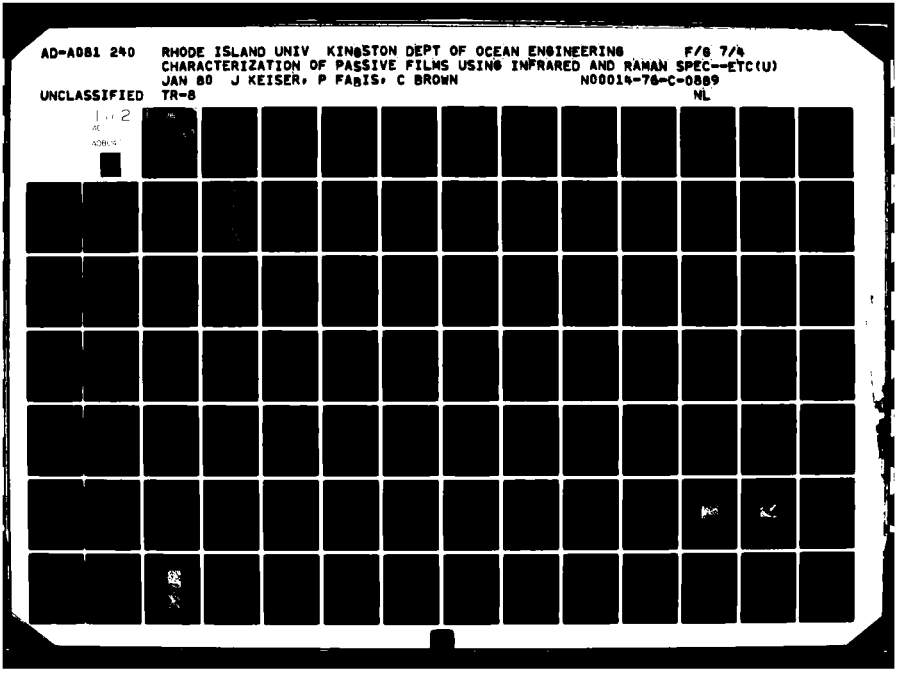

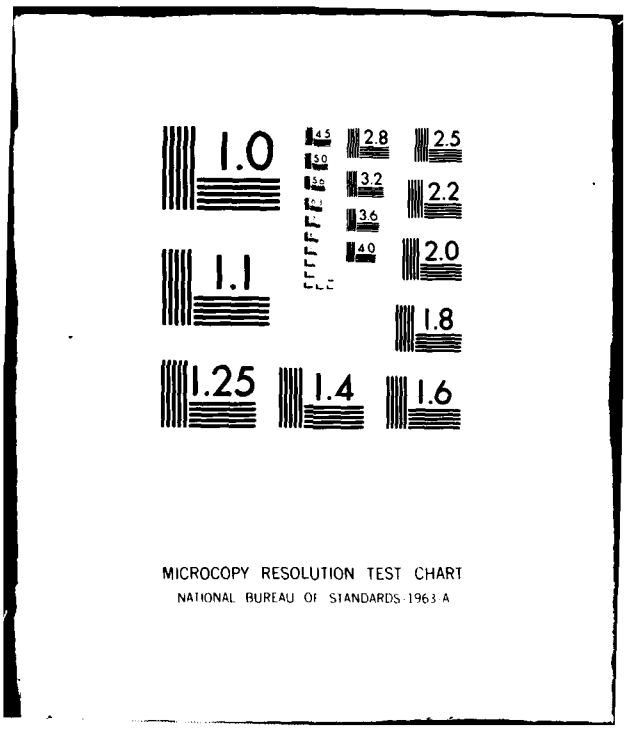
1.0
1.1
1.25
1.4
1.6
1.8
2.0
2.2
2.5
2.8
3.2
3.6
4.0
4.5
5.0
5.6
MICROCOPY RESOLUTION TEST CHART
NATIONAL BUREAU OF STANDARDS-1963-A

LEVEL II (10)

AD A049170 TR 2

CHARACTERIZATION OF PASSIVE FILMS USING INFRARED AND RAMAN SPECTROSCOPY

TECHNICAL REPORT NUMBER 8

FINAL REPORT

CONTRACT NUMBER: N00014-76-C-0889

SUBMITTED TO:

DEPARTMENT OF THE NAVY
OFFICE OF NAVAL RESEARCH
METALLURGY PROGRAM - CODE 471

PREPARED BY:

J. KEISER, P. FABIS, C. BROWN
AND R. HEIDERSBACH
DEPARTMENT OF OCEAN ENGINEERING
UNIVERSITY OF RHODE ISLAND
KINGSTON, RHODE ISLAND 02881

JANUARY 1980

CHARACTERIZATION OF PASSIVE FILMS USING INFRARED AND RAMAN SPECTROSCOPY

TECHNICAL REPORT NUMBER 8

FINAL REPORT

CONTRACT NUMBER: N00014-76-C-0889

SUBMITTED TO:

DEPARTMENT OF THE NAVY
OFFICE OF NAVAL RESEARCH
METALLURGY PROGRAM - CODE 471

PREPARED BY:

J. KEISER, P. FABIS, C. BROWN
AND R. HEIDERSBACH
DEPARTMENT OF OCEAN ENGINEERING
UNIVERSITY OF RHODE ISLAND
KINGSTON, RHODE ISLAND 02881

JANUARY 1980

SECURITY CLASSIFICATION OF THIS PAGE (When Data Entered)

REPORT DOCUMENTATION PAGE

READ INSTRUCTIONS BEFORE COMPLETING FORM

1. REPORT NUMBER: Technical Report No. 8	2. GOVT ACCESSION NO.
3. RECIPIENT'S CATALOG NUMBER	
4. TITLE (and Subtitle): Characterization of Passive Films Using Infrared and Raman Spectroscopy,	5. TYPE OF REPORT & PERIOD COVERED: Final Report.
	6. PERFORMING ORG. REPORT NUMBER
7. AUTHOR(s): J. Keiser P. Fabis, C. Brown and R. Heidersbach	8. CONTRACT OR GRANT NUMBER(s): N00014-76-C-0889
9. PERFORMING ORGANIZATION NAME AND ADDRESS: Department of Ocean Engineering, University of Rhode Island, Kingston, Rhode Island 02881	10. PROGRAM ELEMENT, PROJECT, TASK AREA & WORK UNIT NUMBERS: 12 103
11. CONTROLLING OFFICE NAME AND ADDRESS: Office of Naval Research, Department of the Navy, Arlington, Virginia 22217	12. REPORT DATE: Jan 80
	13. NUMBER OF PAGES: 99
14. MONITORING AGENCY NAME & ADDRESS (if different from Controlling Office): 14 TR-7	15. SECURITY CLASS. (of this report): Unclassified
	15a. DECLASSIFICATION/DOWNGRADING SCHEDULE

16. DISTRIBUTION STATEMENT (of this Report)

This document has been approved for public release and sale; its distribution is unlimited.

17. DISTRIBUTION STATEMENT (of the abstract entered in Block 20, if different from Report)

18. SUPPLEMENTARY NOTES

19. KEY WORDS (Continue on reverse side if necessary and identify by block number)

Passivity, surface chemistry, iron, water, corrosion, oxidation, infrared spectroscopy, Raman spectroscopy

20. ABSTRACT (Continue on reverse side if necessary and identify by block number)

This report summarizes current research into the application of infrared and Raman spectroscopy to the study of passive films on metals.

One section of the report discusses the results of computer interfacing of the Raman spectrometer with a minicomputer to produce signal averaged spectra. The signal-averaged Raman

DD FORM 1 JAN 73 1473 EDITION OF 1 NOV 65 IS OBSOLETE
S/N 0102-LF-014-6601

SECURITY CLASSIFICATION OF THIS PAGE (When Data Entered)

407192

20. Abstract (cont.)

spectra reveal spectral details undistinguishable in a single spectrum.

A parallel study involved exposure of iron, chromium, and two commercial iron-chromium alloys.

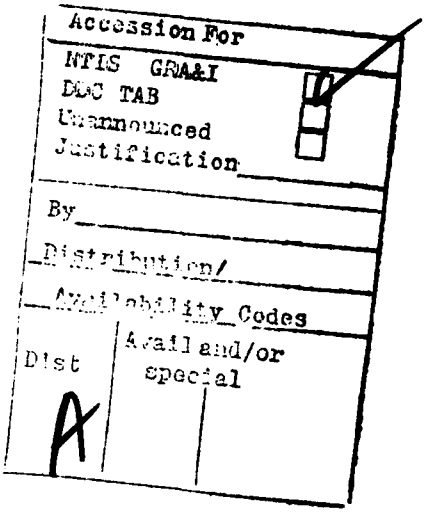

TABLE OF CONTENTS

TABLE OF CONTENTS (CONT.)

AQUEOUS EXPOSURES OF IRON

By

J. Keiser

INTRODUCTION

Previous reports on this project have demonstrated the possible use of Raman spectroscopy for studying the corrosion of iron[1-4]. Included in these reports were the following:

1. The Raman spectra of pure iron oxide and oxyhydroxide powders which were to be used as reference spectra.
2. Spectra which showed that mixtures of these pure powders could be identified by Raman spectroscopy.
3. Raman spectra showing the growth of an oxide film on Armco iron exposed to air at 250° C.
4. The Raman identification of an Fe_3O_4 film formed on Armco iron exposed to boiling 10^{-5} M NaOh.

This has led to the current work which involves the characterization of films formed on iron exposed to different aqueous environments.

EXPERIMENTAL TECHNIQUES

The basic equipment and techniques of Raman spectroscopy have been reviewed in previous reports[1-4]. This report, however, includes additional signal averaging techniques which have been made possible by interfacing the Raman spectrometer to a NOVA 3/12 mini computer.

The computer is capable of sending 5-volt pulses to the Raman monochrometer which can cause it to scan a desired region of the spectrum in either a forward or reverse direction. Any number of repetitive scans may be recorded in this manner. Once the requested number of runs has been scanned, the computer can average the individual spectra and produce a new signal-averaged spectra. This new spectrum will have its signal-to-noise ratio improved by a factor of $\sqrt{N}$, where N is the number of scans averaged[5]. These techniques have enabled the identification of components of iron oxide films which would have otherwise been indistinguishable from the background noise.

Figures 1 through 4 demonstrate the use of signal averaging in identifving different iron oxide films. Figure 1 shows the spectrum obtained from the surface of an Armco iron sample exposed to boiling 10^{-5} M NaOH for 40 hours. Also shown in Figure 1 is a spectrum produced by signal averaging 10 separate runs. When this is compared to the Raman spectra of pure Fe_3O_4 (Figure 2) it can be seen that they are virtually identical. This positive identification would have been difficult without the signal averaged spectrum.

Figure 3 shows the spectrum of another sample of Armco iron versus its 5x signal averaged spectrum. This sample was immersed momentarily in dilute H_2SO_4, rinsed with distilled water and allowed to air dry over night. A light brown "tarnish" developed which was identified as α-FeOOH by comparing its 5x signal averaged spectra with that of pure α-FeOOH (Figure 4).

EXPERIMENTAL RESULTS

Reference Standards: In order to investigate the films formed on iron it was first necessary to synthesize γ-Fe_2O_3 and obtain its Raman spectra. This was a particularly important iron oxide to identify for two reasons:

1. It is often reported as a corrosion product of the aqueous corrosion of iron[6,7].
2. It is almost impossible to distinguish γ-Fe_2O_3 from Fe_3O_4 by either x-ray or electron diffraction methods.

We had included a possible spectra of γ-Fe_2O_3 in our report dated January 1978[2]. The sample used, however, had been prepared in our laboratory and it was discovered that α (and not γ) Fe_2O_3 had been formed. A different synthesis[8] was tried and γ-Fe_2O_3 was produced as confirmed by x-ray diffraction analysis. The Raman spectrum of γ-Fe_2O_3 is very similar to Fe_3O_4. Figure 5 shows spectra of both oxides. Fe_3O_4 shows one broad peak at approximately 667 cm^{-1} while the γ-Fe_2O_3 Raman spectra consists of one broad peak at 720 cm^{-1}. Mixtures of these 2 compounds generally show one broad unresolved band (Figure 5).

Simple Immersion Exposures: Simple immersion experiments were conducted in order to produce films of different compositions for analysis. Alexander and Foley have published a paper demonstrating the soluble corrosion products of iron dissolution and their dependance on the anions in solution[9]. It was thought that perhaps the insoluble corrosion products might also show a dependance on the anions in solution. To investigate this

hypothesis, mechanically polished Armco iron samples were exposed in solutions of NaCl, NaBr, NaI, Na_2SO_4, artificial sea water, $FeCl_3$, $NaClO_4$ and $NaNO_3$ at a pH adjusted to 2 by dropwise addition of H_2SO_4. The concentrations were the same as those used by Alexander and Foley. These samples were allowed to sit in Erlenmeyer flasks for 4-5 weeks. At the conclusion of this time the samples were removed and rinsed with distilled water and methanol before Raman spectra were recorded. A summary of the results appears in Table 1. From this table some possible trends may be noted. Practically all the samples showed a significant amount of γ-FeOOH. The samples exposed to the sodium halides seem to have formed predominantly γ-FeOOH (although some γ-FeOOH and Fe_3O_4 was also detected). The samples which were exposed only to sulfate anions showed the most intense α-FeOOH peaks. Detournay, et.al.[9], have also reported the formation of α-FeOOH in the presence of sulfates. The sample exposed to $NaNO_3$ was the only sample on which γ-Fe_2O_3 was detected. Alexander and Foley also observed that the UV-visible spectra of the iron-$NaNO_3$ solution was unlike that of any of the other solutions they had tested. This sample also corroded much more rapidly than any of the other samples. A light tarnish was visible in about 12 hours as compared to about 2 weeks for the other samples. This is probably due to the oxidizing ability of the nitrate anion.

Potentiostatic Exposures: Raman spectroscopy has been used to investigate the products formed on Armco iron in sulfate solutions under different conditions of potential and pH. The cell

used for these exposures is the same one described in Reference 2. For two of the exposures, some of the "sludge" from the bottom of the cell was collected, dried, pressed into a KBr pellet and the Raman spectra were recorded. It was found in some cases that the products which adhere to the iron surface were different from the iron oxide precipitate that was collected as sludge. Table 2 summarizes the electrochemical conditions and the products seen. In the first exposure listed in Table 1 (potential = + 0.9V SHE, pH = 1.0), only α-FeOOH was detected. This was the product predicted from the iron-sulfate Pourbaix diagram published by Detournay, et.al.[8]. It also confirms previous University of Rhode Island work on simple immersion exposures which implied that α-FeOOH formation is influenced by the presence of sulfates. The third exposure listed in Table 2 (potential +0.8V SHE, pH 6.0) produced a multicomponent film composed of γ-FeOOH, α-FeOOH, γ-Fe_2O_3 and Fe_3O_4. Such a situation cannot be predicted from a Pourbaix diagram since only one compound is predicted for any given condition of potential and pH[10]. The sludge from this cell showed that the precipitates in the solution were very similar to the composition of the surface film. Figures 6 and 7 show the effects of signal averaging the spectra of the surface and sludge. Figure 8 shows the Raman spectra of the surface compared to that of the sludge.

CONCLUSIONS

Raman spectroscopy has been shown to be an effective analytical tool in studying the corrosion of iron. All of the most

important aqueous corrosion products of iron can be identified from their Raman spectra. Interpretation of these spectra is simple and straightforward. Iron films containing up to four different components have been successfully characterized. Both iron surfaces and solution precipitates may be studied.

FUTURE WORK

More research is planned regarding the experimental verification of potential-pH diagrams. This will include work on the iron-sulfate system as well as new work on the iron-chloride system. The effect of drying on iron oxide films will be studied by comparing spectra of dried versus in-situ films. We will also extend this research to include the corrosion products of stainless steels.

REFERENCES

1. R. Heidersbach, C.W. Brown, R.W. Thibeau, A. Goldfarb, "Raman Spectroscopy of Passive Films Formed on Metal Surfaces in Corrosive Environments", Annual Report for the Office of Naval Research, Contract Number: N00014-76-C-0889, 1977.

2. R. Heidersbach, C. Brown, R. Thibeau, and A. Goldfarb, "Characterization of Passive Films Using Infrared and Raman Spectroscopy", Technical Report Number 2, Office of Naval Research, Contract Number: N00014-76-C-0889, January 1978.

3. R.J. Thibeau, C.W. Brown, R.H. Heidersbach, "Raman Spectra of Possible Corrosion Products of Iron", Technical Report Number 3, Contract Number: N00014-76-C-0889, Office of Naval Research, June 1978.

4. R. Thibeau, C. Brown, A. Goldfarb, and R. Heidersbach, "Infrared and Raman Spectroscopy of Aqueous Corrosion Films on Lead", Journal of the Electrochemical Society, 127 (1980) 37.

5. H.A. Strobel, "Chemical Instrumentation: A Systematic Approach", 2nd ed., Addison-Wesley Publishing Co., p. 195, 1973.

6. M.J. Graham, M. Cohen, Corrosion, 32, 432 (1976).

7. M. Cohen, J. Electrochem. Soc., 121, 191C (1974).

8. H.S. Booth, ed., "Inorganic Synthesis", Volume 1, McGraw-Hill, New York, p. 185, 1939.

9. B.J. Alexander, R.T. Foley, Corrosion, 32, 297 (1976).

10. J. Detournay, L. DeMiranda, R. Derie, M. Ghodsi, Corrosion Sci., 15, 295 (1975).

11. R. Thibeau, C. Brown, A. Goldfarb and R. Heidersbach, "Raman and Infrared Spectroscopy of Aqueous Corrosion Films on Lead in 0.1 M Sulfate Solutions", submitted to the Journal of the Electrochemical Society.

TABLE 1

Simple Immersion Exposures of Armco Iron

Solution Composition[1]	Time of Exposure	Compounds Detected By Raman Spectroscopy
0.1 M NaCl	39 days	γ-FeOOH, some Fe_3O_4
0.1 M NaBr	30 days	γ-FeOOH, some α-FeOOH and some Fe_3O_4
0.1 M NaI	39 days	γ-FeOOH, some α-FeOOH, possibly some Fe_3O_4
0.01 M H_2SO_4	39 days	α-FeOOH, γ-FeOOH, Fe_3O_4 and an unknown band at 525 cm^{-1}
Artificial Sea Water[2]	33 days	γ-FeOOH, Fe_3O_4, possibly some α-FeOOH
0.0003 M $FeCl_3$	39 days	α-FeOOH, γ-FeOOH, possibly some Fe_3O_4
0.1 M $NaClO_4$	39 days	γ-FeOOH, α-FeOOH, possibly some Fe_3O_4
0.05 M $NaNo_3$	2 days	γ-Fe_2O_3

[1]All of these solutions were brought to a pH of 2 by dropwise addition of sulfuric acid. The salt concentrations are the same as those used by Alexander and Foley (Ref. 8) with the exception of NaBr.

[2]Made from a synthetic sea salt mixture purchased from Aquarium Systems, Inc., Erstlake, Ohio.

TABLE 2

Potentiostatic Iron Exposures

Conditions	Surface Spectrum Observed	Sludge Spectrum Observed
Pot. + 1.15 V vs SHE pH 1 with H_2SO_4 aerated 23 hrs. 25° C	α-FeOOH	not done
Pot. - 0.30 V vs SHE pH 6.5 0.1 M K_2SO_4 aerated 18 hrs. 25° C	mostly δ-FeOOH, some α-FeOOH and Fe_3O_4	Fe_3O_4
Pot. + 0.8 V vs SHE pH 6.0 0.1 M K_2SO_4 aerated 18 hrs. 25° C	δ and α FeOOH, Fe_3O_4 and δ-Fe_2O_3	δ and α FeOOH and Fe_3O_4

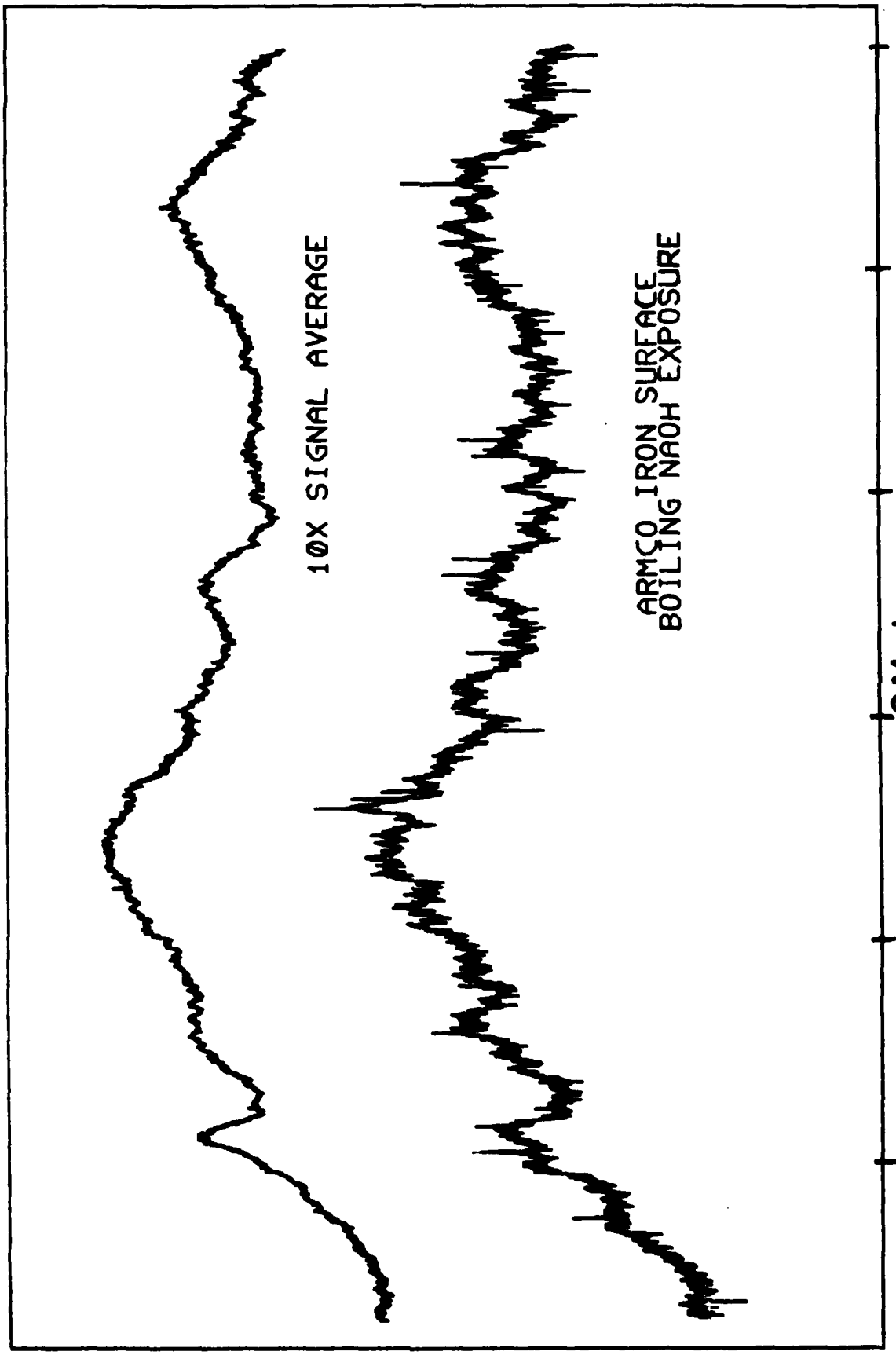

Figure 1. Raman spectra of Armco iron exposed to 10^{-5} M NaOH for 40 hours vs. a 10x signal averaged spectrum of the same sample.

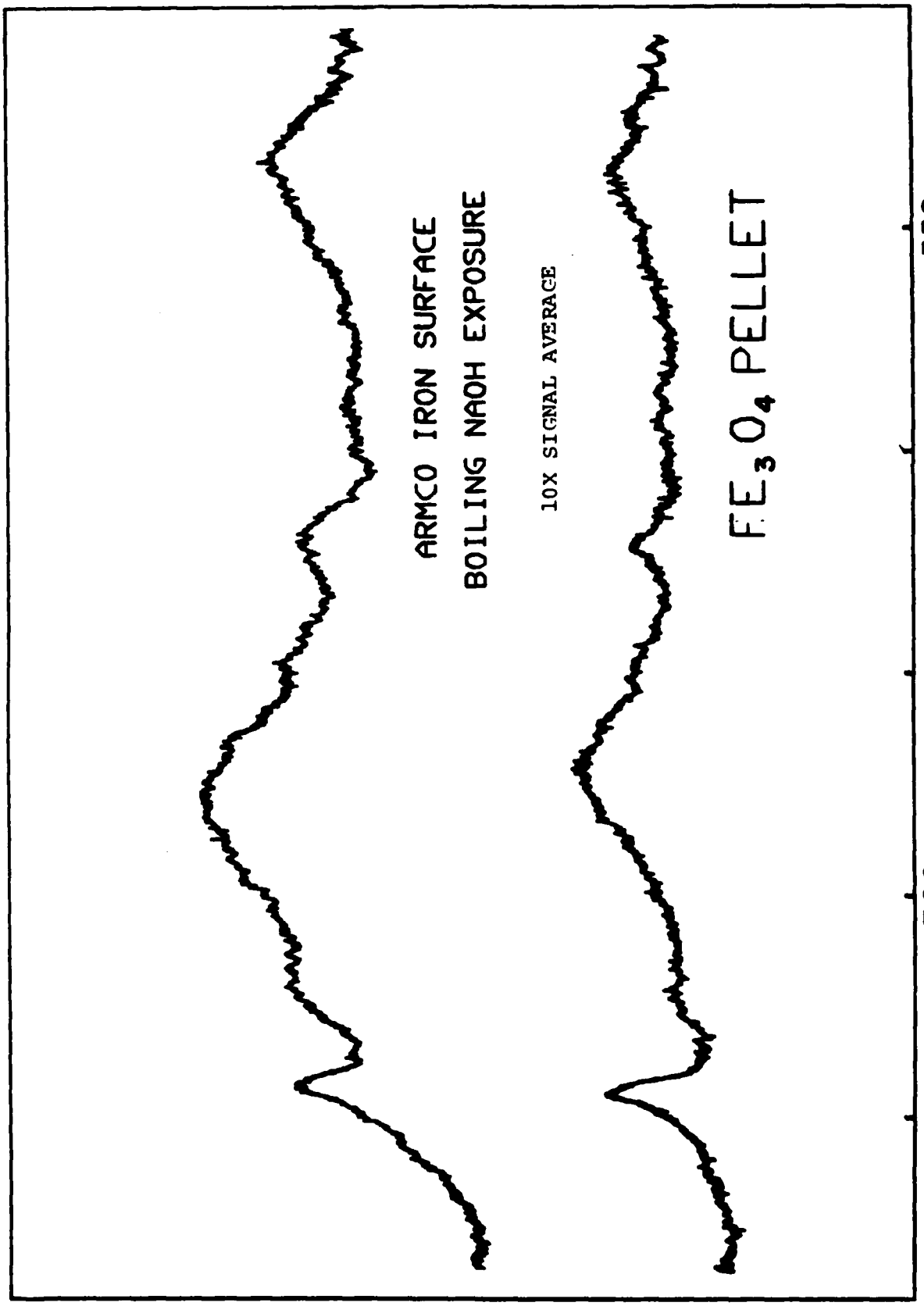

Figure 2. 10x signal averaged spectrum from Figure 1 vs. pure Fe_3O_4.

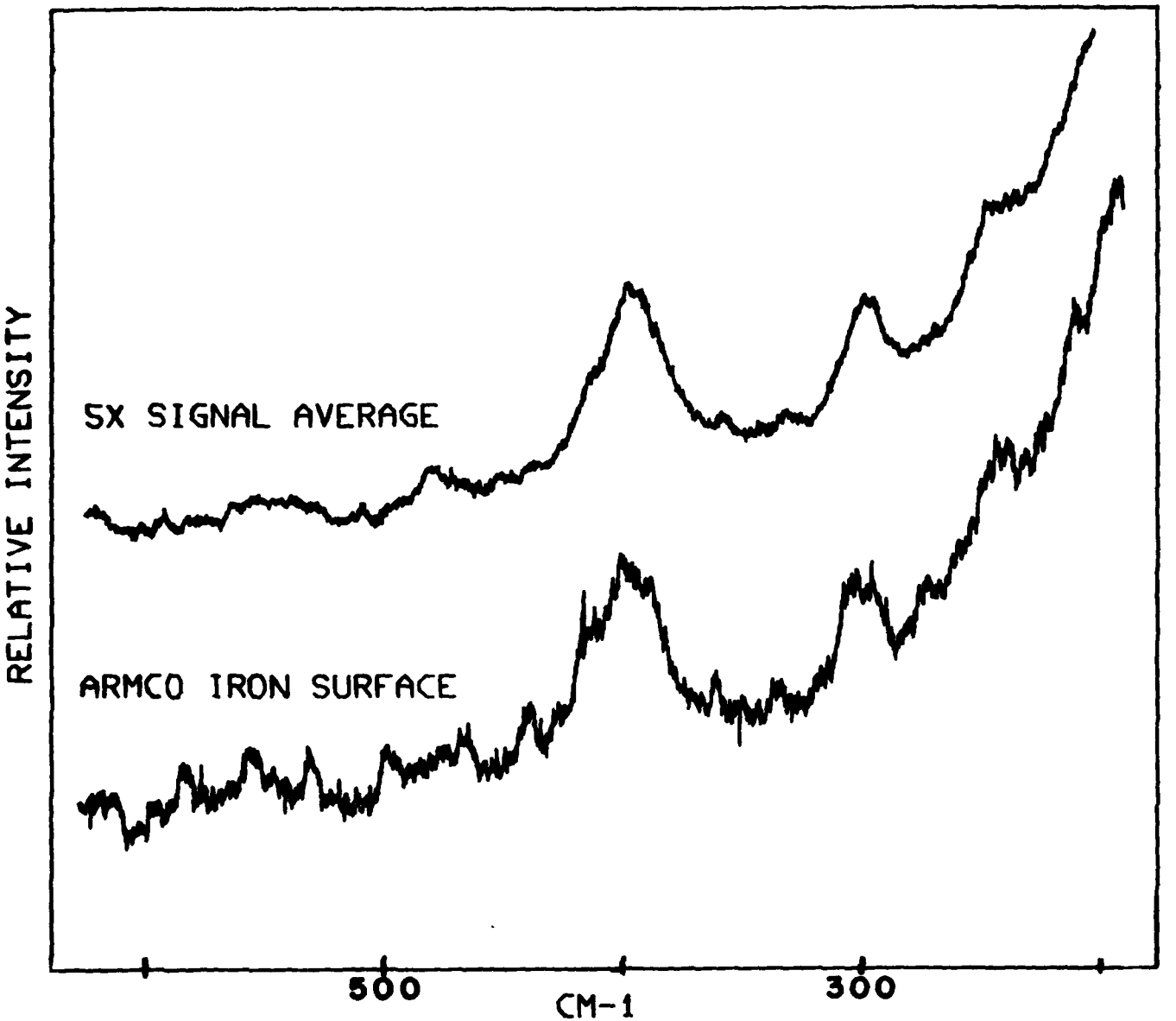

Figure 3. Raman spectrum of an Armco iron surface that was exposed to dilute H_2SO_4 vs. a 5x signal averaged spectrum of the same sample.

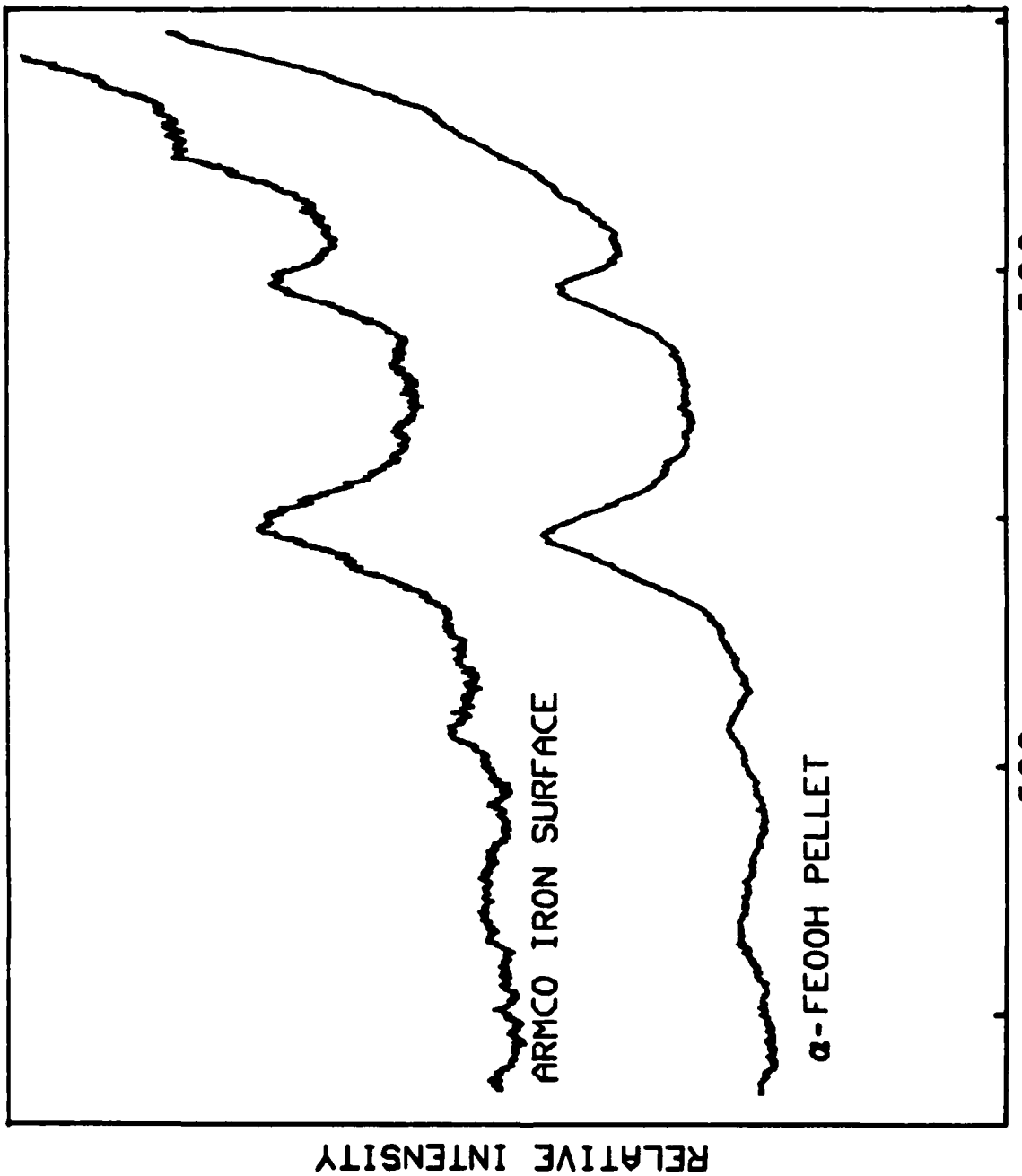

Figure 4. 5x signal averaged spectrum from Figure 3 vs. pure α-FeOOH.

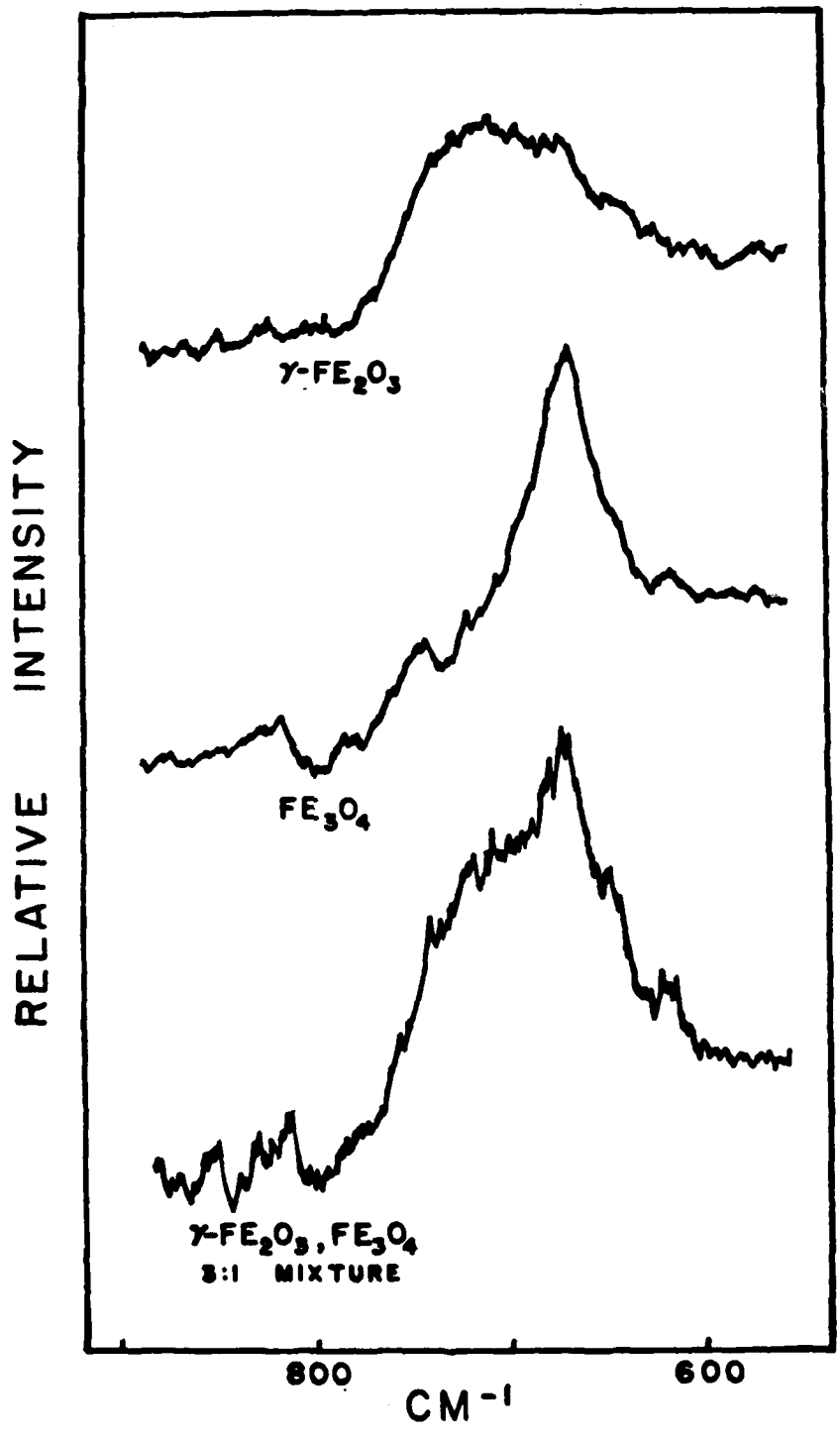

Figure 5. Raman spectra of γ-Fe_2O_3, Fe_3O_4 and a 3:1 mixture of both.

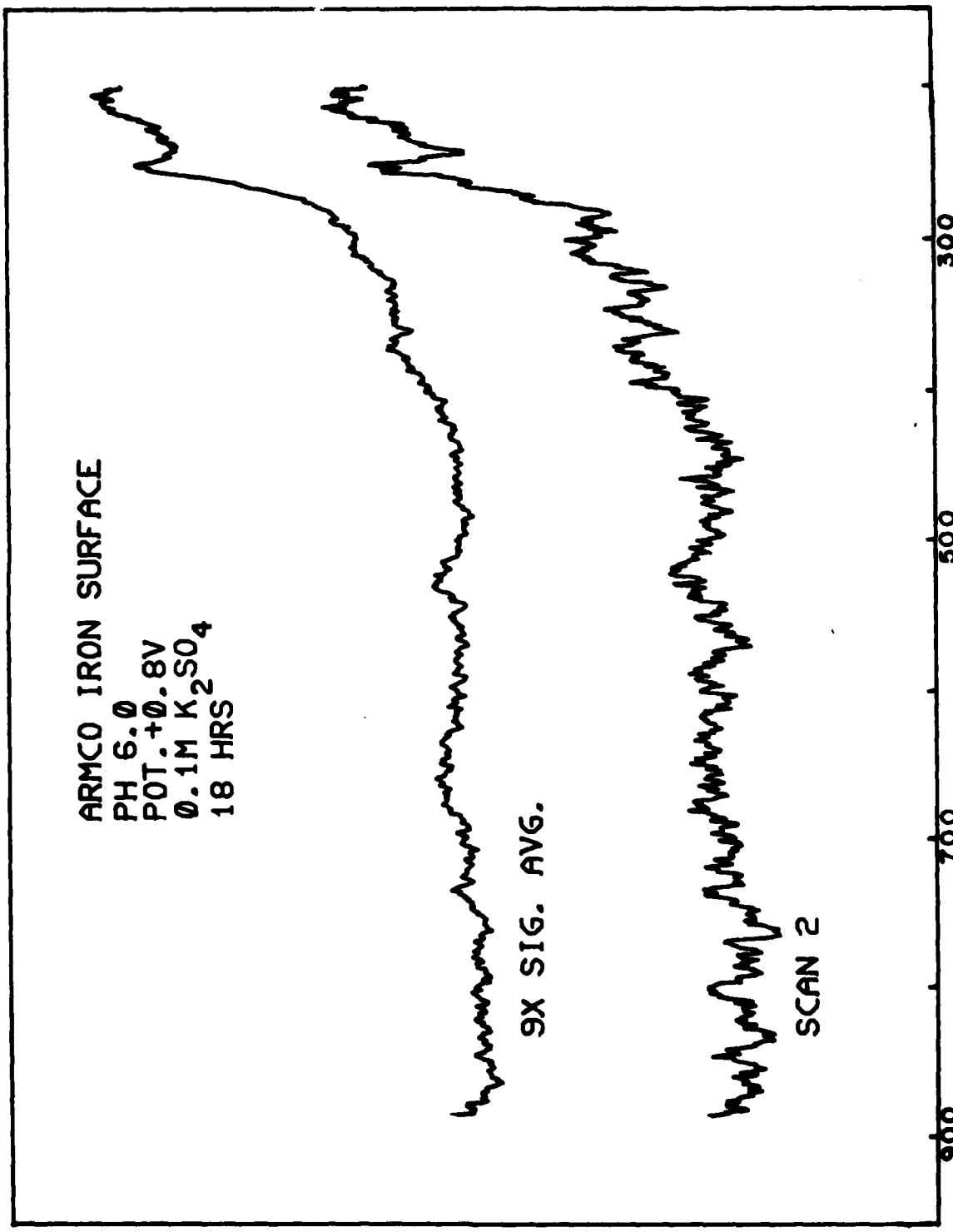

Figure 6. Electrochemical exposure of Armco iron showing the affects of signal averaging.

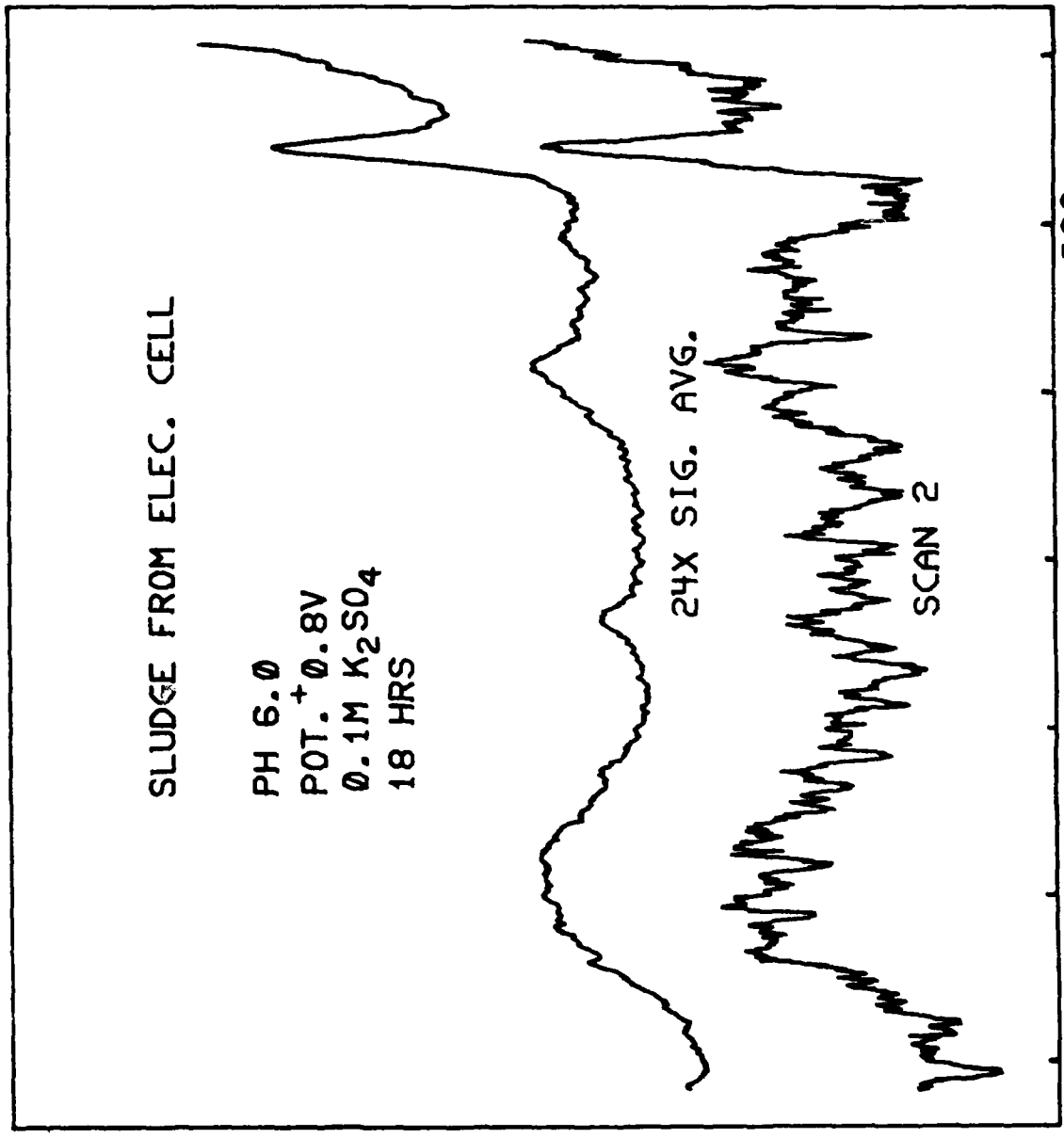

Figure 7. Sludge collected from the bottom of an electrochemical cell (the same exposure as Figure 6) vs. a 24x signal average of the same sample.

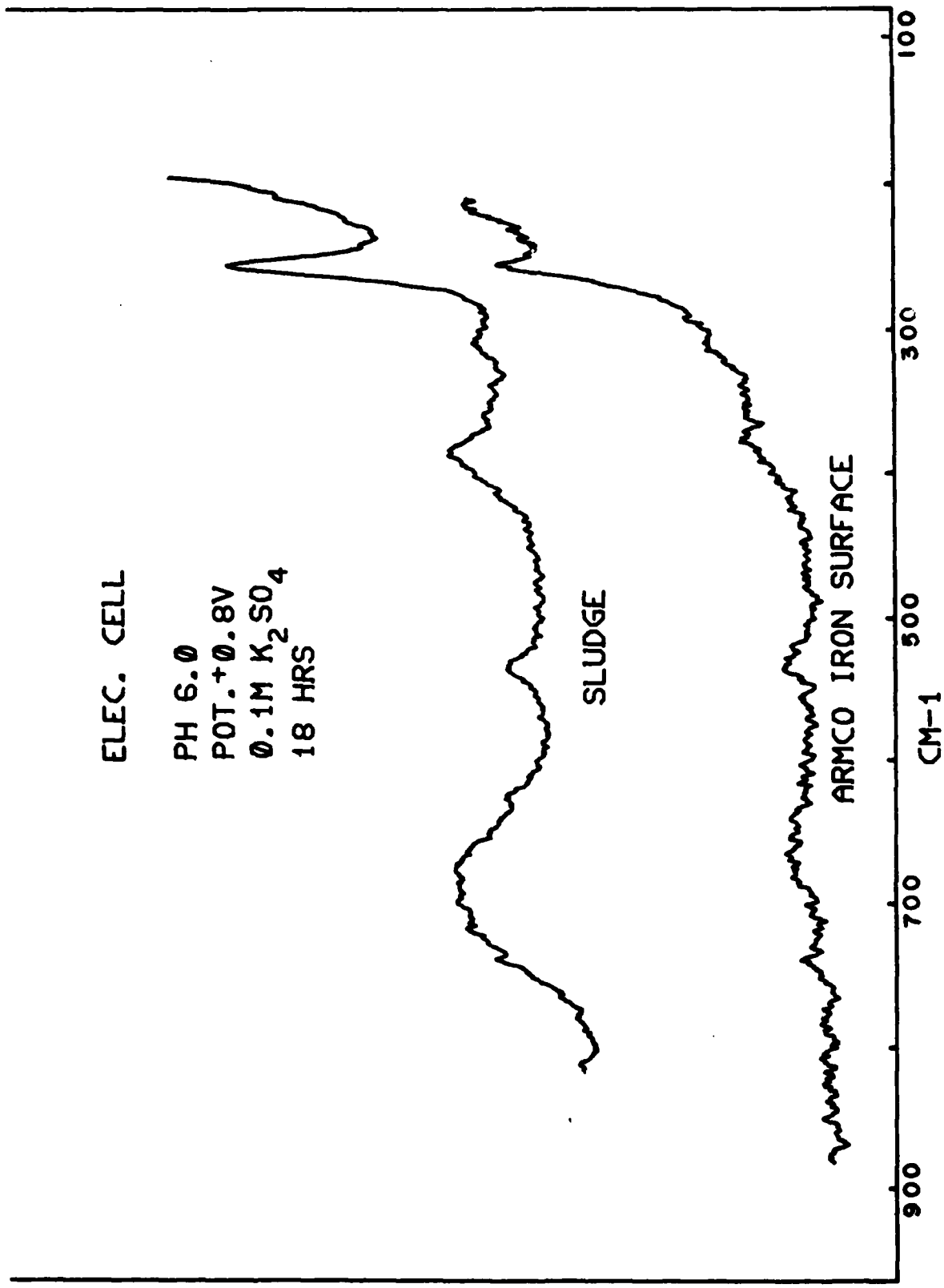

Figure 8. A comparison of the signal averaged spectra from the Armco iron surface and the solution "sludge" shown in Figures 6 and 7.

ELEVATED TEMPERATURE GASEOUS EXPOSURES

By

P. Fabis

INTRODUCTION

The purpose of this phase of research was to provide a series of relatively thick (hundreds of angstroms) oxide films formed on a series of corrosion-resistant alloys. This allowed determination of changes in infrared and Raman spectra on metal substrates under conditions where confirming techniques such as X-ray diffraction could be used to check the results.

The results of the elevated temperature gaseous exposures will allow comparisons with the spectra obtained from aqueous exposures of the same alloys, which can be expected to produce similar, but thinner, oxide surface films.

EXPERIMENTAL ANALYSIS, PROCEDURE, AND APPARATUS

An elevated temperature vacuum/multiple gas purging system was designed and constructed to enable the same exposures to be done while varying both the temperature and gas composition. A schematic of the system is shown in Figure 1. The system consisted of a quartz tube 5.0 cm O.D., a cooling jacket, a female end cap (where samples were loaded, cooled, and unloaded), a gas mixing rotometer, a gas drying and purifying assembly, and an electric tube furnace capable of temperatures between ambient and 1600^{o} C. Temperature maps of the oven at desired experi-

mental temperatures were constructed to obtain the optimum sample position in the oven with regard to temperature stability.

A gas flow system was utilized to prevent, insofar as possible, exhaustion of the corroding gas in the carrier gas. For exposures in air a carrier gas was not used, but for exposures in oxygen and in the hydrogen sulphide-oxygen mixtures oxygen-free nitrogen served as a carrier gas. The gas pressure in the system was monitored by a mercury manometer and maintained at atmospheric pressure.

The goal of the infrared analytical section of this research was to utilize specular and not diffuse reflectance techniques. A schematic of the specular reflectance apparatus can be seen in Figure 2. The sample undergoing analysis had to be flat and its exact orientation in the infrared beam had to be reproducible. A commercially-available Wilks 9D specular reflection attachment was initially used for reflectance work, but modified attachments pictured in Figure 3, similar to those of Mertens[1], were designed and constructed to insure constancy and reproducibility in optimum reflection parameters.

A schematic of the in-situ Raman exposure chamber is pictured in Figure 4. In-situ analysis is advantageous since it insures alteration-free analytical procedures. An in-situ Raman exposure chamber, exposure apparatus, and peripheral equipment were designed and constructed to permit in-situ monitoring of the oxidation process.

Armco iron, AISI Type 446 and AISI Type 502 stainless steels, and two grades of chromium were the sample metals used in this

research. Their compositions are shown in Table 1. The Armco iron, AISI Type 446 and AISI Type 502 stainless steels and the electrolytic grade chromium were chemically cleaned in a dilute solution of glacial acetic and perchloric acid. Samples were then mechanically polished to a mirror surface starting with 60 grit silicon carbide grinding paper, proceeding through a diamond paste to a 0.3 micron alumina powder-distilled water slurry on a lapping wheel. Pure chromium foil did not lend itself to mechanical polishing. The iron, stainless steel, and electrolytic grade chromium were approximately 2.8 x 5.7 cm and the chromium foil was approximately 2.0 x 2.0 cm. After surface preparation, all samples were thoroughly rinsed in distilled water, ultrasonically cleaned in spectroscopic grade methanol, and dried in nitrogen gas. They were then vacuum desiccated to minimize ambient temperature air oxidation.

Following removal from desiccation, the desired samples were loaded into the quartz-tube vacuum system, the system was evacuated, and then extra-dry research purity hydrogen gas was purged into the tube at 120^{o} C to insure a "clean" unoxidized surface. The hydrogen was then bled out of the system, and the carrier-reaction gas mixture was purged through the quartz tube at variable exposure temperatures and exposure periods as shown in Table 2. Following exposure, samples were distilled water quenched, nitrogen gas dried, and mounted for spectral analysis. An exception to distilled water quenching was ambient atmosphere cooling upon termination of in-situ exposures. Atmospheric cooling was utilized to observe the formation of compounds not stable following a water quench.

To examine surface preparation effects on spectrum quality chemical cleaning followed by mechanical polishing, as well as solely mechanical polishing preceeded various oxidation exposures. Raman and infrared reflection spectra were then recorded and compared on the basis of resolution, intensity, and instrument noise level.

Raman and infrared spectra of possible iron and chromium oxides present in surface films were needed for reference and comparison. The dominant oxides of iron (Fe_2O_3, Fe_3O_4, FeO), and chromium (Cr_2O_3), under proposed experimental conditions were obtained from commercial suppliers and/or synthesized and their Raman and infrared spectra recorded. Reagent grade powdered oxide samples were hydraulically pelletized with a KBr matrix[2], mounted in the instrument, and their spectra recorded while purging the sample compartment with nitrogen gas. The infrared spectra were recorded in the transmission mode,and the Raman spectra were recorded with the samples mounted at an angle of 20^{o} from vertical. Double oxides, also known as spinels, of varying composition were synthesized and used for surface oxidation product identification on the stainless steel samples.

Infrared Reflectance System: A Perkin-Elmer 521 grating infrared spectrophotometer with modified reflectance attachments and a Beckman 42-POL grating polarizer were used to record the infrared reflection spectra. This is a modification of the instrumentation used in previous studies of the aqueous corrosion of lead at the University of Rhode Island. A schematic of the reflection system is shown in Figure 5. Radiant energy from a

polychromatic source is split into a sample and a reference beam which are parallel. A commercially available reflection attachment was initially used for reflectance work, but modified attachments, similar to those of Mertens[4], were designed and constructed to insure constancy and reproducibility in the optimum reflection parameters -- the beam incidence angle and the number of reflections.

The multiple reflection attachment allowed radiation reflection between a sample-mirror pair in the sample beam and a mirror-mirror pair in the reference beam, at adjustable angles of incidence from 30° to 70°. These attachments were previously shown in Figure 3. The rectangular morphology of the aluminum-coated mirrors and of the sample in the reflectance attachment dictated orientation are such that radiation was reflected along the major axes of the sample and the mirrors to maximize the signal to noise ratio. Multiple-sized precision spacers allowed interchangability and sensitivity control. A maximum of about 40 reflections could be obtained with quality mirrors and sample surfaces. The focusing scheme was executed with three spherical mirrors and one planar mirror. The reflection attachment was mounted on the optical chassis of a Wilks 9D specular reflectance apparatus.

The spectrometer was adjusted for spectrum recording by careful beam balancing. Maximum reflectivity in the reference beam was obtained by operating the spectrometer in the single-beam mode and simulataneously adjusting the aluminum-coated mirrors in the reflection apparatus. Once a satisfactory re-

flectivity was obtained, the polarizer was mounted directly in front of the main slits. Samples were mounted versus an aluminum planar mirror in the reflection attachment,and the sample apparatus was positioned in the spectrometer light path. Adjustments to maximize the number of reflections and the beam incidence angle were performed by mirror alignment procedures.

The reference beam is identical to the sample beam with the exception of a mirror assuming the sample position in the reference reflection attachment. The reference beam then encounters an optical attenuator to equalize the sample and reference beam intensities. A sector mirror in the monochromator compartment then modulates the beam to establish a switching frequency allowing time for detector response. After sample and reference beam combination, the beam passes through a wire grid polarizer. Polarizer adjustment allows only the electric vector of light parallel to the plane of incidence to be transmitted. The advantage of spectral polarization is shown in Figure 6. The components of radiation perpendicular to the incident plane, E, are selectively filtered to increase instrument sensitivity. To insure that the maximum sensitivity was obtained in the E_{11} modes (electric vector of radiation parallel to incident plane) all spectra were recorded in the E_{11} and E_1 modes. Next, the beam is directed into the monochromator where the radiation is dispersed into its component frequencies and transmitted to the detector. The detector, a sensitive thermocouple, transduces the temperature due to the impinging infrared radiation to an electrical signal indicating the magnitude of the inci-

dent power. A servo motor controls the optical attenuator and the resulting reflection spectrum is a record of attenuator position. The actual "reflection" spectrum is a combination transmission-reflection spectrum since the radiation is transmitted through the film and reflected from the substrate metal surface.

In all cases, a preliminary spectrum was recorded and from it the necessary adjustments in polarizing angle, incidence angle, and number of reflections to maximize instrument sensitivity were determined. The beam incidence angle was between 65^{o} and 72^{o} and from two to eight reflections were usually employed. Polarizer settings were determined by adjusting the polarizing angle while the instrument wavelength was centered on one of the reflection-absorption bands. Once optimum conditions were obtained, the spectrum was recorded from 2500 wavenumbers to 250 wavenumbers. The sample compartment was continuously purged with nitrogen gas during spectrum recording to minimize carbon dioxide and water vapor band interferences. This problem was an important experimental consideration since both water vapor and metal oxides have absorption bands in the long wavelength region (below 600 cm^{-1}) of the spectrum. Scale expansion techniques were available but were unnecessary since all infrared spectra were well defined. Goldfarb[5] reported the use of scale expansion techniques to enhance infrared reflectance spectra of lead in phosphate buffers.

In-situ infrared spectroscopy was attemped, but due to sample chamber size limitations and reflecting mirror surface oxidation problems, the recording of spectra was impossible.

Raman System: The Raman system is composed of a laser, a sample compartment and exposure cell, optical monochromators and a photon detection system. The laser is a source of monochromatic radiation which impinges on the sample. Most of this radiation is reflected from the sample and does not undergo a wavelength change. There is an interaction between the incident radiation and the surface which results in an energy loss and an emission of radiation at wavelengths other than that of the incident radiation. This emitted radiation is measured as the Raman spectrum.

Using a Spex Industries Model 1401 double monochromator with a photon counting system, Raman spectra were recorded employing the 5145 A^{o} green excitation wavelength radiation. An optical schematic of the instrument layout is pictured in Figure 7. A coherent Radiation Laboratories Model CR-3 Argon ion laser was located beneath the monochromator, and the monochromatic radiation was reflected by a mirror through the sample compartment to the sample. Some of the radiation is scattered and a focusing lens is positioned allowing the beam to be sharply focused on the entrance slits of the monochromator. Radiation passing through the slits is collimated by a mirror and dispersed by a grating. The radiation is then frequency sorted and directed by a collimating mirror and a plane mirror to a set of intermediate slits. This narrow frequency band of radiation, which has passed through the first monochromator, then passes through a second monochromator to maximize the rejection of stray radiation; it then reaches the photomultiplier tube.

The number of photons per unit time interval is converted to an analog signal which drives the strip chart recorder. A frequency range is scanned by turning the two gratings in the monochromator simultaneously so the frequency of the radiation reaching the detector is changed. Therefore, the Raman spectrum recorded is a plot of radiation intensity versus frequency difference from the excitation frequency. This concept is pictorially represented in Figure 8.

In order to optimize observation of Raman scattered radiation, the oxidized metal sample was oriented at an angle of 20^{o} from vertical. Greenler and Slager[6] indicated that the incident beam-sample surface angle determines the intensity of the reaction between the incident radiation electric vector and the surface film. This angle also regulates the amount of stray radiation entering the monochromator. Since only the scattered component of impinging radiation should reach the entrance slits, the sample orientation must prohibit specularly reflected radiation from reaching the focusing lens and eventually the monochromators and detector.

As previously mentioned, in-situ analysis is advantageous because it insures alteration-free analytical procedures. The high temperature in-situ Raman exposure apparatus is composed of a standard exposure cell, similar to that used by Thibeau[7], modified for high temperature gaseous exposures. Samples to be oxidized in-situ were mounted with the unpolished surface against the coils of a platinum wire contact resistance heater arranged in the elevated temperature Raman cell as shown in Figure 4.

The oxidation temperature and its stability was monitored by a chromel-alumel thermocouple. The entrance and exit gas ports allowed thorough oxidation atmosphere exchange during metal exposures.

There is a beam modulator incorporated in the system for in-situ elevated temperature analysis. The scattered radiation necessary for Raman spectrum generation must be separated from the interferring emission radiation. The emission radiation decreased instrument sensitivity by overloading the monochromators with unwanted radiation. This difficulty was eliminated by modulation of the laser source. The intensity of the laser beam was fluctuated at a constant frequency. The photomultiplier detector then received two types of signals, an alternating one from the source and a continuous one from the elevated temperature emission. These signals were converted to corresponding electrical signals. A simple electronic system was utilized to respond to and amplify the AC signal component and ignore the unmodulated DC component. A circular sectored disk was interposed in the beam between the laser source and the heated sample. The disk was sectored to create modulated radiation pulses. Rotation of the disks at a constant rate provided an intermittent beam that was chopped to the desired frequency by control of the motor speed. The design of the beam modulation system was adapted and modified from a discussion by Skoog and West[8].

X-Ray Diffraction: The X-ray diffraction patterns of synthesized compounds, of analytical reagents, and of selected surface film compounds were recorded. These patterns were recorded on a

General Electric 11GJ1 X-ray unit with copper and chromium targets. The beam slit width was 3 degrees; filtration -- 2 nickel; soller slit -- medium; time constant -- 1 second; scaling -- linear and logarithmic; and a maximum 2000 counts per second at full scale deflection.

Scanning Electron Microscope: Samples to be observed were cut to enable them to fit in the vacuum-observation chamber of the SEM. The sample size was approximately 5 mm x 5 mm. Following a previously outlined surface preparation procedure, the samples were exposed under the desired experimental conditions. Upon cooling, samples were epoxy glued to a mounting stud, silver painted on non-conducting surfaces, and left to dry for 24 hours.

All samples, though good conductors, were coated with a gold-palladium film utilizing a vapor deposition apparatus to enhance the resolution of the microscope. A Hitachi Model USG-46B vacuum evaporator was used.

SEM observation utilized a Hitachi Scanscope SSM-2 and all magnifications were between (50x) and (2000x).

Micrographs were taken using a Tektronix oscilloscope camera Model C-27 with F 1.4 to F 16 optics and a 1:1 magnification ratio.

Polaroid #665 positive-negative land film with an ASA rating of 75 was used for all pictures with a photometer reading of 80-85 and an aperture setting of F 16.

Interference Microscopy -- Film Thickness: Upon completing all other analyses, the oxidized samples were partially etched in

a solution of nitric acid (23 percent by volume), hydrofluoric acid (4 percent by volume), and water (73 percent by volume). The samples were immersed in the above solution at about 50-55° C for 1 to 5 minutes. Prior to etching the desired etch area was dipped in hot water to aid in increasing the rate of film removal. Upon completion of the etching process, samples were distilled water rinsed, nitrogen gas dried, and desiccated.

The sample was then placed in a vacuum evaporator and coated with silver. The over-coating faithfully contoured the step produced by the etching procedure. The overcoated silver had on it a step equal in metrical thickness to that of the film. In this technique there was an inherent assumption that the film, before overcoating, is continuous. Silver is used as a reflective coating due to its high reflectivity and low absorption characteristics. This process is shown in Figure 9.

A Unitron MeC Series N inverted stage metallographic microscope and the interference microscopy attachments were utilized in measuring the film thickness. Samples were observed soon after the silver coating procedure since the silver film can oxidize rapidly and produce spotty images. The oxidation product also is able to absorb more light and decrease the sensitivity of the method. To prevent silver oxidation problems, a thin layer of SiO_2 may be evaporated on to the silver[9].

The Model NUM-INT Interference accessories converted a Unitron Series N Metallograph into a multiple-beam micro interferometer. The accessories consisted of a 10x interference objective, an accurate "proof plate" which attached to the objective, and a cadmium interference filter used in conjunction

with the light source. In use, the fine focus control was used to bring the objective proof plate into contact with the specimen surface. Interference fringes were produced by multiple reflections between the specimen and the plate. The fringes superimpose a contour map on the specimen image. Since the distance between adjacent fringes corresponds to a difference in height of one-half the wavelength of the illuminating light, the extent of the surface irregularity could be measured. Table 2 presents the film thickness measurements for the exposures of this investigation.

RESULTS AND DISCUSSION

AIR EXPOSURES

Oxide Films Formed on Iron: Infrared reflectance spectra of Armco iron exposed at various temperatures in air are shown in Figure 10. These spectra closely resemble those obtained by Poling[10], Goldfarb[5] and Mertens[1]. Between the oxidizing temperatures of 250° C and 460° C the relative band intensities increase approximately three-fold. From 460° C to 880° C the band frequency shifts become the dominant feature while the band intensities remain approximately constant or decrease slightly. At lower temperatures, 250° C to 460° C, initial oxidation products observed were Fe_2O_3 and Fe_3O_4. It was difficult to distinguish between α - Fe_2O_3 and γ - Fe_2O_3 due to the close proximity of spectral bands for each polymorph and due to the poorly defined bands for γ - Fe_2O_3. X-ray analysis confirmed the presence of γ - Fe_2O_3. At lower oxidizing tempera-

tures the oxide film composition consisted of intricate structures of Fe_2O_3 polymorphs and Fe_3O_4 similar to those reported by Mertens[1]. The lower oxidation temperatures produced bands of greatest spectral intensity at 655 cm^{-1} which could be attributable to γ - Fe_2O_3 and Fe_3O_4. Moderate band intensities at 320 cm^{-1}, 465 cm^{-1} and 560 cm^{-1} indicate the presence of α - Fe_2O_3. As the temperature was increased to 670° C and 880° C, α - Fe_2O_3 bands were the prevalent spectral features. At 670° C an unassignable band at 762 cm^{-1} vanishes at 850° C and a moderate band at 650 cm^{-1} with a 635 cm^{-1} shoulder appears. The intensity of the α - Fe_2O_3 bands increased with a 660 cm^{-1} band intensity reduction.

Figure 11 shows the Raman spectra for Armco iron under identical exposure conditions. These spectra closely resemble those obtained by Thibeau[7]. The presence of spectral bands at 230 cm^{-1}, 245 cm^{-1}, 300 cm^{-1}, 415 cm^{-1}, and 610 cm^{-1}, at all oxidizing temperatures confirms the presence of α - Fe_2O_3 and a band at 663 confirmed the presence of Fe_3O_4. At oxidizing temperatures above 570° C, FeO is a stable oxide phase. The Raman spectra for FeO and Fe_3O_4 are identical, with bands at 615 cm^{-1} and 665 cm^{-1}, so alternate analytical methods were employed to distinguish between these components. X-ray diffraction patterns of these samples indicated the presence of FeO and Fe_3O_4 at 460° C, 670° C and 880° C. Evidence for FeO existence in the 460° C, 15 hour exposure obtained from X-ray analysis confirmed earlier reports by Gulbransen and Ruka[11] of FeO stability below 570° C. Two explanations can be offered for the similarity of Raman spectra of FeO and Fe_3O_4. The

Fe - O bond vibrations in FeO and Fe_3O_4 may be nearly the same, thus the same spectral bands are observed for both compounds. The other possibility is that FeO is metastable below 570° C and decomposes into the more stable Fe_3O_4 and elemental iron due to laser heating and absorption of radiation. Since FeO and Fe_3O_4 are black in color, visible light can be strongly absorbed causing thermal decomposition[7]. The effect of sample decomposition via laser heating can be offset by diminishing the laser power and/or by inserting neutral density filters in the beam path. Sample rotation during Raman analysis was contemplated as well as utilizing an alternate excitation radiation wavelength, 4880 A°, to minimize sample decomposition. Other methods mentioned previously, such as using neutral density filters proved to be more effective in these analyses.

Oxide Films Formed on Chromium: Raman spectra for pure chromium oxidized in air for 15 hours at elevated temperatures are presented in Figure 12. The strongest spectral band is at 569 cm^{-1}, with secondary dominant peaks at 303 cm^{-1} and 348 cm^{-1}, and weaker bands at 612 cm^{-1} and 437 cm^{-1}. The above mentioned bands are common to all elevated temperature chromium exposures and indicate the oxidation product to be Cr_2O_3. Only the 880° C exposure had additional distinguishable bands which were located at 392 cm^{-1}, 648 cm^{-1}, and 656 cm^{-1}. These additional bands could be attributable to the effect of chromium existing at a higher oxidation state as reported by Mertens[2] from his infrared reflection spectra of oxidized chromium in oxygen. Infrared reflection spectra were not obtained for pure chromium due to sample size limitations.

Chromia, Cr_2O_3, is reported to be an oxidation product of elevated temperature air exposure of chromium[12,13]. The elevated temperature oxide film component on chromium was found to be only Cr_2O_3. The scale spalled and flaked off quite easily after exposure to higher temperatures, so scale adherence seemed poor. At high oxidation temperatures, nitrogen has been reported to be taken into solid solution and form Cr_2N upon cooling in air[12]. A water quench following oxidation would retain the nitrogen in solution[14]. In this investigation, all elevated temperature chromium exposures were distilled water quenched so bands attributable to Cr_2N should not have been and were not observed.

Cr_2O_3 has also been reported as the sole oxidation product on chromium after heating in oxygen at various temperatures[12]. This is valid for temperatures below 1600° C, but above this temperature and at higher oxygen pressures, CrO_2, Cr_5O_7, Cr_2O_5, Cr_3O_8 and CrO_3 may form[15]. These may be metastable phases and a higher oxygen pressure may be a necessity for their formation. Cr_3O_4 is reported as a stable product in strongly reducing conditions and at temperatures greater than 1600° C[15].

Oxide Films on Stainless Steels: A pai. of commercial iron-chromium alloys, AISI Type 446 and AISI Type 502 was selected on the basis of chromium content. AISI Type 446 stainless steel contained 24.6 weight percent chromium and AISI Type 502 stainless steel contained 5.14 weight percent, relative to AISI 446 with only 0.37 weight percent silicon.

Examples of infrared reflectance spectra for AISI Type 446 stainless steel and AISI Type 502 stainless steel oxidized at various temperatures in air for 15 hours are shown in Figure 13 and Figure 14, respectively. The bands of greatest intensity are located in the 425 cm^{-1} to 750 cm^{-1} range. Bands of lesser intensity were observed on both sides of this range, the higher temperature exposures resulting in the higher frequency bands becoming the more dominant bands. The 880° C exposures exhibited greater band multiplicity below the dominant bands in the proximity of 730 cm^{-1}. The 460° C exposures had a greatly decreased band intensity and a negligible band multiplicity below the most dominant peak.

Bands suggesting FeO, Fe_3O_4, and α - Fe_2O_3 are present, but the dominant band at 737 cm^{-1} suggests a spinel phase perhaps consisting of $FeO \cdot Cr_2O_3$[1]. According to Mertens[1], the stoichiometric spinel, $FeO \cdot Cr_2O_3$, would produce a single, symmetrical band in this region since all metal oxides that were investigated gave symmetrical longitudinal modes at specific frequencies. McCullogh, et.al., have identified this phase on 18-8 chromium-nickel and 16 percent chromium steels[16]. The bands attributable to the spinel phase vanish in the lower temperature exposures since the spinel phase may only be stable to about 800° C[12], but a Cr_2O_3 phase remains evident. The oxide film at lower exposure temperatures exhibits some heterogeneous mixture of Fe_2O_3 and Cr_2O_3.

The solitary, dominant band at 638 cm^{-1} on AISI Type 502 stainless steel at 460° C for 15 hours was assigned to γ -Fe_2O_3.

Other characteristic bonds were observed. Although Cr is selectively oxidized to Cr_2O_3 in elevated temperature exposures on stainless steels[12], the strong bands of Cr_2O_3 at 710 cm^{-1} and 522 cm^{-1} were not observed. This may be due to the low chromium content of this alloy. Higher frequency bands may be attributable to Si-O bonds. Mertens[1] makes no definite assignment, but suggests a SiO_2 component, metal-silicate phases, or chromium existing in higher oxidation states as possible causes for higher band frequencies on AISI Type 304, AISI Type 316, and AISI Type 410 stainless steels at 850° C in pure oxygen. If metal silicates are present this would hint at layer which is nonprotective against oxidation since the metal silicates are low melting eutectics. Metal silicates such as $FeSiO_4$, were not observed on AISI Type 502 or AISI Type 446 using Raman, infrared, or X-ray analysis.

Raman spectra for these alloys subjected to identical conditions are shown in Figure 15 and Figure 16. The bands of greatest intensity tend to be wide when compared with the bands of the pure oxides. This is an indication of the presence of compound mixtures. Due to the simplicity and relatively distant spacing of bands in the Raman spectra of iron oxides and chromium oxide, the identification of compounds in such a mixture at low exposure temperatures is not difficult. Unlike the broad overlapping bands in the infrared spectra of these compounds, the relatively narrow Raman bands allow a more rapid identification of compounds comprising a given mixture. Lower exposure temperature spectra for AISI Type 502 stainless steel exposed for 15

hours in air are presented in Figure 16 and suggest α - Fe_2O_3 and Cr_2O_3 components and an emerging and increasing Fe_3O_4 component. At the maximum exposure temperature of 880° C bands attributable to the spinel phase, $FeO \cdot Cr_2O_3$, appeared at the expense of decreasing and eventually vanishing FeO bands which can be observed in Figure 16. The spinel occurrence was confirmed by comparison with Raman and X-ray analyses of laboratory synthesized spinels. Cr_2O_3 bands were present at all exposure temperatures.

Spectra at lower temperatures on AISI Type 446 stainless steel oxidized in air for 15 hours are seen in Figure 15. AISI Type 446 and AISI Type 502 stainless steel exposures exhibited somewhat similar spectral trends. Initial formation of α - Fe_2O_3, Fe_3O_4 and Cr_2O_3 is indicated. With increasing exposure temperatures a heterogeneous surface mixture of Fe_2O_3 and Cr_2O_3 is prevalent and once the maximum exposure temperature of 880° C is attained, a spinel phase emerges as $FeO \cdot Cr_2O_3$. At these elevated temperatures, Cr_2O_3 and Fe_3O_4 bands are also observable. Faint, higher frequency bands could be attributable to FeO, but spinel presence can exclude a FeO phase. Although not very strong, contrary to information reported by Saksena[17], The Raman band for SiO_2 (α - quartz) at 466 cm^{-1} was observed on both alloys during the elevated temperature exposures in air. The Raman bands for α - cristobalite at 493 cm^{-1} and 456 cm^{-1} for vitreous silica, as reported by Reitzel[18], were also not well defined in any spectra as would be expected.

Figures 17 and 18 show scanning electron micrographs of the surface oxides of AISI Type 502 and AISI Type 446 stainless steels after 15 hours exposure in air at 670° C. Scale breakdown is apparent. The breakthrough sites are highly localized and randomly distributed on the surface; this results in the warts or nodules of a duplex structure consisting of an inner layer of spinel oxide and an outer layer of "doped" ferric oxide[19,20]. Depending upon alloy composition and oxidizing conditions, the nodules may expand laterally until the entire surface is covered with a stratified scale[21]. Two theories have been proposed for the scale alteration. There may be a chemical mechanism that is operative where the protective scale is penetrated by iron ions causing transformation to the spinel oxide and producing ferric oxide at the outer surface[22]. The other possibility is that scale cracking occurs and the underlying alloy, depleted in chromium reacts directly with the atmosphere producing the spinel oxide and outer iron oxides[22]. In either case, a stratified scale is generated over the whole or part of the surface. AISI Type 446 stainless steel, the higher chromium content alloy, had very few nodular growths at 670° C. The 460° C and 250° C exposures exhibited no nodules, and the scale was apparently continuous. AISI Type 502 stainless steel, the lower chromium, higher silicon content alloy, exhibited nodule growth down to 460° C. There were also scale cracks at 670° C which could be attributed to silica accumulation at the metal-oxide interface[22]. An alternate explanation is that the scale fracturing may be due to compressive

stresses in the oxide resulting in nonuniform oxide growth. The thermal expansion characteristics of oxide and substrate metal are also considerably different and this may result in tensile stress nonuniformity. Hobby and Wood[23] have noted that scale breakdown does not seem to occur for alloys of high chromium content, particularly at low service temperatures. This is evident in the AISI Type 446 stainless steel micrographs at lower exposure temperatures. Whether a spinel oxide scale is beneficial in the protective sense is still a debatable topic[12].

The Effects of Exposure Period: The effect of exposure period was also investigated for AISI Type 446 and AISI Type 502 stainless steels. Shown in Figure 19 are the infrared reflectance spectra for these alloys at 670° for 10 and 24 hours exposure in air. Noticible with increased exposure period was increased band intensity and multiplicity, greater band resolution, and overall spectral enhancement. Longer exposure periods increase oxide film thickness so relative band intensities attributable to a specific compound may be assessed as a qualitative measurement of the quanity of an oxide phase present. The Raman spectra for the same samples are shown in Figure 20 and analogous interpretations can be made for these spectra as for the infrared reflectance spectra.

In-Situ Raman Spectra: In-situ Raman exposures of AISI Type 446 and AISI Type 502 stainless steels at 880° C for varying exposure periods in air are depicted in Figure 21. AISI Type 446 stainless steel exhibited the initial formation of a spinel phase, $FeO \cdot Cr_2O_3$, after a 3 hour exposure. Bands attributable to α - Fe_2O_3, Fe_3O_4, and Cr_2O_3 are observable but faint. Continuing

the exposure period to 8 hours produced bands of a dominant Cr_2O_3 phase, a spinel phase, $FeO \cdot Cr_2O_3$, and the iron rich phases of Fe_2O_3 and Fe_3O_4.

Also shown in Figure 21 is an in-situ Raman exposure of AISI Type 502 stainless steel under identical conditions. The three hour exposure in air produced Raman bands suggesting α - Fe_2O_3, FeO, and Cr_2O_3. The spectrum after eight hours exposure in air exhibited a decreasing FeO component and the initial formation of a $FeO \cdot Cr_2O_3$ phase. The bands attributable to Cr_2O_3 were also present, but of greater intensity on the AISI Type 446 alloy exposure. Following the three and eight hour in-situ exposure analyses, air cooling of the samples was permitted. Once cooled to ambient temperatures, Raman analysis was performed to investigate the possibility of Cr_2N formation. This phase is expected to nucleate on pure chromium upon air cooling from elevated temperatures. The Raman spectral analysis did not detect a Cr_2N component in the film. Upon completion of the Raman analysis, the air cooled sample was mounted and prepared for scanning electron microscopy investigations. Following comparison with an identically exposed, but water quenched sample, it was apparent that surface morphological features can be considerably affected by cooling rate and method. The micrographs can be compared in Figure 22.

The in-situ spectra in Figure 21 can be compared to the ex-situ spectra in Figure 15 and Figure 16. The majority of in-situ Raman spectral bands also appeared in the ex-situ Raman spectra. This was evident in both the AISI Type 446 and AISI Type 502 stainless steel sample exposure spectra. The shorter

exposure periods for in-situ investigation show initial surface oxidation products which may be different than longer exposure term oxidation products. The in-situ spectra exposure period may not have been long enough to allow all bands to fully develop. Surface preparation techniques could have introduced surface impurities which, not being exactly reproducible, lead to spectral differences. In general, the ex-situ and in-situ spectra are similar. In-situ investigation may not be as necessary in elevated temperature oxide film investigation as in aqueous passive film studies where hydration and dehydration of the film is an important consideration. O'Grady[4] discusses the film hydration mechanism and the role of water in passive film structures on iron.

The Effects of Surface Preparation: Surface preparation procedures had observable influences upon infrared reflection spectra, but were unnoticible on Raman spectra. Chemical cleaning followed by mechanical polishing as well as soley mechanical polishing preceeded various oxidation exposures. Chemical cleaning followed by oxidation produced poor infrared reflectance spectra, but had little effect on Raman spectra quality. It was determined that mechanical polishing was required for good quality infrared reflectance spectra, but was not required to obtain decent Raman spectra.

OXYGEN EXPOSURES

Armco Iron Oxidation: The infrared reflection spectra of Armco iron exposed at various temperatures in pure oxygen are shown in Figure 23. A close resemblance exists between these spectra and those obtained by Mertens[1].

Increases in exposure temperatures produced band intensity increases probably resulting from surface film thickening. Certain band frequencies were common to all spectra suggesting similar surface oxidation products. A marked change in band intensities occurred between the 460° C and 880° C exposures as indicated by the 427 cm, 501 cm^{-1} and 667 cm^{-1} bands. The 427 cm^{-1} and 501 cm^{-1} bands exhibited a decreasing intensity trend at 670° C, but returned to approximately one-half the 460° C exposure intensity at the 880° C exposure. An opposite trend was observed for the 667 cm^{-1} band through the 460° C to 880° C exposure sequence. The 667 cm^{-1} band at 670° C was almost double the intensity exhibited by the same band in the 460° C and 880° C exposures.

The oxidation process on iron at the specified exposure temperatures probably results in the formation of surface oxidation products initially rich in γ - Fe_2O_3 and Fe_3O_4. Fe_3O_4 is believed to be a "secondary" oxidation product in this case due to its limited presence. The pure oxygen oxidizing atmosphere favors the Fe_2O_3 formation over Fe_3O_4.

The lower exposure temperatures produced surface oxidation products of Fe_3O_4 and Fe_2O_3. The utilization of X-ray analysis permitted the identification of both polymorphs of Fe_2O_3, α - Fe_2O_3 and γ - Fe_2O_3, as well as Fe_3O_4.

Initial growth of the 667 cm^{-1} band suggested a dominant γ - Fe_2O_3 phase in the surface oxidation product. With increased exposure temperature, the γ - Fe_2O_3 component of the surface oxidation product decreased while the α - Fe_2O_3 bands were en-

hanced at 427 cm^{-1} and 505 cm^{-1}. X-ray analysis confirmed the compound identifications.

Figure 24 presents the Raman spectra for Armco iron exposed at various temperatures in pure oxygen. The spectra obtained contain certain bands at 230 cm^{-1}, 300 cm^{-1}, 421 cm^{-1}, and 617 cm^{-1} at all oxidizing temperatures which demonstrated the presence of α - Fe_2O_3 and Fe_3O_4. The bands at 617 cm^{-1} and 662 cm^{-1} were evidence for the existence of FeO at the 670° C and 880° C exposure temperatures. X-ray methods confirmed the presence of an FeO component in the surface oxidation product. FeO was not positively identified via infrared reflectance analysis, as were Fe_2O_3 and Fe_3O_4, so X-ray analysis was utilized to confirm the Raman spectral results.

Chromium Oxidation: The infrared reflectance spectra of chromium exposed in pure oxygen at various elevated temperatures are presented in Figure 25. The band of greatest intensity appeared at 715 cm^{-1} which was inherent in all spectra. Above the 460° C exposure temperature numerous other bands appeared at 595 cm^{-1}, 524 cm^{-1}, 438 cm^{-1}, and 404 cm^{-1}. The bands at 595 cm^{-1}, 438 cm^{-1} and 404 cm^{-1} did not develop significantly in the lower exposure temperature spectra. Perhaps this is related to a minimum film thickness limit being attained before these bands are spectrally resolvable.

The only surface oxidation product identified on chromium under these conditions was Cr_2O_3. Mertens[1] reports a major band in the reflectance spectra between 720 cm^{-1} and 740 cm^{-1} and attributes this to a longitudinal vibration mode. This

band was not present in either the reflectance or transmission spectra in this experiment. However, the 715 cm^{-1} band could be attributed to the longitudinal modes reported by Mertens[1]. McDevitt and Baun[24] do not report any absorption bands of Cr_2O_3 in the 720-740 cm^{-1} region either. The very low intensity bands above the 850 cm^{-1} region could be attributed to chromium existing in a higher oxidation state than normally found in Cr_2O_3[1]. Scale adherence was poor and sample handling was minimized to prevent scale flaking.

The Raman spectra for chromium exposed in pure oxygen at elevated temperatures are shown in Figure 26. The spectral band of greatest intensity is at 563 cm^{-1}. Lower intensity bands are located at 610 cm^{-1}, 342 cm^{-1}, and 305 cm^{-1}. All of the above-mentioned bands were common to all spectra regardless of exposure temperature and differed only in their relative intensities. The sole surface oxidation product was determined to be Cr_2O_3. As previously mentioned, Cr_2O_3 has been reported to be the sole oxidation product on chromium after heating in oxygen at various temperatures below 1600° C[15]. Experimental evidence in this investigation confirmed this finding.

Stainless Steel Oxidation: Figures 27 and 28 show the infrared reflectance spectra for AISI Type 446 and AISI Type 502 stainless steel oxidized in pure oxygen at various temperatures for a 15 hour period. The most prominent bands in both cases are between 550 cm^{-1} and 750 cm^{-1}. Bands of lesser intensity were observed below the 550 cm^{-1} region.

At higher exposure temperatures, band multiplicity was greater and low intensity bands arose in the higher wavenumber regions of 1150 cm^{-1} to 1300 cm^{-1}. The dominant bands at higher exposure temperatures were between 600 cm^{-1} and 750 cm^{-1} and can be attributed to spinel formation. According to Mertens[1], a stoichiometric spinel ($FeO \cdot Cr_2O_3$) would produce a single, reasonably symmetric band in this wavenumber region. Due to compositional differences between the AISI Type 446 and AISI Type 502 stainless steels, identical oxidation conditions produced spinels of unequal stoichiometry. AISI Type 446 stainless steels, being richer in chromium, produced a surface spinel richer in chromia than in iron oxides and this caused slight band frequency shifts to higher wavenumbers relative to a stoichiometric spinel. AISI Type 502 stainless steel, containing about 21% of the amount of chromium in AISI Type 446 stainless steel, produced a surface spinel more rich in the iron oxides. This had the effect of producing band frequency shifts to lower wavenumber values relative to a stoichiometric spinel.

Multiple shoulders on the low frequency side of a dominant 713 cm^{-1} band on the 880° C exposure of AISI Type 502 stainless steel hints at the existence of a spinel and a possibility of an α - Fe_2O_3 constituent. Bands in the region of 710 cm^{-1} to 720 cm^{-1} are attributable to Cr_2O_3, but the bands at 530 cm^{-1} are direct evidence of a Cr_2O_3 component in the surface oxidation product.

The higher frequency bands, which occurred in both AISI Type 446 and AISI Type 502 stainless steel spectra at 1150 cm^{-1} to 1300 cm^{-1}, may be attributed to Si-O bands in a SiO_2 surface

oxidation product, metal silicate phases, or chromium of a higher oxidation state. Through the analytical techniques utilized in this investigation, the presence of metal silicate phases was not discovered.

Spectra at lower exposure temperatures exhibited bands in the 650 cm^{-1} to 660 cm^{-1} region. When compared to the reflectance spectra of pure iron where bands of similar frequency were assigned to α - Fe_2O_3, it is possible to make an analogous assignment due to this fact. Spectral bands arising at lower frequencies, 340 cm^{-1} to 550 cm^{-1} can be assigend to γ - Fe_2O_3 and Cr_2O_3 components of the surface oxidation product.

The Raman spectra for these alloys subjected to identical conditions are shown in Figure 29 and Figure 30. The lower exposure temperatures produced Raman bands of less intensity than the exposures of higher temperatures. Bands located at 225 cm^{-1}, 293 cm^{-1}, and 415 cm^{-1} can be attributed to an α - Fe_2O_3 component, at 663 cm^{-1} for the Fe_3O_4 component, and 563 cm^{-1} and 305 cm^{-1} for a Cr_2O_3 component in the surface oxidation product. Both AISI Type 446 and AISI Type 502 stainless steels exhibited similar low exposure temperature oxidation product compositions. The main difference in spectra was the relative intensities of the bands attributable to a specific compound. For example, the Cr_2O_3 bands in AISI Type 446 stainless steel spectra were initially of greater intensity than those same bands on the AISI Type 502 stainless steel spectra. This difference could be of either kinetic or compositional origin; perhaps AISI Type 446 stainless steel initially oxidizes at a more rapid rate producing "thicker", more spectrally detectable films, than AISI Type

502 stainless steel, or perhaps the AISI Type 446 stainless steel has more chromium at the metal-gas interface available for oxidation.

With increasing exposure temperatures the band frequency shifts and band intensity increases indicate changes in the surface oxidation products. The presence of $\alpha - Fe_2O_3$ is confirmable through the bands at 227 cm^{-1}, 293 cm^{-1}, and 414 cm^{-1}. Cr_2O_3 is present as evidenced by the bands positioned at 563 cm^{-1}, 342 cm^{-1}, and 305 cm^{-1}. An emerging FeO component, bands at 616 cm^{-1} and 663 cm^{-1}, was identifiable in the 670° C exposure. X-ray diffraction methods were utilized to confirm the FeO presence since the Raman bands of both FeO and Fe_3O_4 are identical. The X-ray methods were utilized before Raman analysis to insure that the FeO was truly an oxidation product due to the elevated temperature exposure and not due to laser decomposition of Fe_3O_4. At the maximum exposure temperature of 880° C bands attributable to the spinel phase, $FeO \cdot Cr_2O_3$, appeared. The spinel formation on AISI Type 502 stainless steel occurred to a smaller extent than on AISI Type 446 stainless steel. The bands attributable to Cr_2O_3 were of equal intensity so perhaps the surface oxidation product on AISI Type 502 stainless steel remains rich in Cr_2O_3 rather than contributing all Cr_2O_3 to form a dominant spinel phase.

The Raman bands attributable to SiO_2 (α-quartz) at 446 cm^{-1} were observed on both AISI Type 446 and AISI Type 502 stainless steel indicating the possiblity of a silica component in the surface oxidation product.

Exposure Period: The effect of exposure period in pure O_2 was investigated for the AISI Type 446 and AISI Type 502 stainless steels. In Figure 31 the infrared reflectance spectra for these alloys at 670° C for 10 and 24 hours is shown. The effect of increased exposure period was to increase band intensities, band multiplicity, and achieve a greater band resolution. An analogous interpretation can be obtained for the Raman spectra of those alloys under identical conditions which are shown in Figure 32.

Caution must be used during interpretation of the effect of exposure period on spectral characteristics. The optical constants (reflectivity, absorptivity, index of refraction) play an important part in the morphology and intensity of a spectrum. For example, the absorption constants (k_1) for iron oxides have such variety that the sensitivity to detect each oxide varies markedly. For this reason, relative band intensities do not necessarily suggest the composition of the thickness of a surface film. Francis and Ellison[25] as well as Greenler[26] discuss this problem in detail.

The exposure periods of 10 and 24 hours may not have been extensive enough to observe the nucleation of some possible surface oxidation products. Kinetic effects were not of direct importance in this investigation, and the possibility of the formation of compounds which may form under different exposure lengths is realized.

"In-Situ" Spectra: In-situ Raman spectra for AISI Type 446 and AISI Type 502 stainless steels are presented in Figure 33. Both

the AISI Type 446 and AISI Type 502 stainless steel samples were run under identical conditions -- 880° C in pure oxygen for 3 and 8 hour exposure periods.

The 3 hour exposure of AISI Type 446 stainless steel exhibited bands attributable to α - Fe_2O_3 at 227 cm^{-1}, 293 cm^{-1}, and 416 cm^{-1}. Also, Cr_2O_3 bands were observed, though faint, at 305 cm^{-1}, 342 cm^{-1}, and 563 cm^{-1}. A spinel phase, $FeO \cdot Cr_2O_3$, was nucleated at 625 cm^{-1} with a small shoulder at 630-635 cm^{-1}. The upward shift in wavenumbers relative to a stoichiometric spinel indicated a spinel phase rich in chromia. A band at 463 cm^{-1} indicated the possible presence of a SiO_2 component in both the 3 and 8 hour exposure periods. The 8 hour exposure of AISI Type 446 stainless steel resulted in greater band intensities than the 3 hour exposure under identical conditions. The 8 hour exposure resulted in a decreasing band intensity of the Cr_2O_3 surface oxidation product component and a resulting increase in the spinel band at 625 cm^{-1}.

The 3 hour exposure of AISI Type 502 stainless steel produced bands also attributable to α - Fe_2O_3 at 229 cm^{-1}, 295 cm^{-1}, and 415 cm^{-1}. Bands assignable to Cr_2O_3 were exhibited, faintly again, at 305 cm^{-1}, 342 cm^{-1}, and 563 cm^{-1}. Both the 3 and 8 hour exposures exhibited a 466 cm^{-1} band suggesting the possibility of a silica component in the surface oxidation product. Again, an increased exposure period resulted in an increase in band intensity under identical oxidizing conditions. The spinel phase of the surface oxidation product arose in both the 3 and 8 hour exposures at 592 cm^{-1}. The band frequency shift to lower wavenumber values relative to a stoichiometric spinel composi-

tion suggest a spinel phase rich in iron oxides. There was not a corresponding Cr_2O_3 band intensity decrease with an increase in the spinel band intensity when comparing the 3 and 8 hour exposures. There were, however, small changes in the band attributable to α - Fe_2O_3.

With little or no alteration of bands attributable to Cr_2O_3 when comparing 3 and 8 hour in-situ spectra and some changes in Fe_2O_3 band morphologies it is possible to see a spinel phase with a dominant iron oxide component in the AISI Type 502 stainless steel exposures. This is not the case for AISI Type 446 stainless steel and Cr_2O_3 band alterations did occur. These band alterations along with band frequency shifts to higher wavenumber values relative to a stoichiometric spinel composition suggest a spinel phase rich in a chromia component.

SUMMARY AND CONCLUSIONS

The use of Raman and infrared reflectance spectroscopy simplifies existing analytical techniques for oxide film analysis. Film alteration is virtually eliminated during analysis with in-situ methods and they can easily be adapted to suit experimental conditions. These spectroscopic disciplines were complementary in the sense that where one technique was not sensitive, the other could be relied upon for the required structural information.

It was demonstrated that Raman spectroscopy is an effective analytical method for oxide film investigation. In-situ techniques are simple and provide easily interpretable results. Synthesized spinel compounds compared well with the surface

species formed at elevated exposure temperatures on the stainless steel alloys. X-ray confirmation of the infrared and Raman analyses satisfied the confirmability stipulation placed on the ideal surface analysis techniques. Although sample decomposition due to radiation absorption could be a problem with the darker colored surface compounds, decomposition due to the excitation beam was a less serious problem with the brown, red, and orange colored surface compounds.

Infrared reflectance spectroscopy was also demonstrated to be a sensitive oxide film analysis technique. The use of high surface area powders, necessary for transmission spectra of solids, is eliminated by using reflectance spectroscopy. This minimizes thermal decomposition problems. Also, in an attempt to thermally stabilize these powders, an inert binding matrix such as KBr or Nujol, is used which may limit the spectral regions that can be scanned unobstructively. For these reasons reflectance spectroscopy is easily utilized for oxide film analysis with minor optical considerations.

Oxide film analysis on AISI Type 446 stainless steel indicated the prevalent oxide phases to be Fe_2O_3 and Cr_2O_3 at lower exposure temperatures. The AISI Type 502 stainless steels analyses were similar to the AISI Type 446 analyses with the exception of lower intensity Cr_2O_3 bands. Higher exposure temperatures produced spinels, $FeO \cdot Cr_2O_3$, and Cr_2O_3 as oxidation products. The presence of Fe_3O_4 is noted, but bands attributable to this phase were of low intensity.

AISI Type 502 stainless steel displayed spinel spectral characteristics similar to those synthesized spinels which were

iron oxide rich. There was a band frequency shift to higher frequencies for chromium oxide rich spinel phases.

Scanning electron microscopy showed scale flaking and cracking. Morphological surface features, such as nodules, suggested localization of scale breakthrough sites. The stratified nature of the scale is evident. Air cooling produced noticible surface morphology differences from water quenching as shown by scanning electron microscopy in Figure 22.

In-situ Raman analysis exhibited increasing spectral enhancement and resolution with increasing exposure period. Unfortunately, the noise level also increased, but with the use of computer of average transient (CAT) devices spectral averaging techniques can reduce this interference[27]. Band intensities increased due to thickening films. Initial Fe_2O_3 and Cr_2O_3 formation was noticible on AISI Type 446 stainless steel with faint traces of FeO and Fe_3O_4. As the exposure period increased, the spinel phase $FeO \cdot Cr_2O_3$, emerged at the expense of FeO which vanished. AISI Type 502 stainless steel followed a similar reaction, but due to a lower chromium content than AISI Type 446 stainless steel, the bands attributable to Cr_2O_3 were of lower intensity.

The effects of the two exposure media, air and pure oxygen, were very similar. Microstructural surface morphologies were not distinguishable between the samples exposed to air and those exposed to oxygen. As previously mentioned, the major differences result from quantitative variations between the stable oxides under the given exposure conditions.

Since Raman analyses required no mechanical polishing, surface preparation time was minimal. Infrared analysis, due to the reflection process involved, required a mechanical surface preparation. The more superior the surface quality obtained, the more efficient the substrate reflection and the less of an intensity loss will be experienced.

REFERENCES

1. F.P. Mertens, Corrosion, Vol. 34, No. 10, p. 359, 1978.

2. A.D. Cross and R.A. Jones, An Introduction to Practical Infrared Spectroscopy, Plenum Press, p. 22, 1969.

3. R.H. Heidersbach, C.W. Brown, R.J. Thibeau, A.Z. Goldfarb, "Raman and Infrared Spectroscopy of Aqueous Corrosion Films on Lead",Technical Report No. 2, University of Rhode Island, Department of Ocean Engineering, p. 135, 1978.

4. F.P. Mertens, Surface Science, Vol. 70, p. 161, 1978.

5. A.Z. Goldfarb, "Characterization of Corrosion Films on Lead by Infrared Reflectance Spectroscopy", M.S. Thesis, University of Rhode Island, p. 135, 1978.

6. R.L. Greenler and T.C. Slager, Spectrochemica Acta, 29A, 193, 1973.

7. R.J. Thibeau, "Characterization of Oxidation Product Films on Lead in Aqueous Media by In-Situ Raman Spectroscopy". Ph.D. Dissertation, University of Rhode Island, 1978.

8. O.A. Skoog and D.M. West, Principles of Instrumental Analysis, Holt, Rinehart and Winston, Inc., pp. 248-252, 1971.

9. S. Tolansky, Multiple-Beam Interference Microscopy of Metals, Academic Press, New York, p. 96, 1970.

10. G.W. Poling, J. Electrochem. Soc., Vol. 116, p. 958, 1969.

11. E.A. Gulbransen and R. Ruka, J. Metals, N.Y., Vol. 188, p. 1500, 1948.

12. O. Kubachewski and B.E. Hopkins, Oxidation of Metals and Alloys, Butterworths, p. 222, 1962.

13. Per Kofstad, High Temperature Oxidation of Metals, John Wiley and Sons, Inc., p. 132, 1966.

14. C.A. Phalinker, E.B. Evans, and W.M. Baldwin, J. Electrochem. Soc., Vol. 103, p. 429, 1956.

15. A. Muan and E.F. Osborn, Phase Equilibria Among Oxides in Steelmaking, Addision Wesley Publishing Co., p. 33, 1965.

16. H.M. McCullogh, M.G. Fontana and F.H. Beck, Trans. Amer. Metals, Vol. 43, p. 404, 1951.

17. B.O. Saksena, Proc. Indian Acad. Sci., A12, p. 93, 1940.

18. J.B. Reitzel, Jour. Chem. Phys., Vol. 23, No. 12, p. 2407, 1955.

19. J.E. Croll and G.R. Wallwork, Oxid. Metals, Vol. 1, p. 55, 1969.

20. A. DesBrasunas, J.T. Sow and O.E. Harder, Symposium on Materials for Gas Turbines, Am. Soc. Test. Matr. Proc., Vol. 46, p. 870, 1946.

21. M. Vykucky and M. Mericka, Br. Corros. J., Vol. 5, p. 162, 1970.

22. H.J. Yearion, H.E. Boun, Jr. and R.E. Warr, Corrosion, Vol. 12, p. 561t, 1956.

23. M.G. Hobby and G.C. Wood, Oxid. Metals, Vol. 1, p. 23, 1969.

24. N.T. McDevitt and W.C. Baun, Spectrochemica Acta, Vol. 20, p. 801, 1964.

25. S.A. Francis, A.H. Ellison, J. Opt. Soc. Amer., Vol. 49, p. 131, 1959.

26. R.G. Greenler, J. Appl. Phys., Supp. 2, Pt. 2, P. 265, 1974.

27. O. Howarth, Theory of Spectroscopy and Elementary Introduction, Halsted Press, p. 95, 1973.

TABLE 1

CHEMICAL COMPOSITIONS OF METALS USED IN OXIDATION INVESTIGATIONS

	Iron	Chromium	Nickel	Molybdenum	Manganese	Carbon	Silicon
Armco Iron[1]	99.991	.006	.005	.005	.045	.00135	.002
Chromium[2]	--	99.995+	--	--	--	--	--
Electrolytic Grade[3] Chromium	.15	99.9	--	.001	.005	.01	.005
AISI Type 446	≈74.9 (Bal.)	24.6	.50	.10	.71	.10	.37
AISI Type 502	≈92.2 (Bal.)	5.14	.17	.49	.39	.05	1.52

[1]Armco Ingot Iron High Purity

[2]Alpha-Ventron Chromium Foil (m4N+)

[3]Union Carbide Elchrome

TABLE 2

EXPOSURE CONDITIONS AND FILM THICKNESS MEASUREMENTS

Material	Exposure Temperature (^{o} C)	Exposure Medium	Exposure Period	Film Thickness (A^{o})
Armco Fe	880	Air	15	6065
	880	O_2	15	5713
	670	Air	15	1810
	670	O_2	15	1777
	460	Air	15	1416
	460	O_2	15	1462
	250	Air	15	305
	250	O_2	15	329
Chromium	880	Air	15	1820
	880	O_2	15	2030
	670	Air	15	1320
	670	O_2	15	1190
	460	Air	15	560
	460	O_2	15	400
	250	Air	15	(Undetectable)
	250	O_2	15	(Undetectable)
AISI Type 446	880	Air	3*	--
	880	Air	8*	--
	880	Air	15	2405
	670	Air	10	--
	670	Air	15	1730
	670	Air	24	--
	460	Air	15	515
	250	Air	15	370
AISI Type 446	880	O_2	3*	--
	880	O_2	3*	--
	880	O_2	15	2510
	670	O_2	10	--
	670	O_2	15	1400
	670	O_2	24	--
	460	O_2	15	725
	250	O_2	15	415

*Indicates In-Situ Analysis was Performed.

TABLE 2 (CONT.)

Material	Exposure Temperature (^{o}C)	Exposure Medium	Exposure Period	Film Thickness (A^{o})
AISI Type 502	880	Air	3*	--
	880	Air	8*	--
	880	Air	15	3110
	670	Air	10	--
	670	Air	15	1880
	670	Air	24	--
	460	Air	15	900
	250	Air	15	400
AISI Type 502	880	O_2	3*	--
	880	O_2	8*	--
	880	O_2	15	2850
	670	O_2	10	--
	670	O_2	15	2170
	670	O_2	24	--
	460	O_2	15	735
	250	O_2	15	420

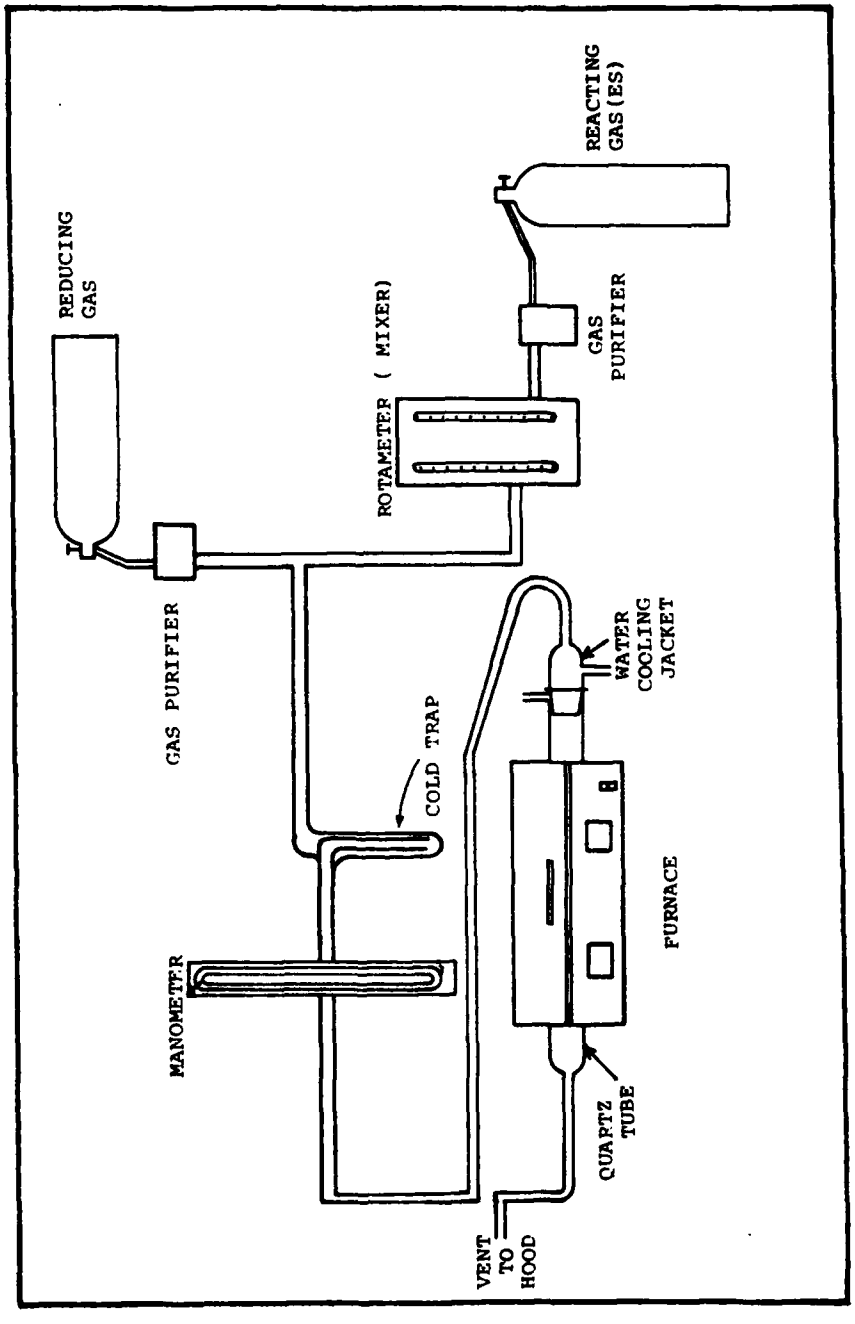

Figure 1. Schematic of the elevated temperature-vacuum-multiple gas purging system.

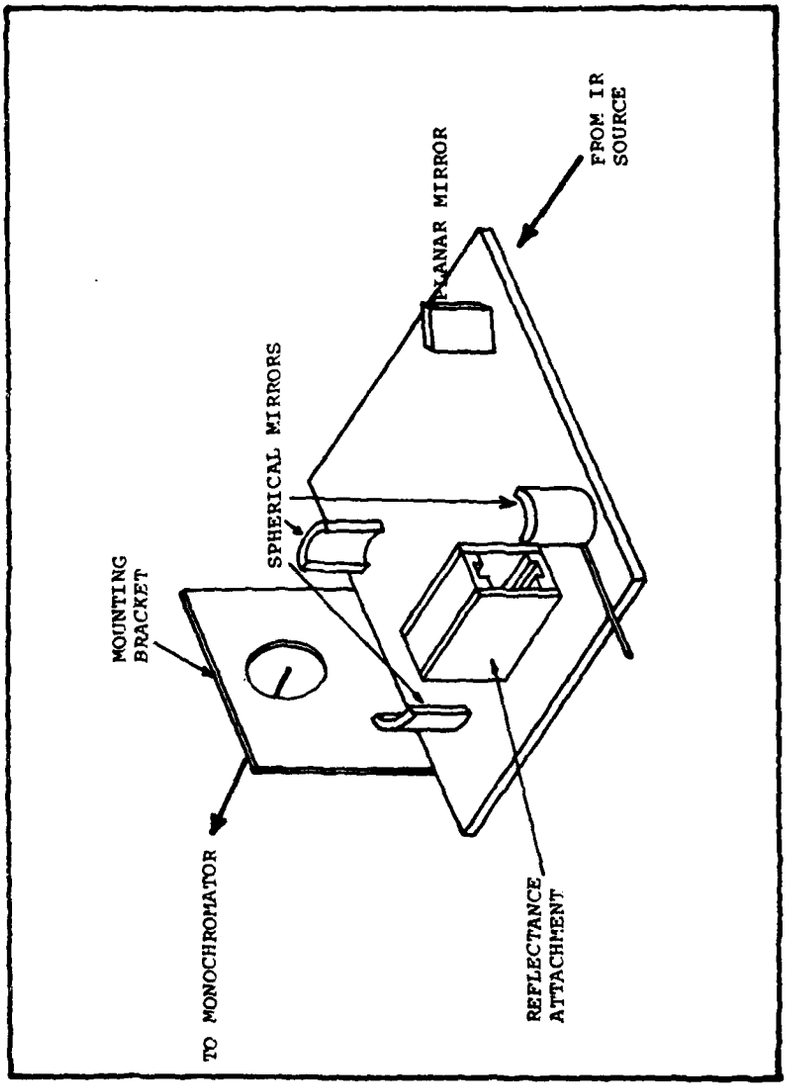

Figure 2. Schematic of the specular reflectance apparatus.

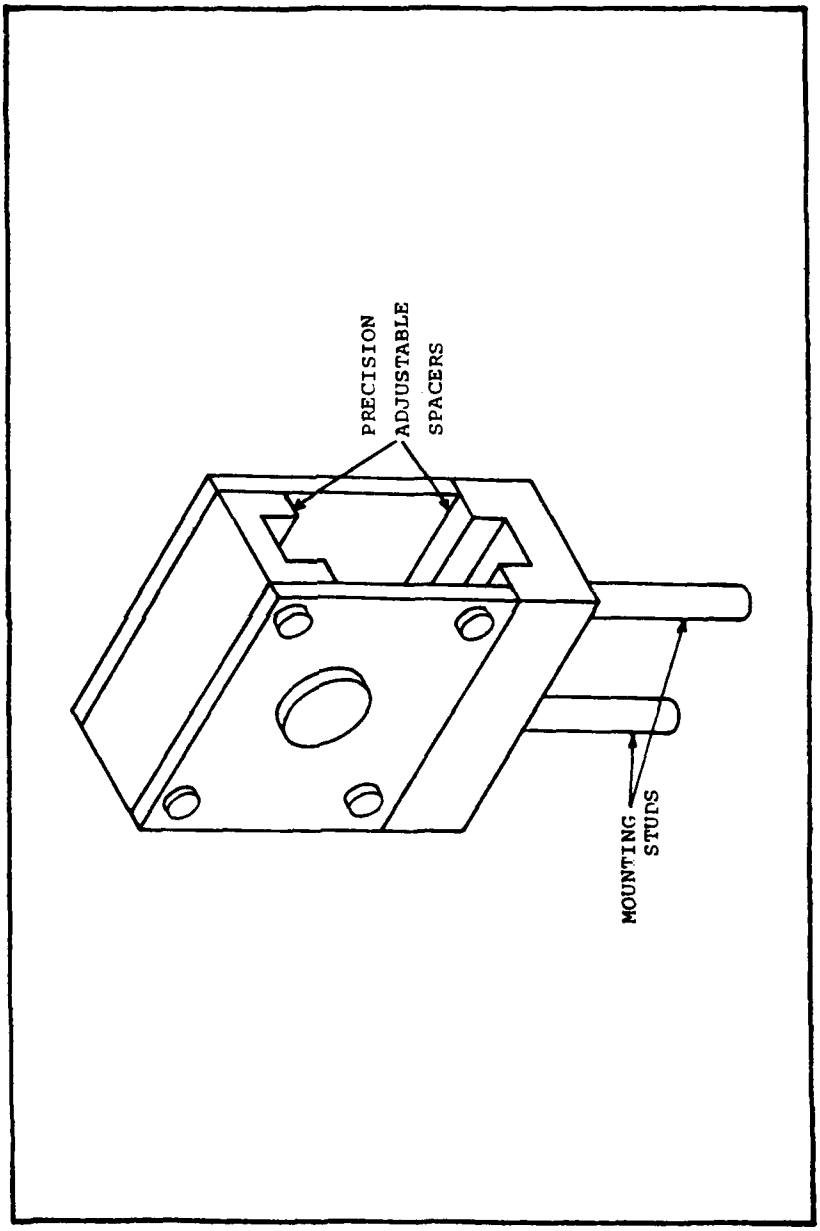

Figure 3. Schematic of the infrared reflectance attachments.

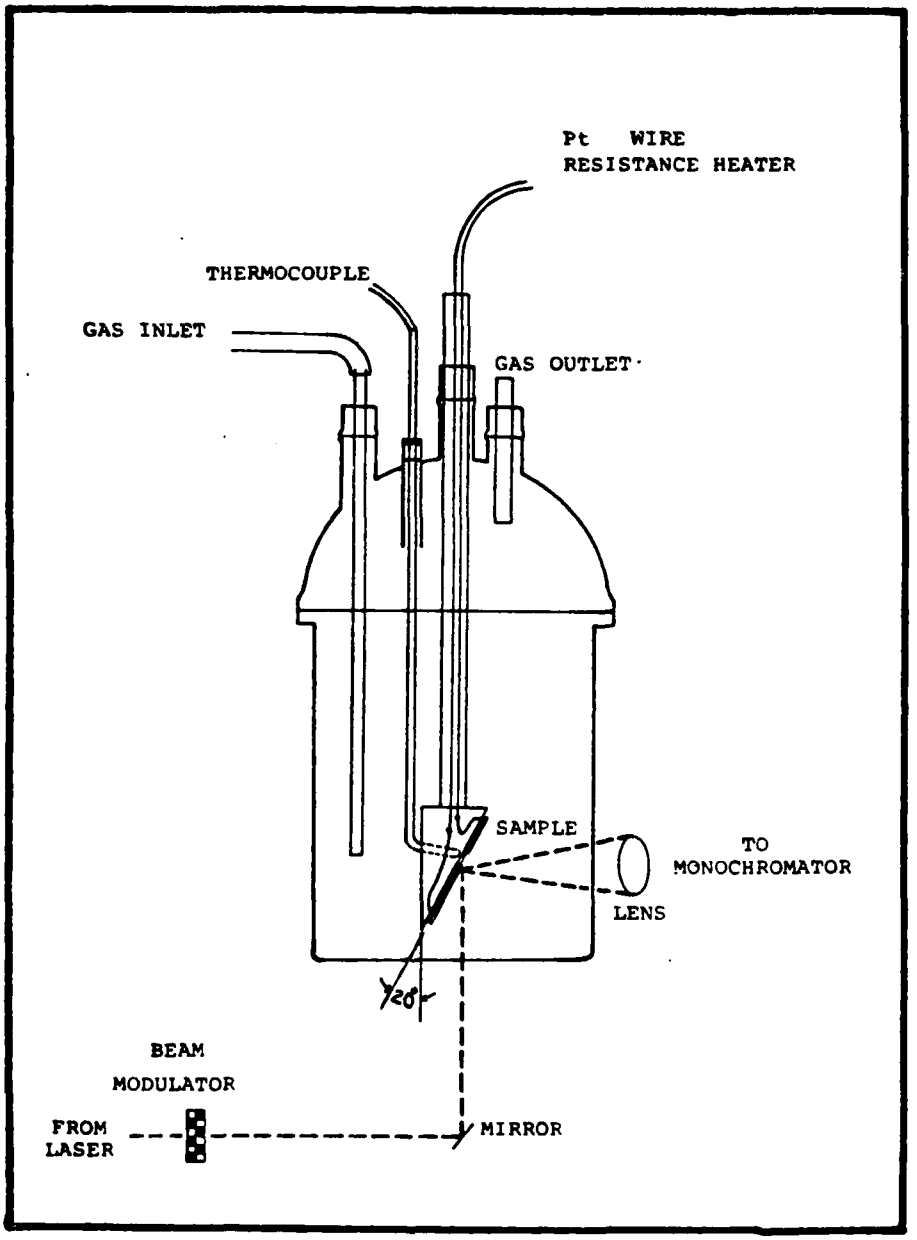

Figure 4. Schematic of the in-situ Raman exposure chamber.

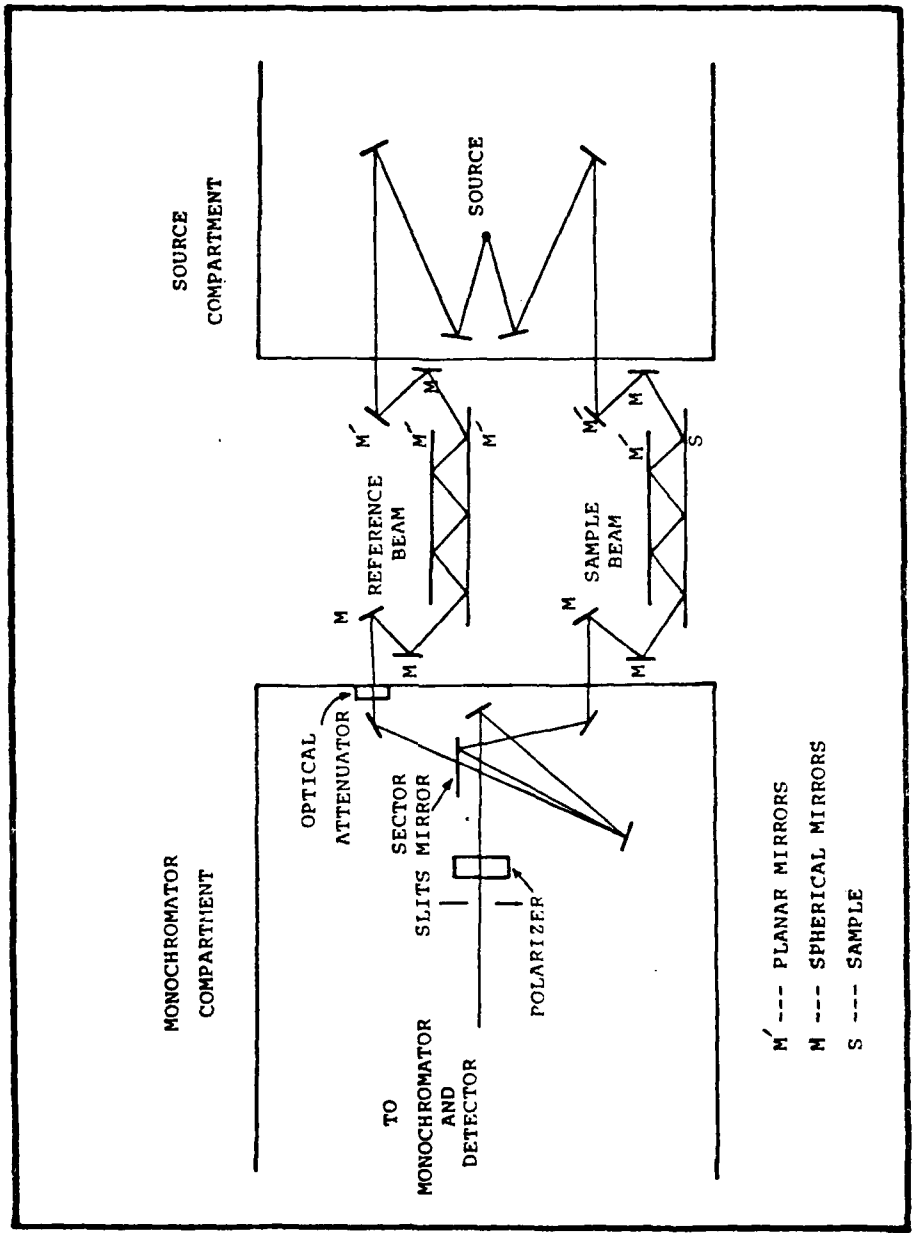

Figure 5. Schematic of the reflectance system.

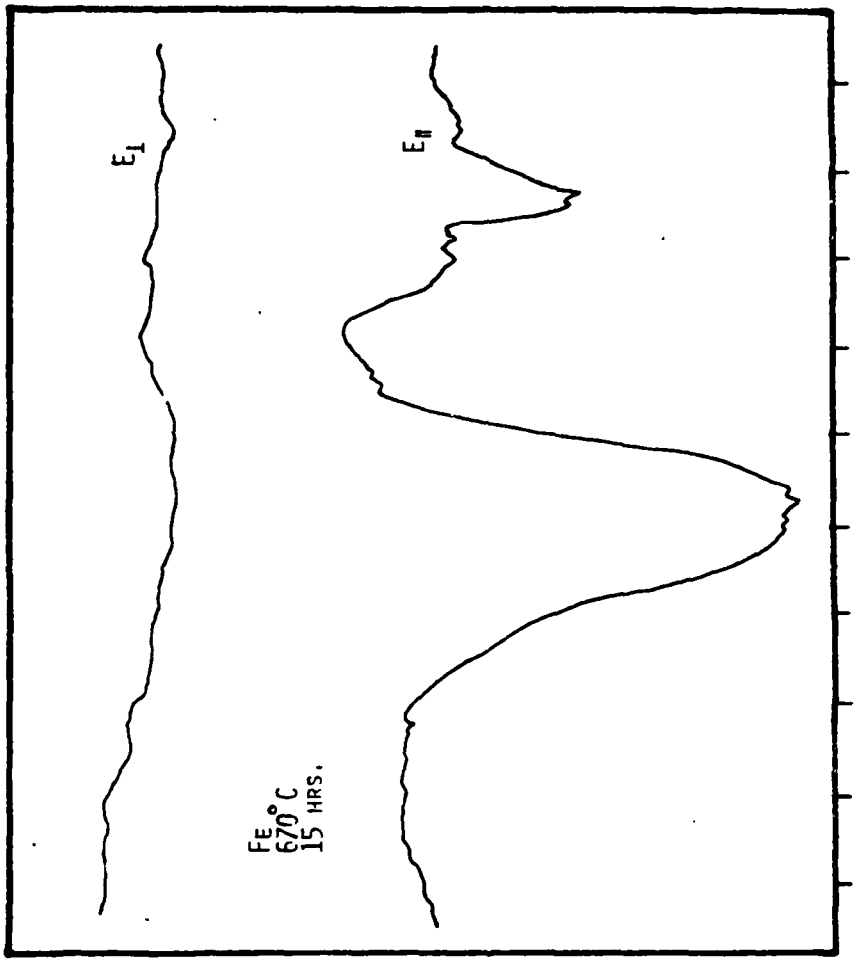

Figure 6. Infrared reflectance spectra demonstrating the necessity of spectral polarization.

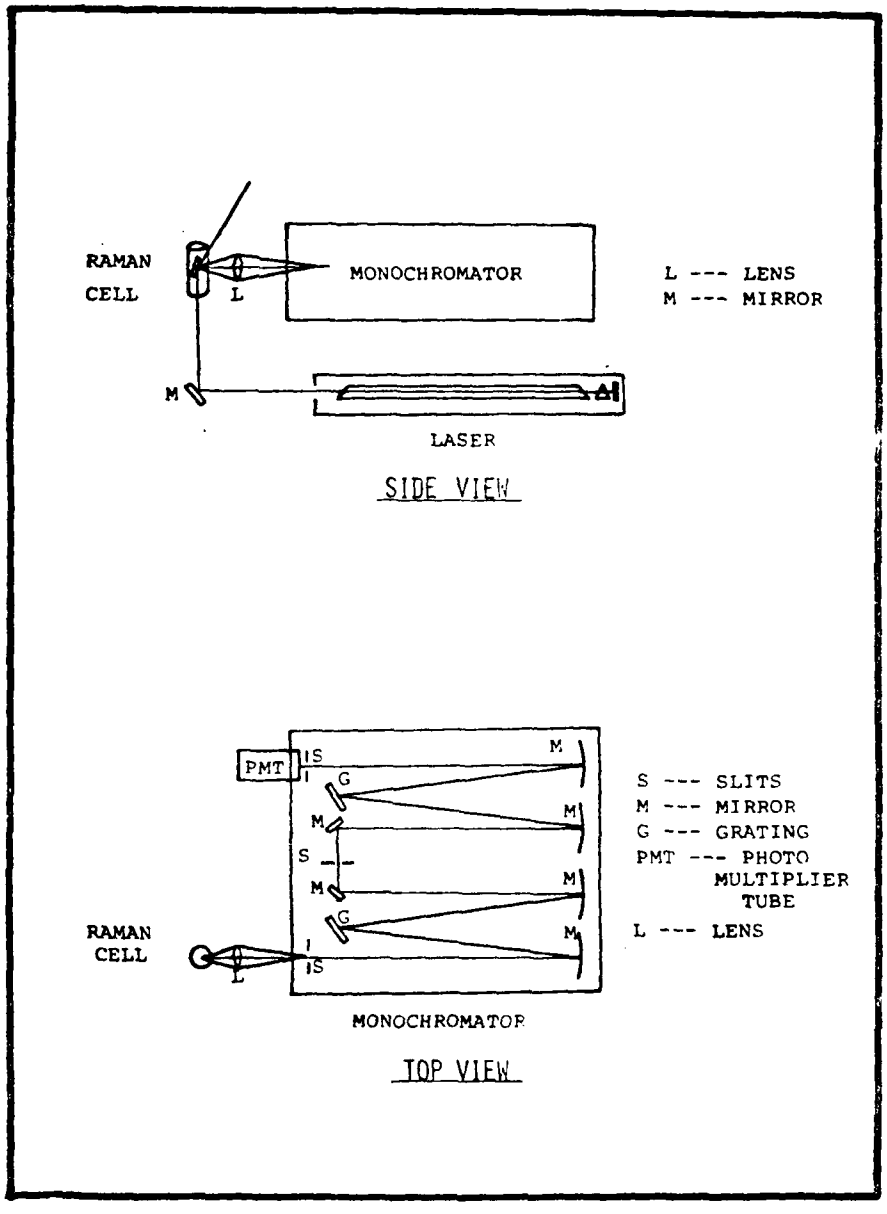

Figure 7. Schematic of a typical Raman spectrometer.

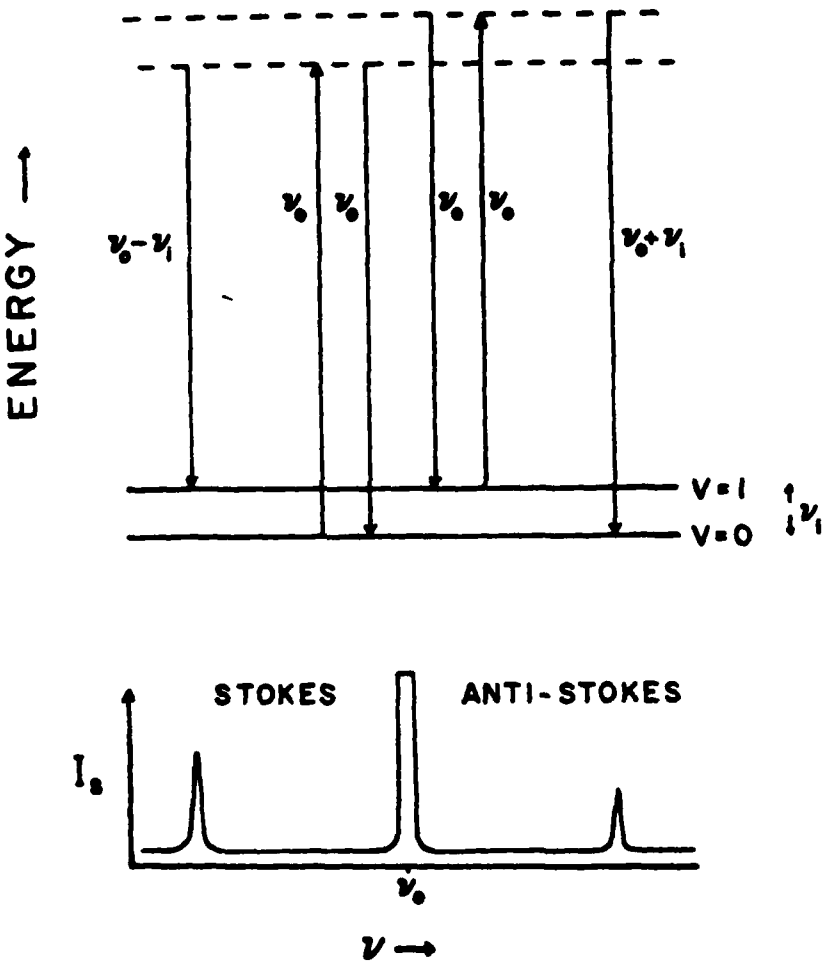

Figure 8. Schematic of a model Raman spectrum.

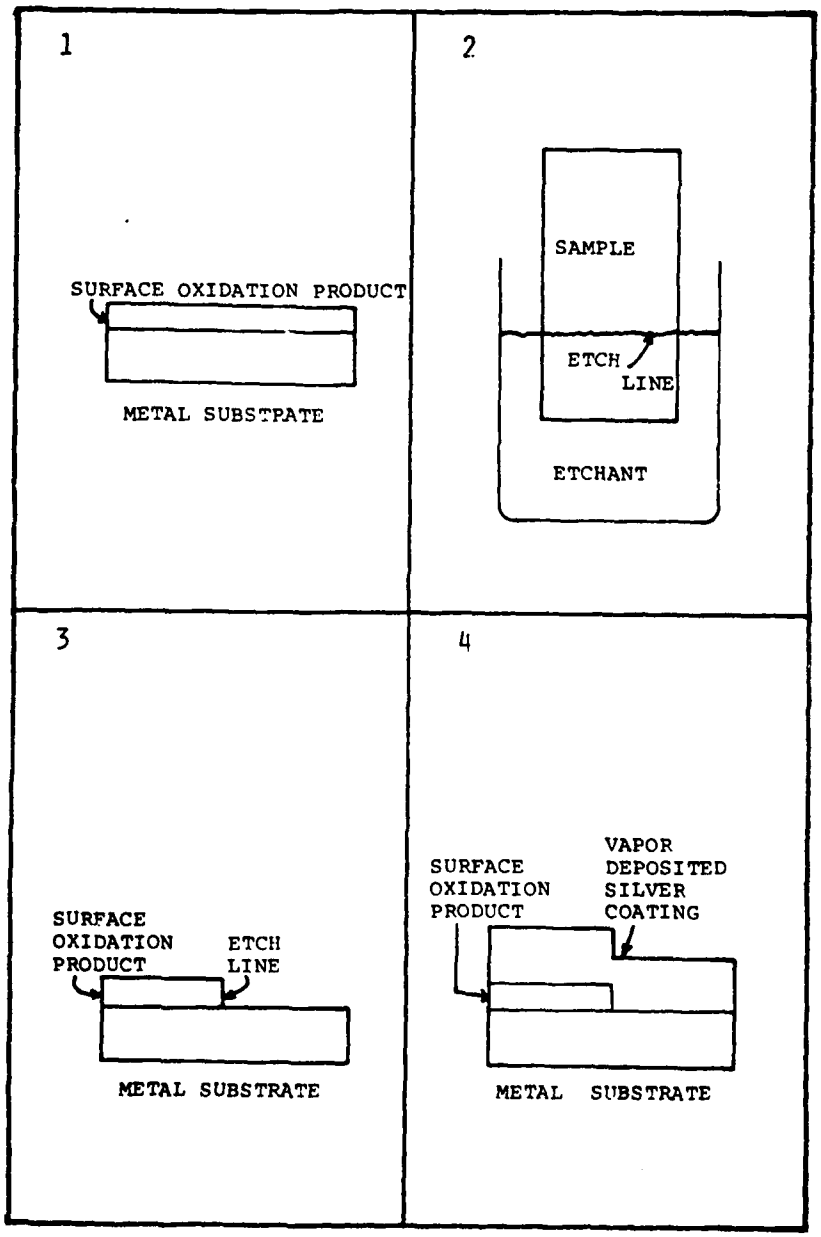

Figure 9. Schematic of the etching procedure utilized in sample preparation for interference microscopy.

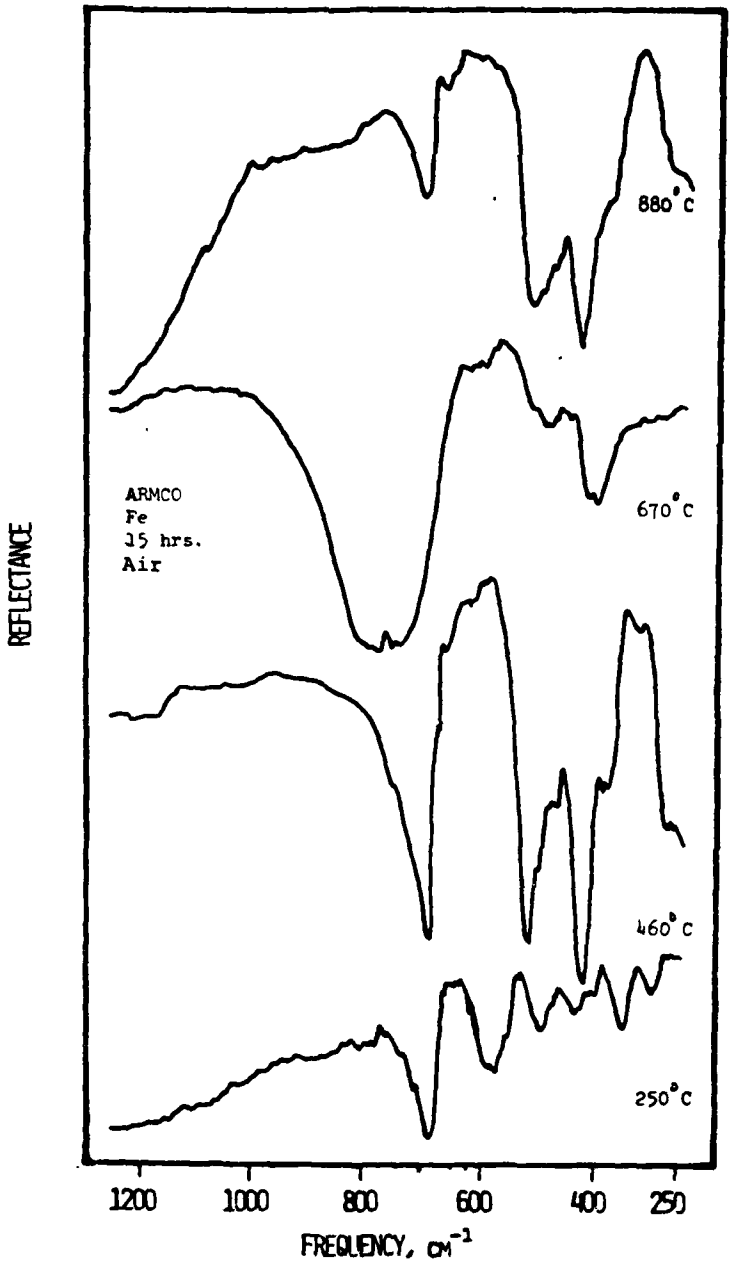

Figure 10. Infrared reflectance spectra of Armco iron exposed at various temperatures in air for 15 hours.

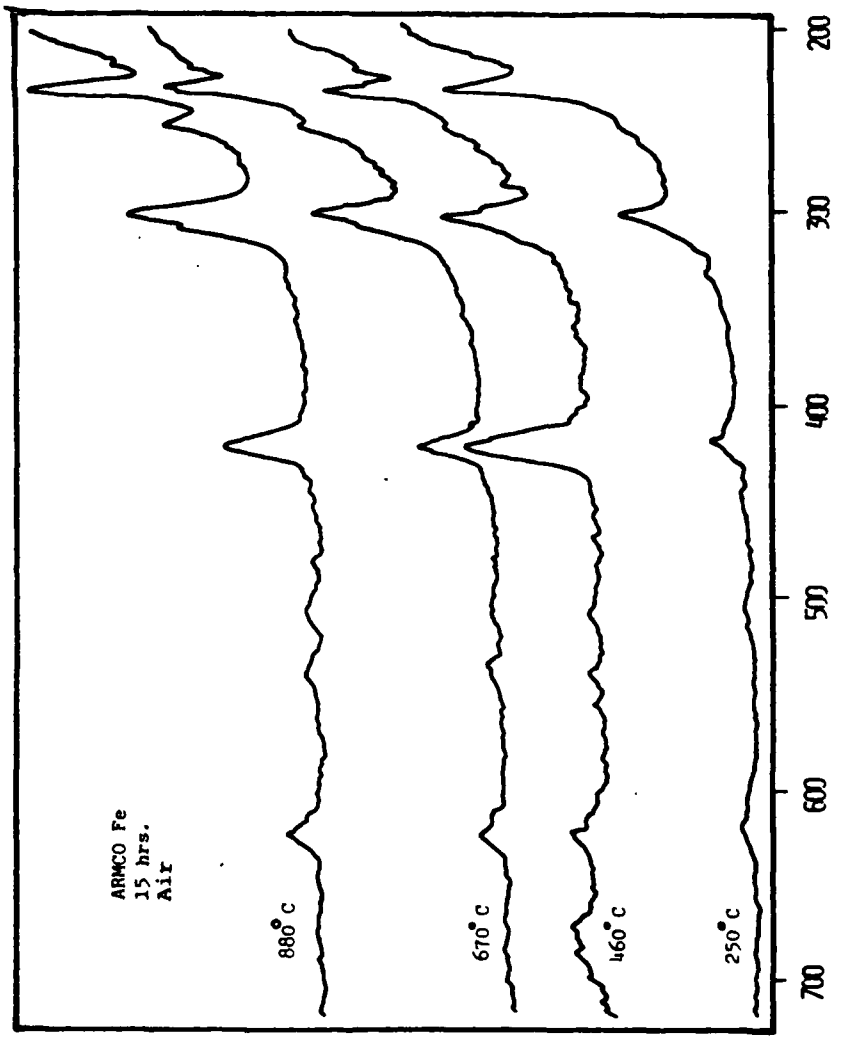

Figure 11. Raman spectra of Armco iron exposed at various temperatures in air for 15 hours.

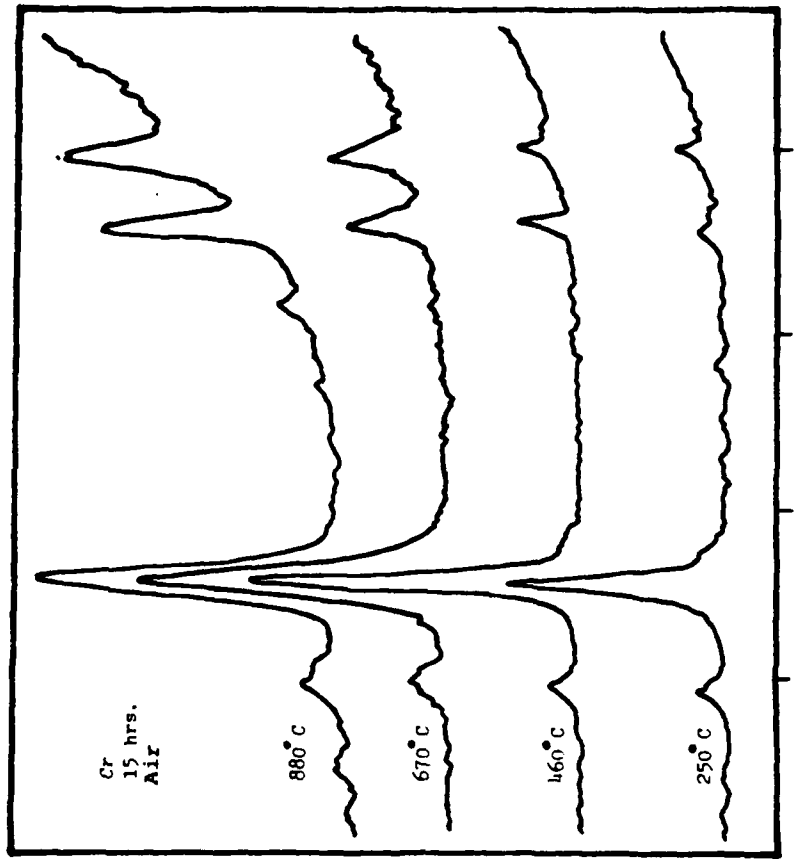

Figure 12. Raman spectra for pure chromium exposed in air for 15 hours at elevated temperatures.

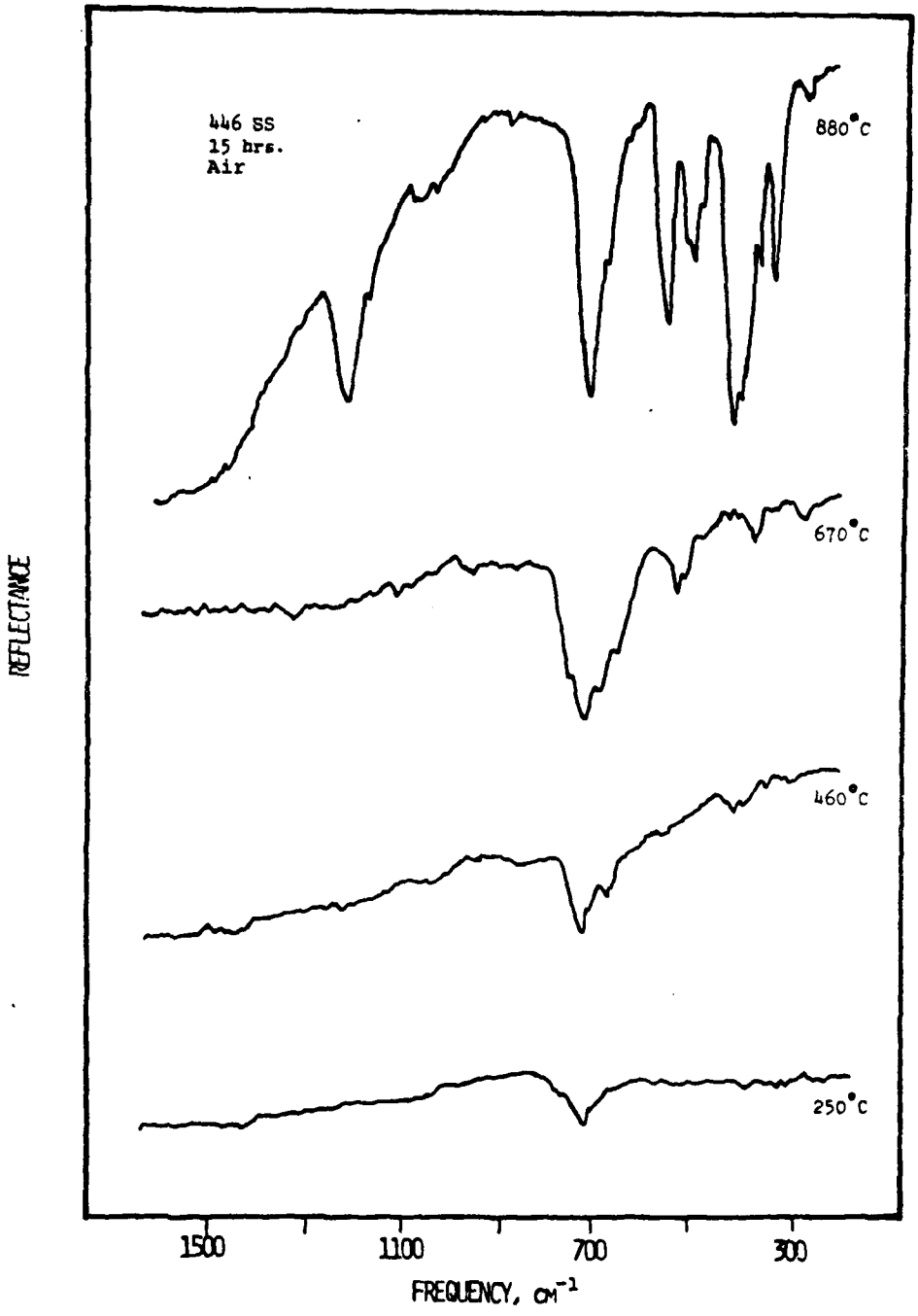

Figure 13. Infrared reflectance spectra for AISI Type 446 stainless steel oxidized in air for 15 hours at elevated temperatures.

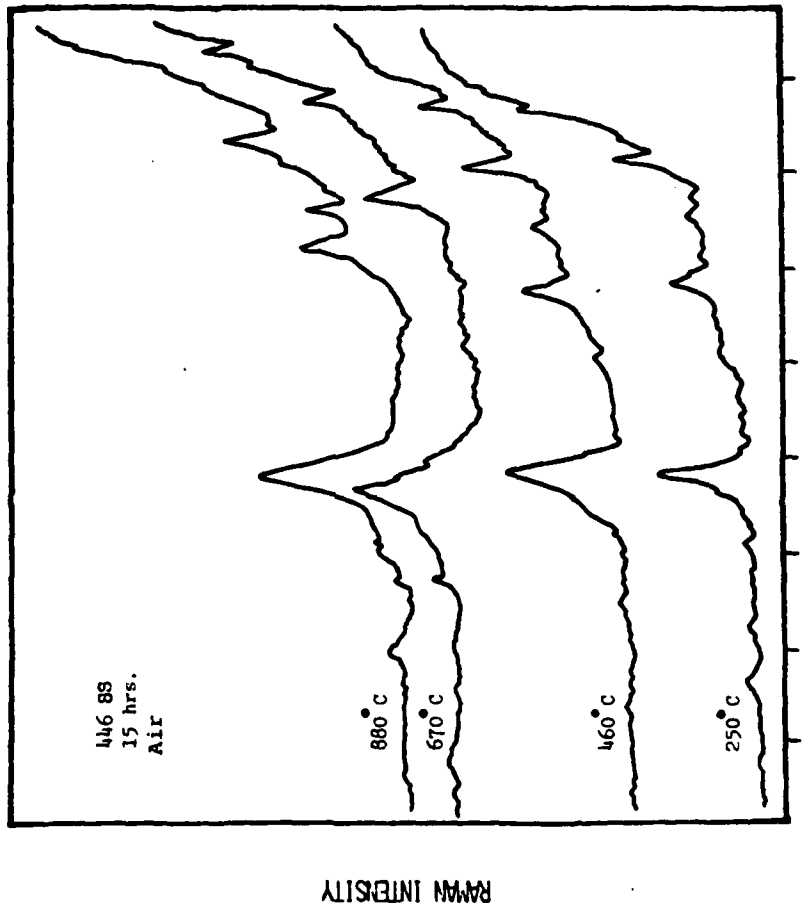

Figure 14. Raman spectra for AISI Type 446 stainless steel oxidized in air for 15 hours at elevated temperatures.

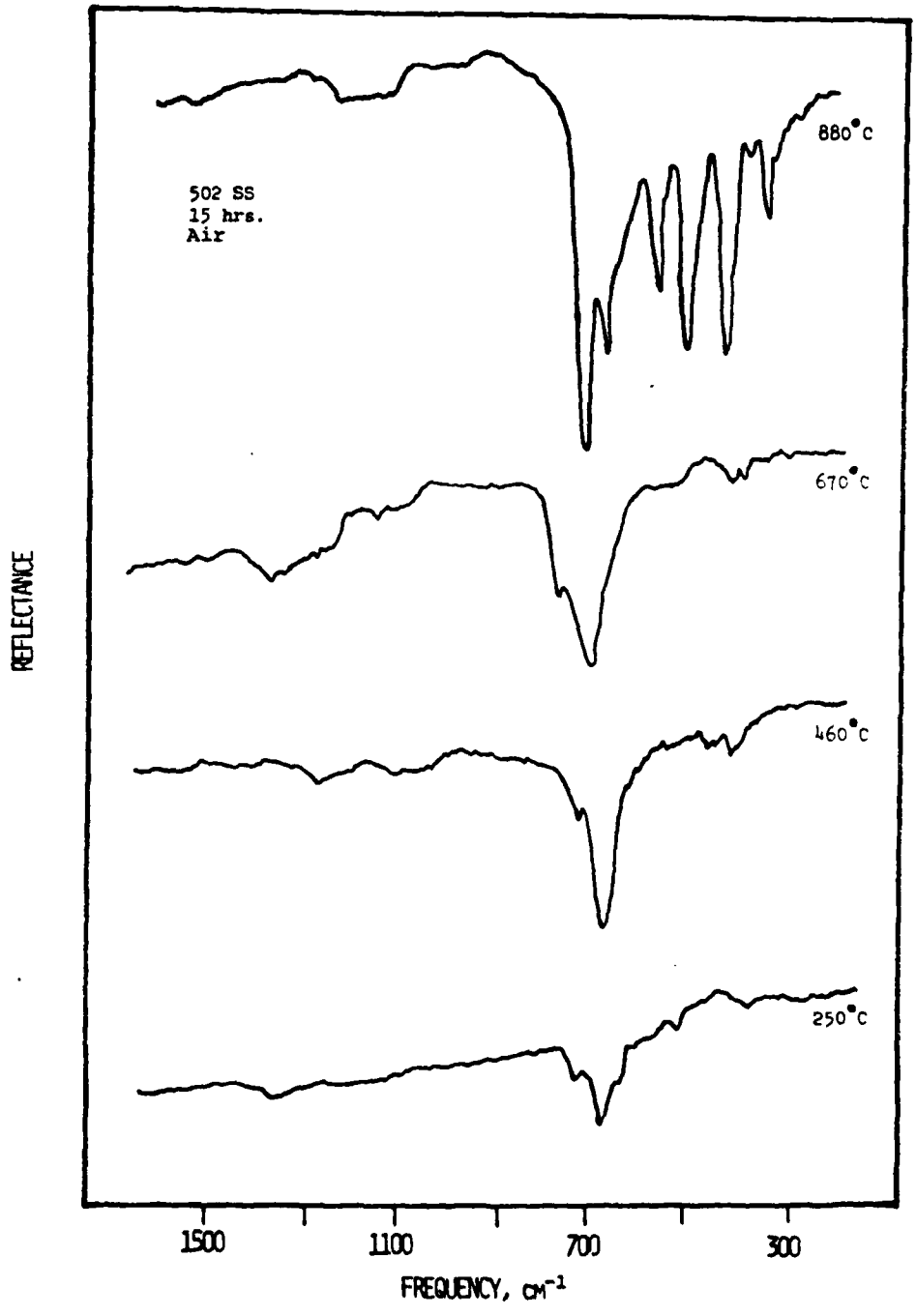

Figure 15. Infrared reflectance spectra for AISI Type 502 stainless steel oxidized in air for 15 hours at elevated temperatures.

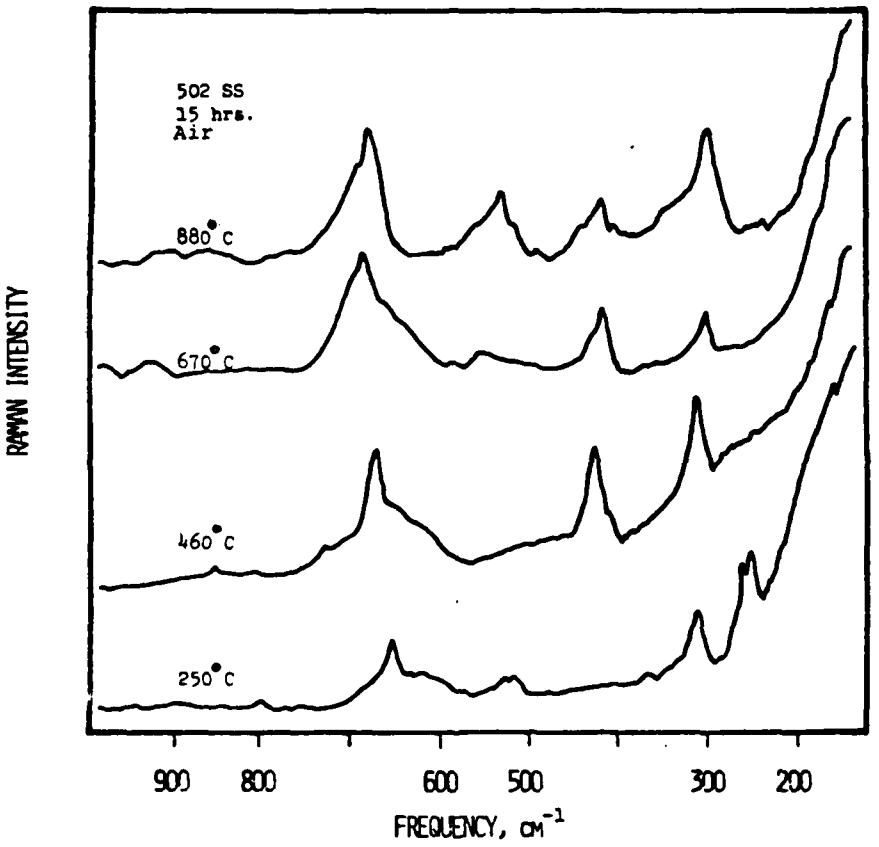

Figure 16. Raman spectra for AISI Type 502 stainless steel oxidized in air for 15 hours at elevated temperatures.

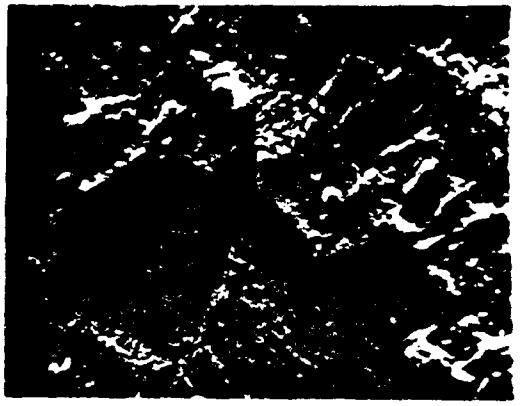

Figure 17. Scanning electron micrograph of AISI Type 502 stainless steel after 15 hours exposure in air at 670°C.

Figure 18. Scanning electron micrograph of AISI Type 446 stainless steel after 15 hours exposure in air at 670°C.

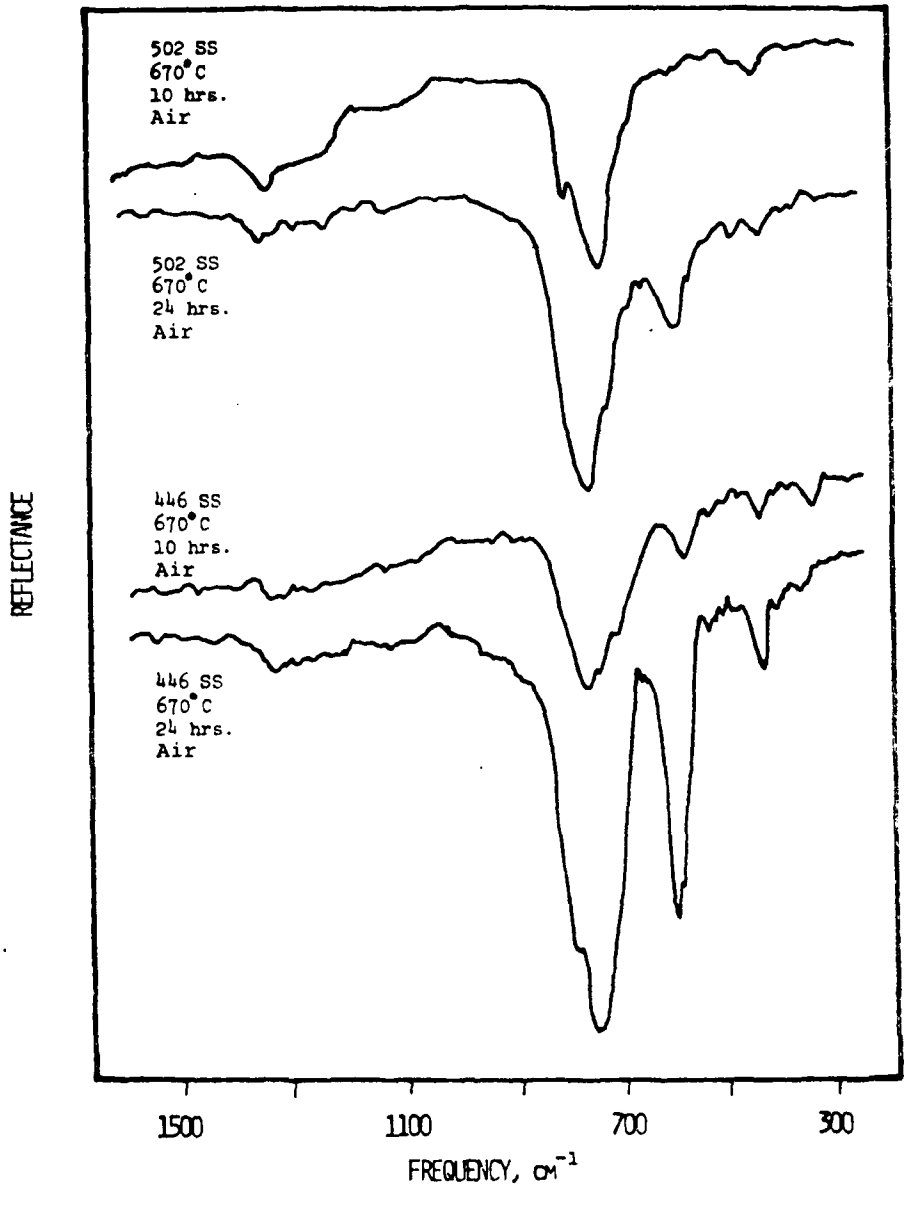

Figure 19. Infrared reflectance spectra for AISI Type 446 and AISI Type 502 stainless steels oxidized in air at 670°C for 10 and 24 hours.

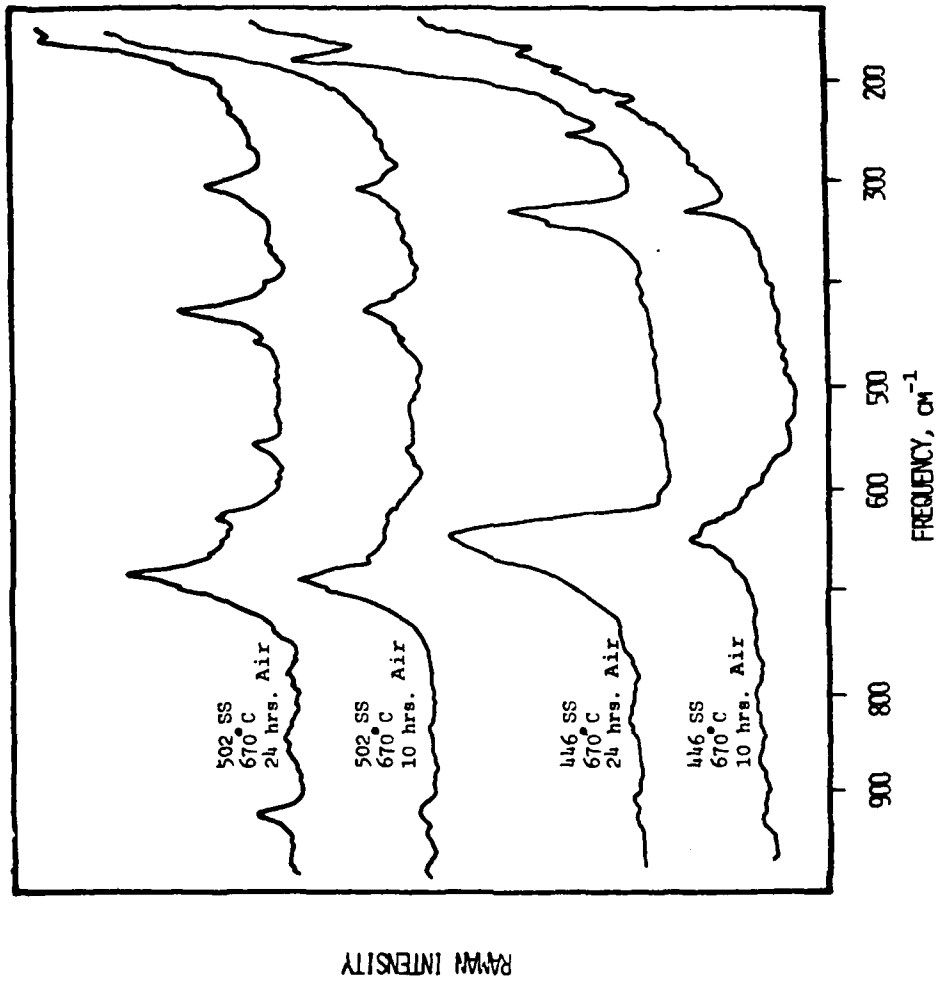

Figure 20. Raman spectra for AISI Type 446 and AISI Type 502 stainless steels oxidized in air at 670°C for 10 and 24 hours.

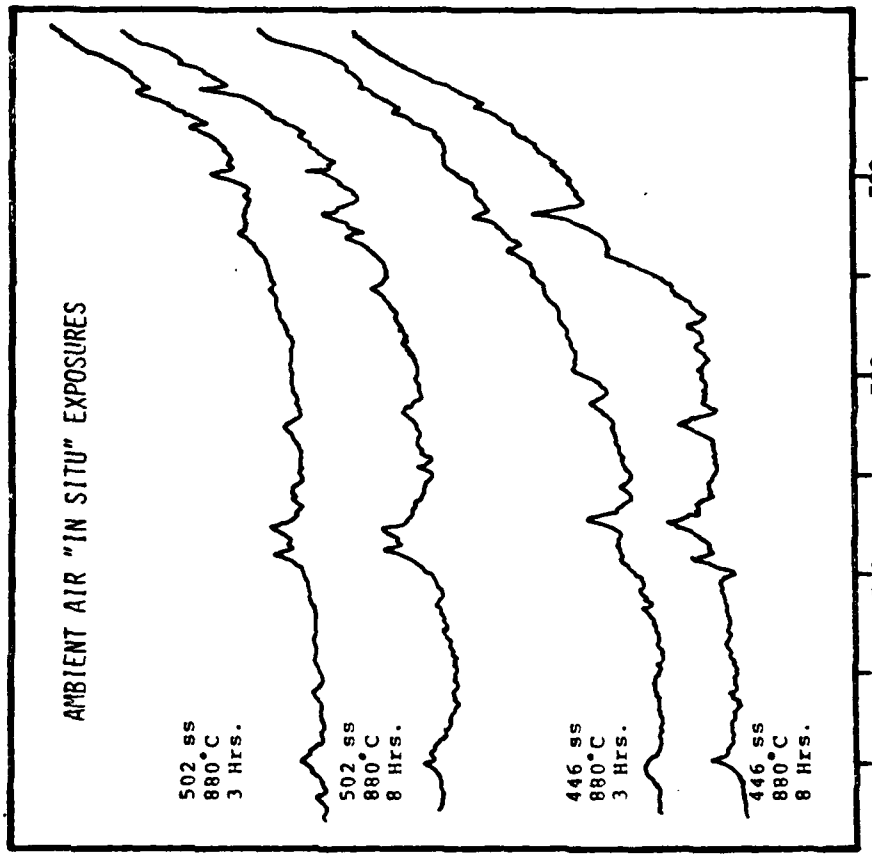

Figure 21. In-situ Raman spectra for AISI Type 446 and AISI Type 502 stainless steels during exposure in air at 880°C for 3 and 8 hours.

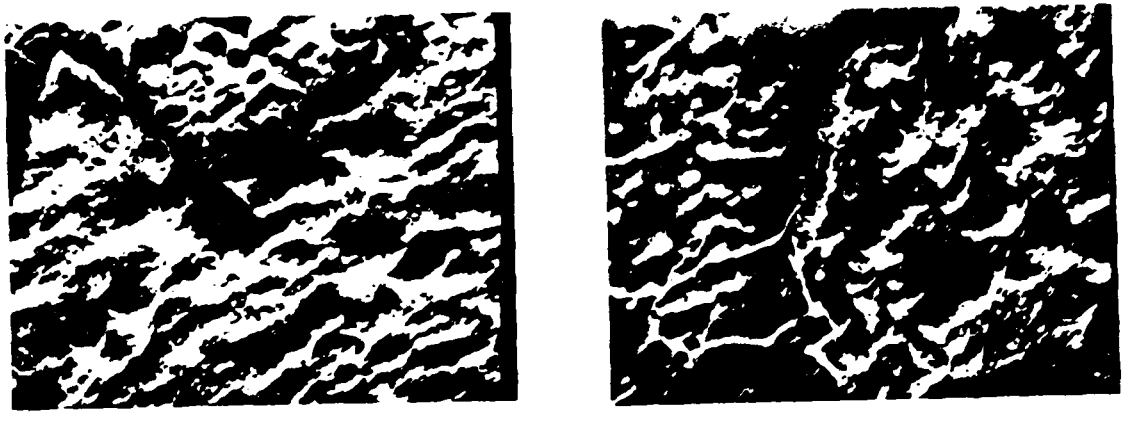

Figure 22. Scanning electron micrographs of surface morphologies on water quenched versus air cooled samples of stainless steel.

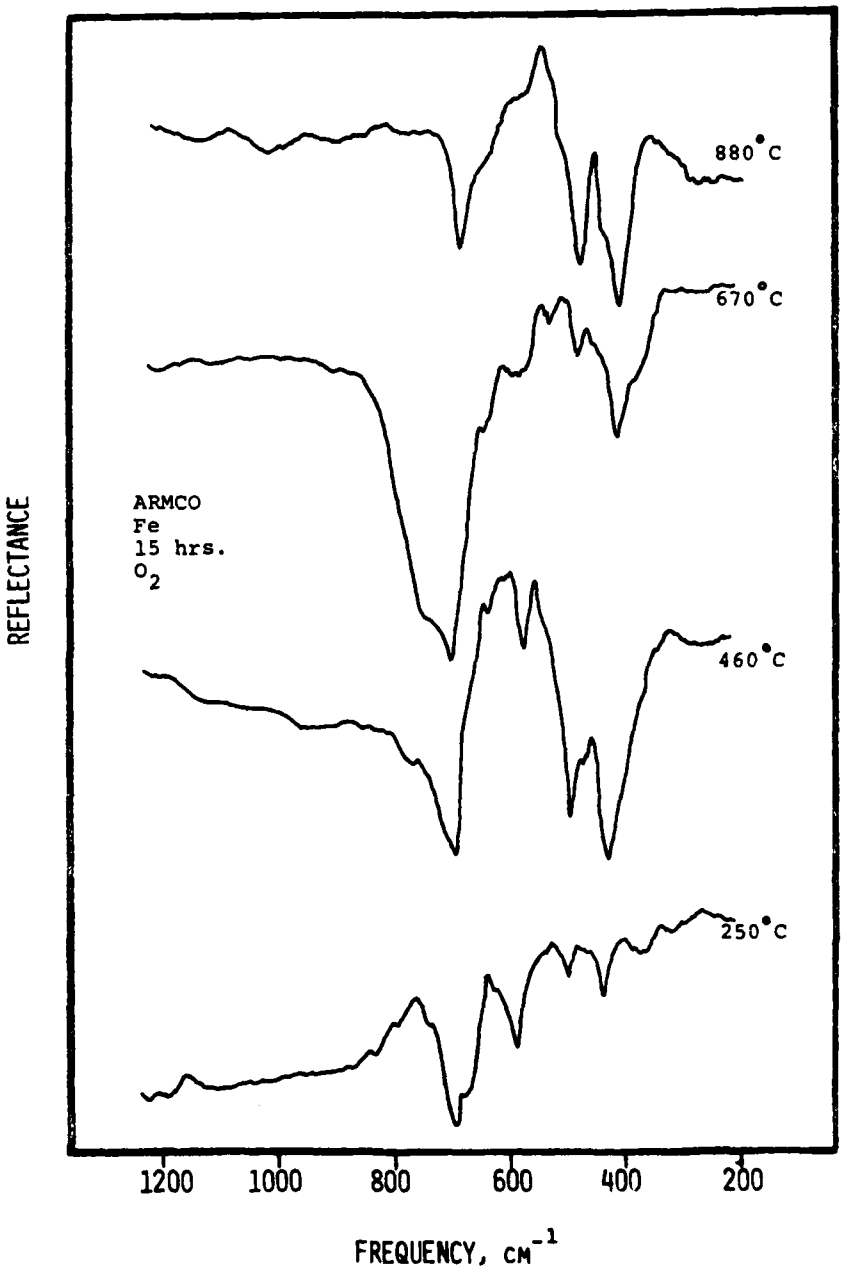

Figure 23. Infrared reflectance spectra of Armco iron exposed at various temperatures for 15 hours in pure oxygen.

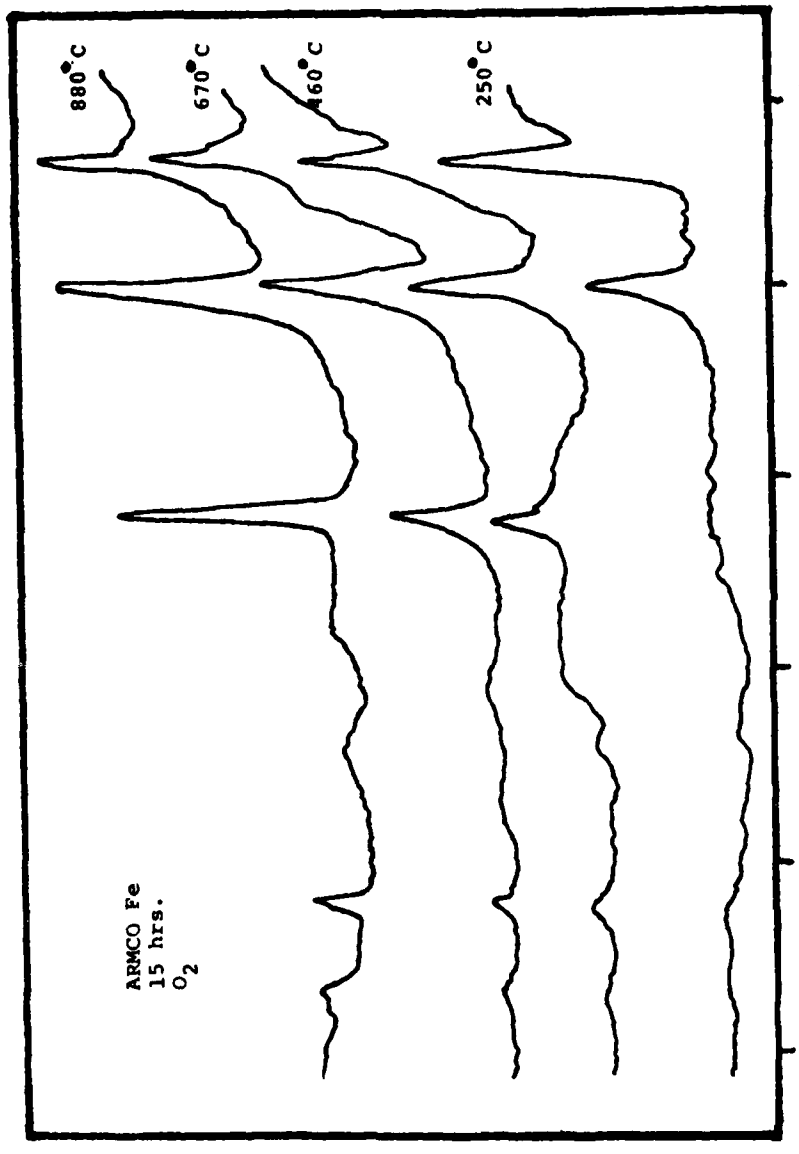

Figure 24. Raman spectra of Armco iron exposed at various temperatures for 15 hours in pure oxygen.

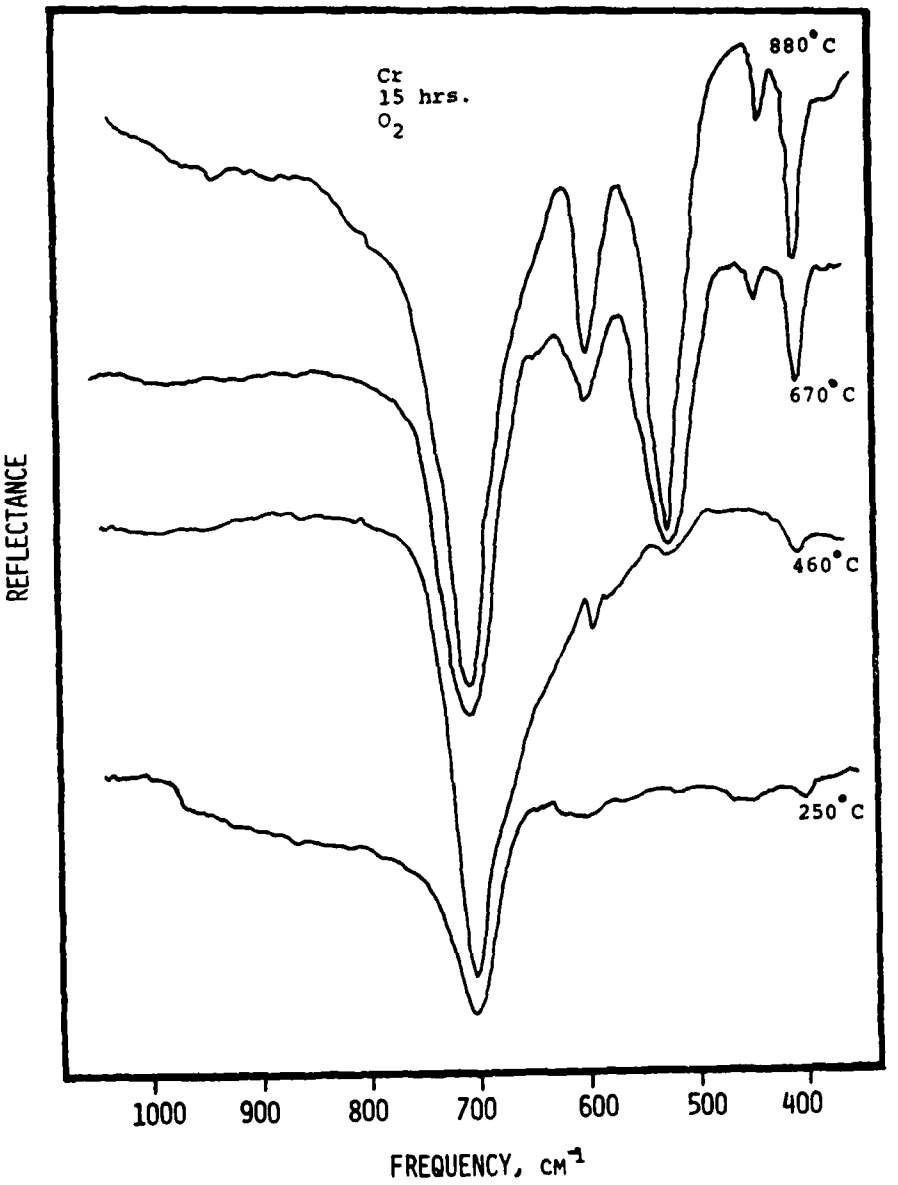

Figure 25. Infrared reflectance spectra of chromium exposed at various temperatures for 15 hours in pure oxygen.

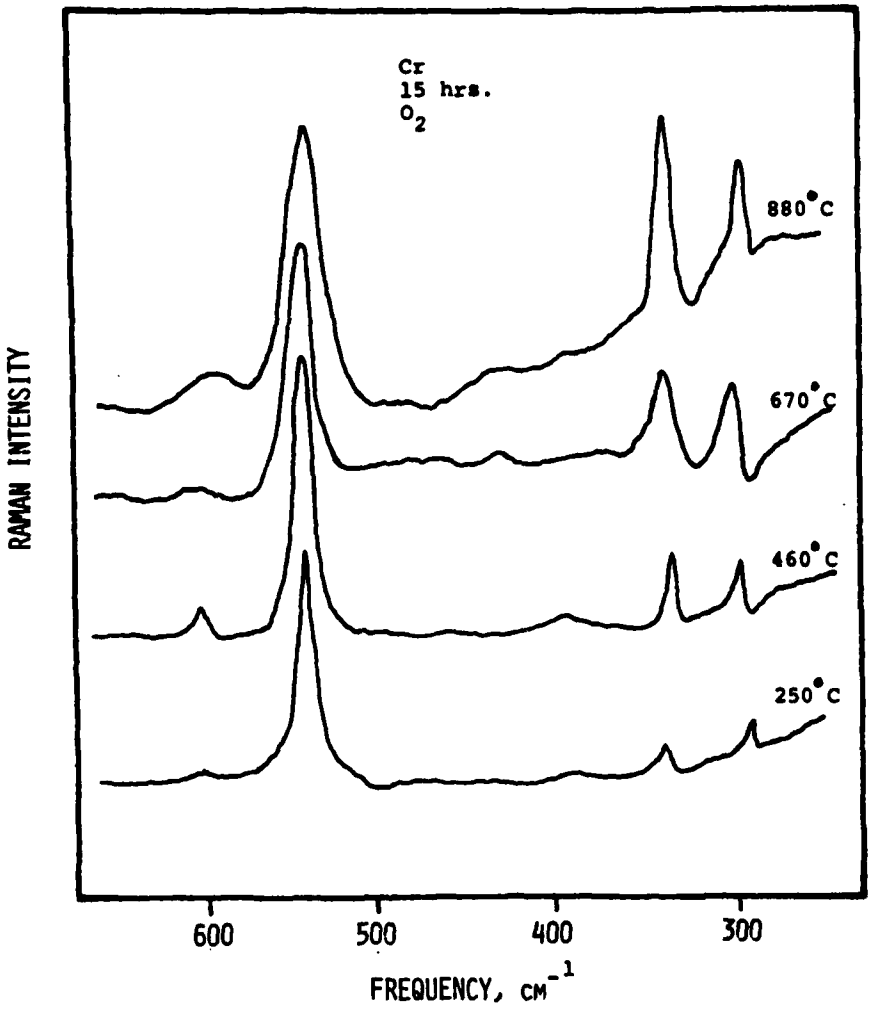

Figure 26. Raman spectra of chromium exposed at various temperatures for 15 hours in pure oxygen.

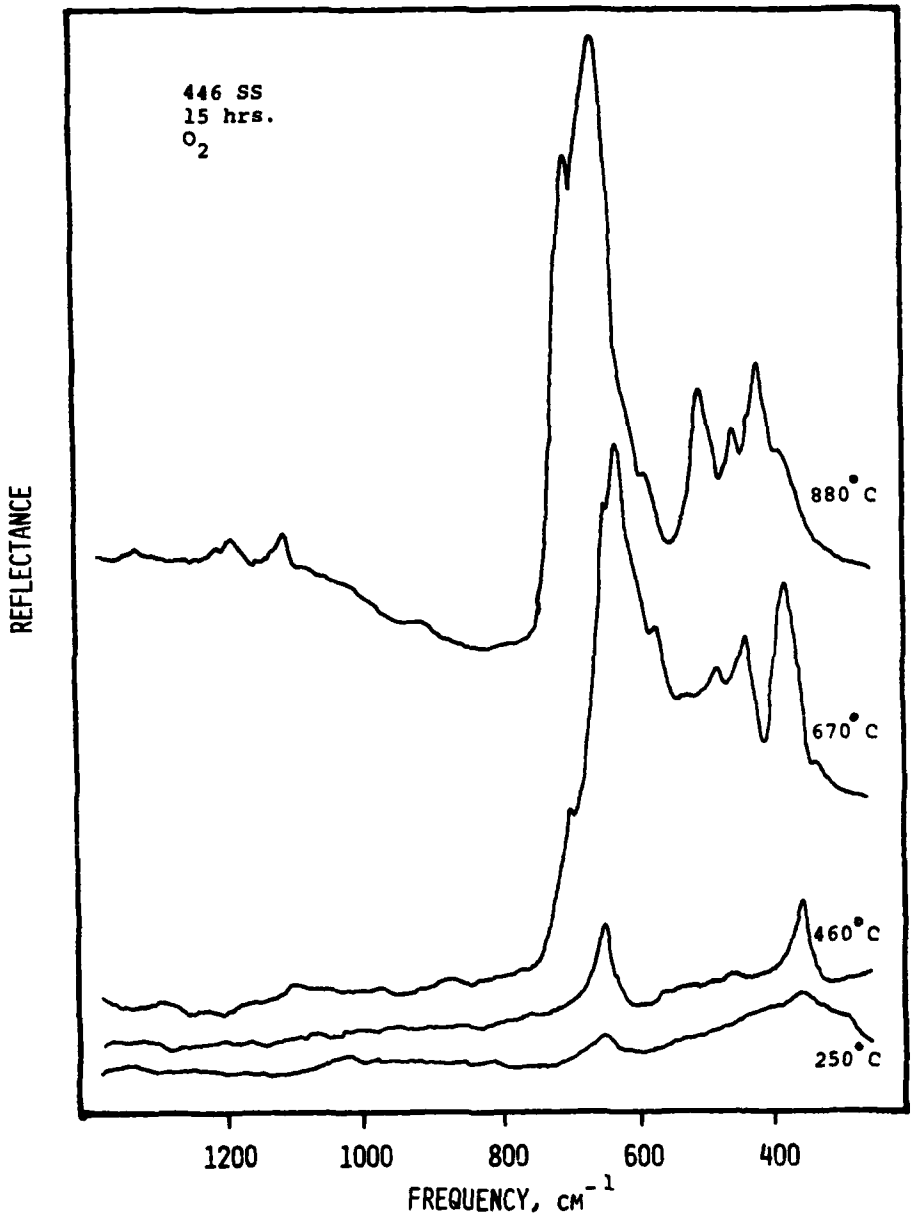

Figure 27. Infrared reflectance spectra of AISI Type 446 stainless steel exposed at various temperatures for 15 hours in pure oxygen.

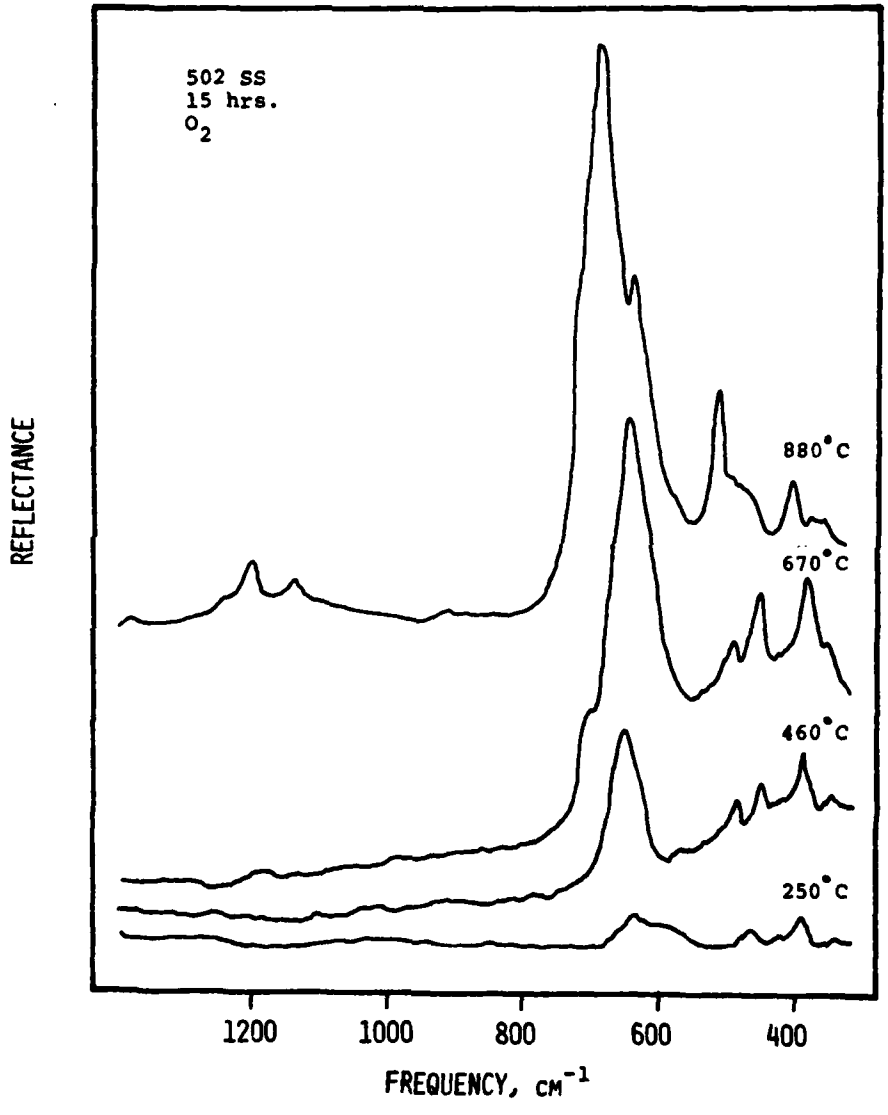

Figure 28. Infrared reflectance spectra of AISI Type 502 stainless steel exposed at various temperatures for 15 hours in pure oxygen.

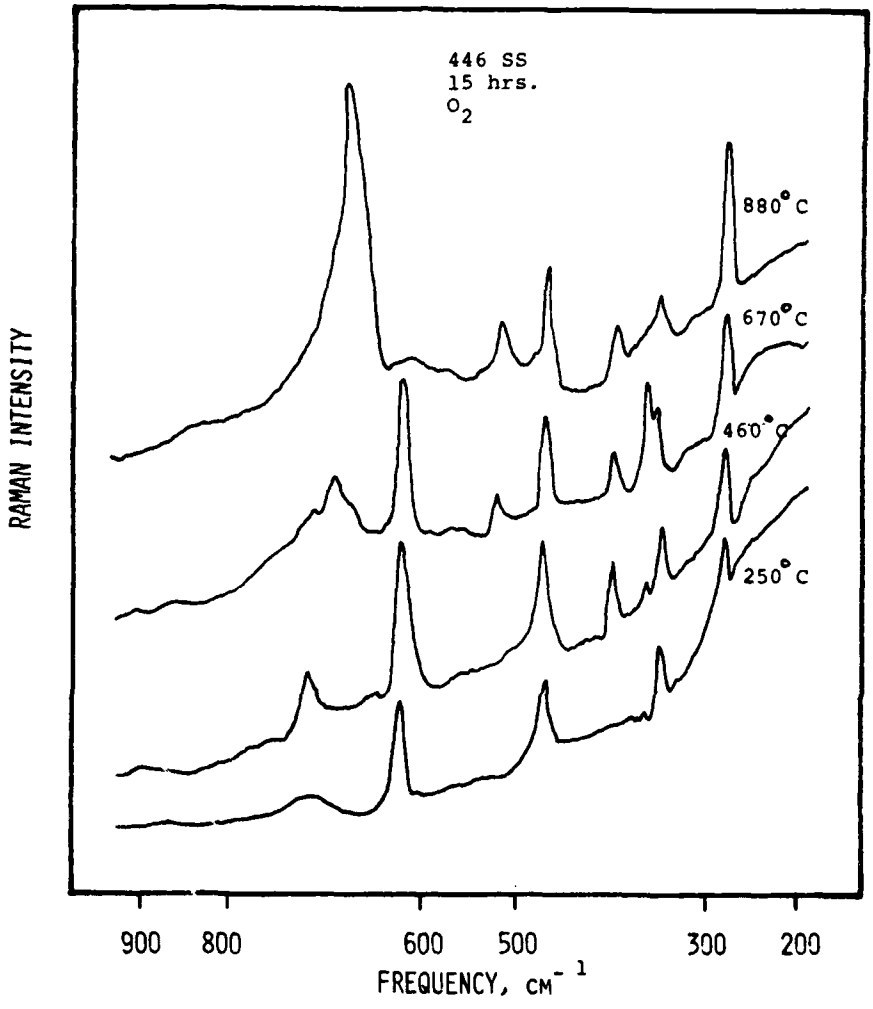

Figure 29. Raman spectra of AISI Type 446 stainless steel exposed at various temperatures for 15 hours in pure oxygen.

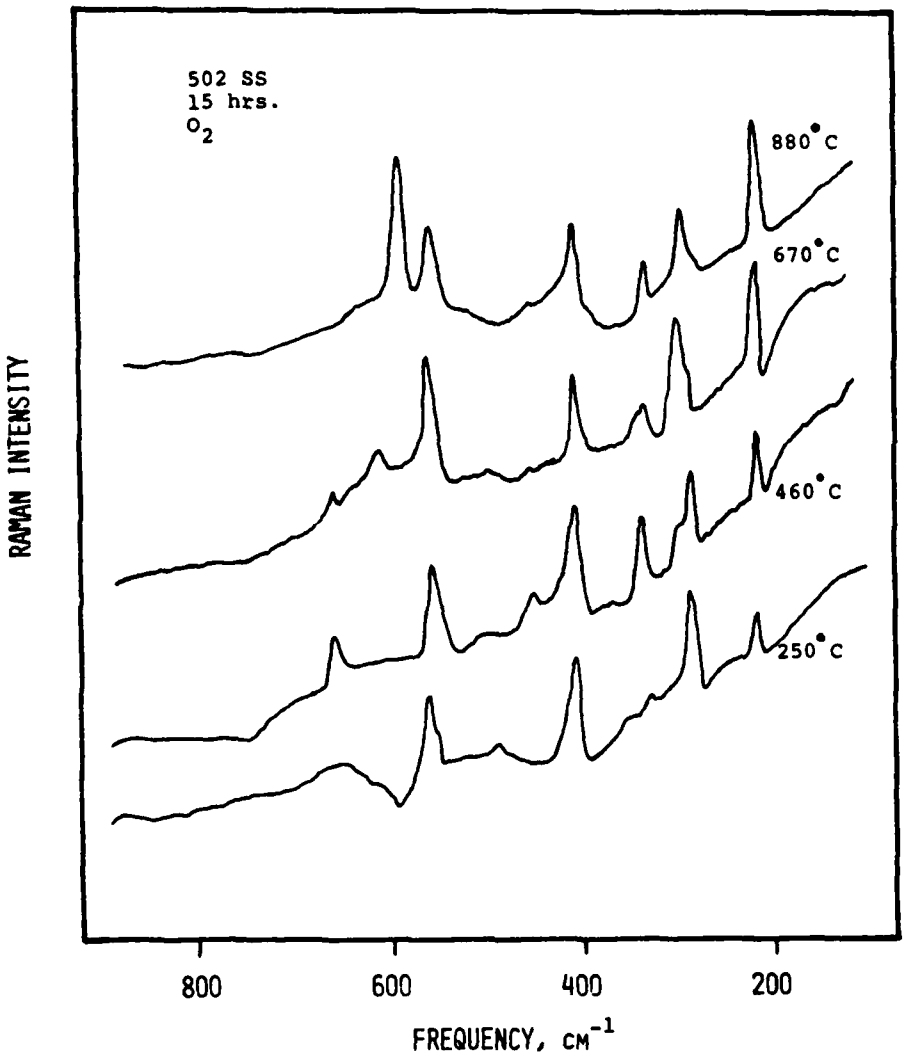

Figure 30. Raman spectra of AISI Type 502 stainless steel exposed at various temperatures for 15 hours in pure oxygen.

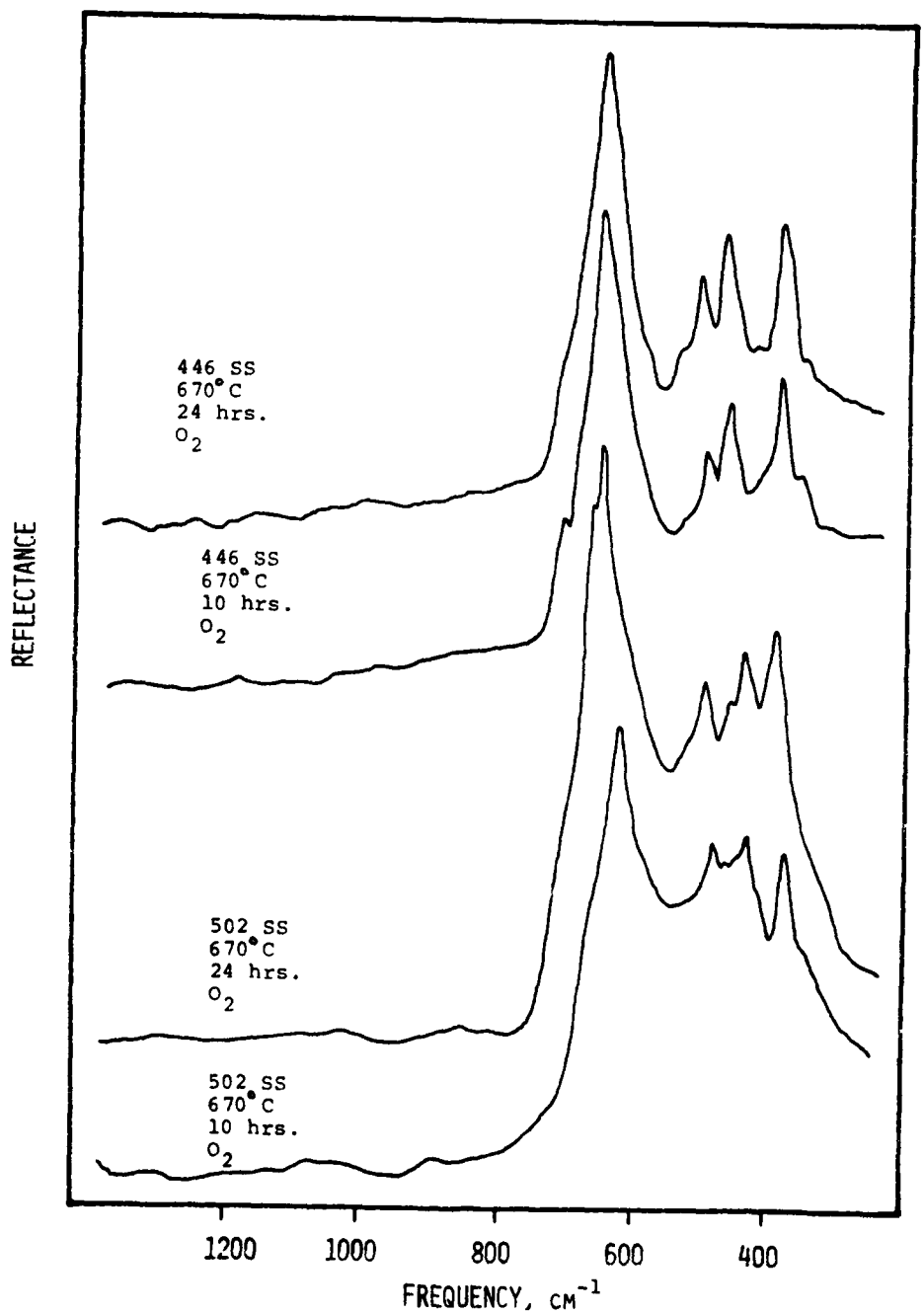

Figure 31. Infrared reflectance spectra for AISI Type 446 and AISI Type 502 stainless steels exposed at 670°C for 10 and 24 hours in pure oxygen.

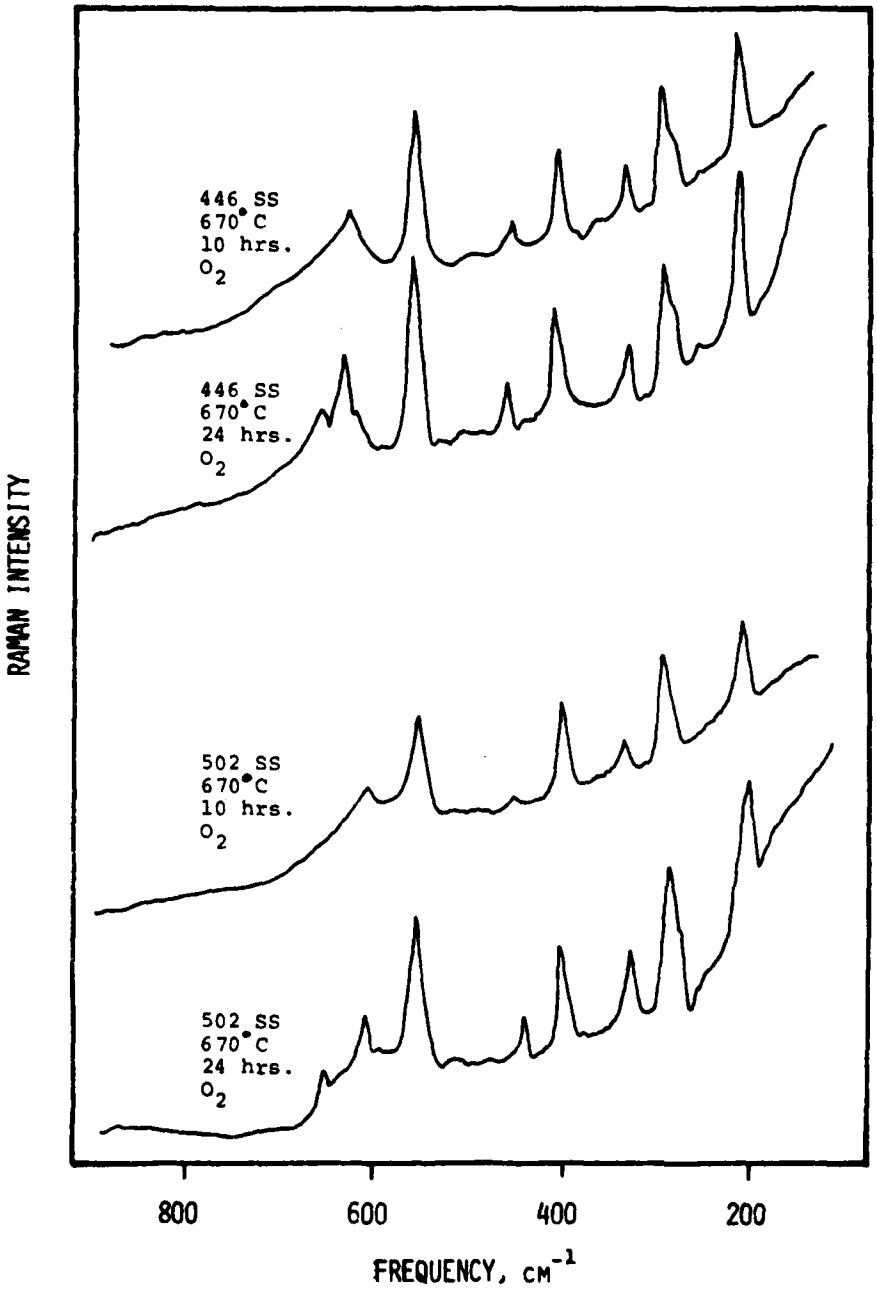

Figure 32. Raman spectra for AISI Type 446 and AISI Type 502 stainless steels exposed at 670°C for 10 and 24 hours in pure oxygen.

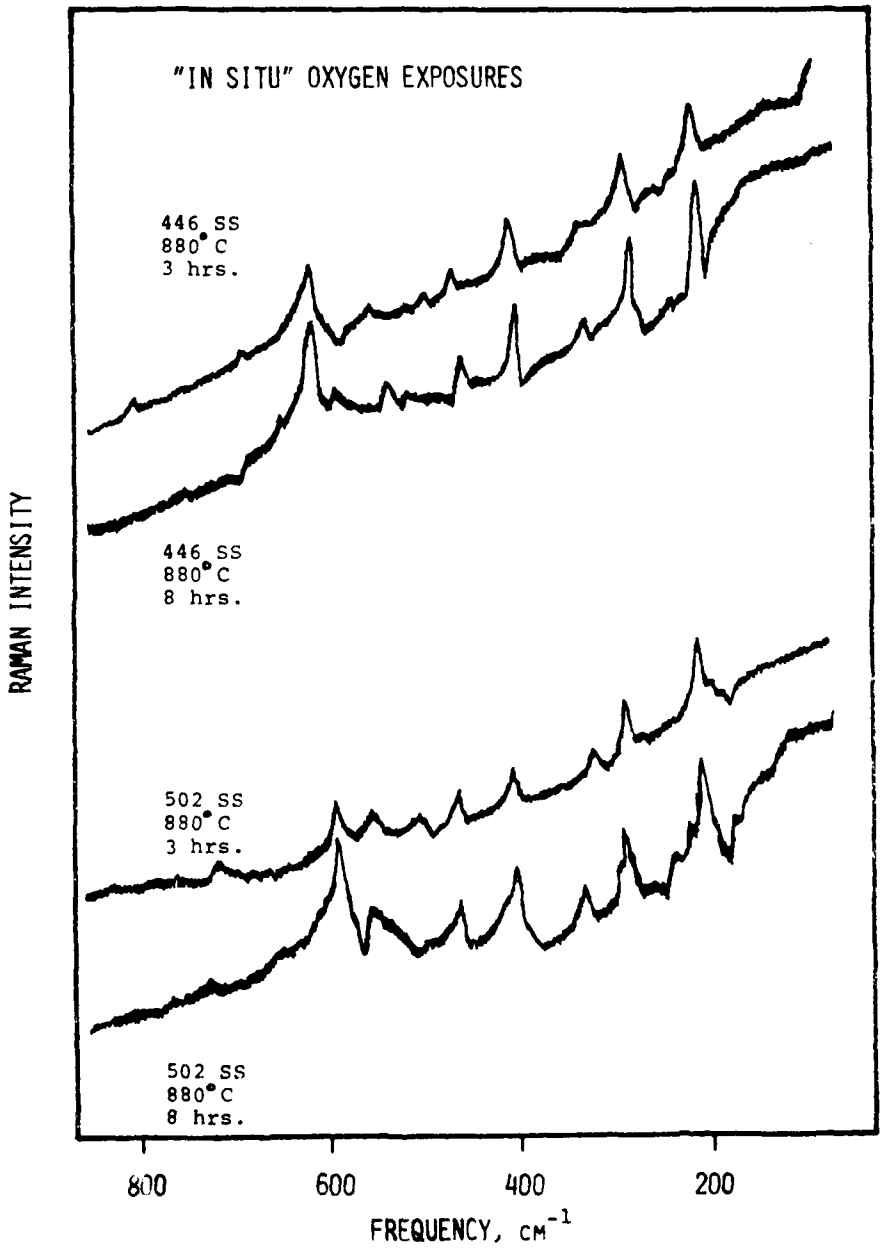

Figure 33. In-situ Raman spectra for AISI Type 446 and AISI Type 502 stainless steels during exposure in pure oxygen at 880°C for 3 and 8 hours.

AD-A081 240 RHODE ISLAND UNIV KINGSTON DEPT OF OCEAN ENGINEERING F/G 7/4
CHARACTERIZATION OF PASSIVE FILMS USING INFRARED AND RAMAN SPEC--ETC(U)
JAN 80 J KEISER, P FABIS, C BROWN N00014-78-C-0889
UNCLASSIFIED TR-6 NL

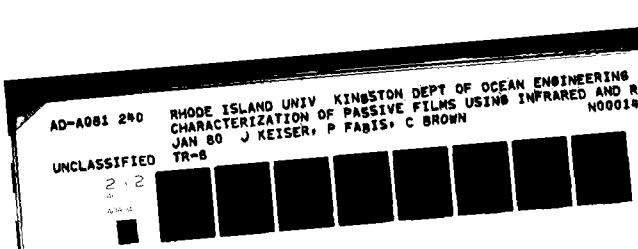

END
DATE FILMED
3 80
DTIC

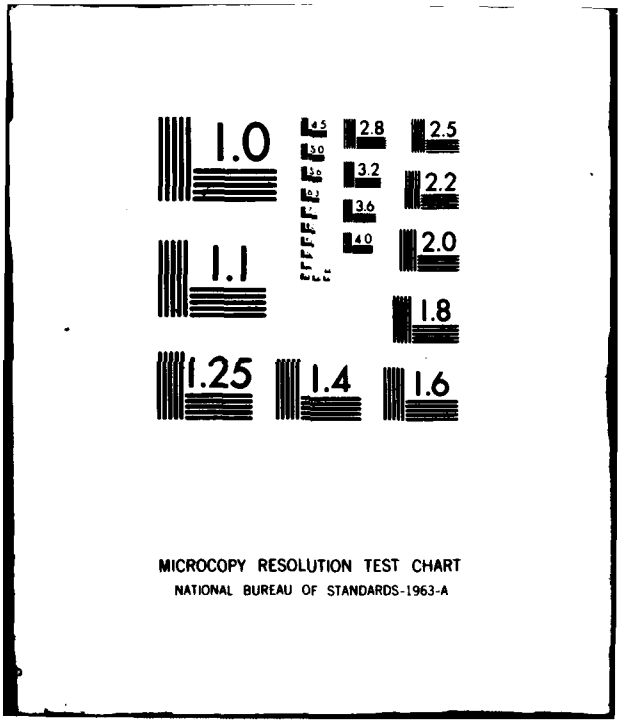
1.0
1.1
1.25
1.4
1.6
1.8
2.0
2.2
2.5
2.8
3.2
3.6
4.0
4.5
5.0
MICROCOPY RESOLUTION TEST CHART
NATIONAL BUREAU OF STANDARDS-1963-A

C
July 1977

SUPPLEMENTARY DISTRIBUTION LIST

Technical and Summary Reports

Dr. T. R. Beck
Electrochemical Technology Corporation
10035 31st Avenue, NE
Seattle, WA 98125

Professor I. M. Bernstein
Carnegie-Mellon University
Schenley Park
Pittsburgh, PA 15213

Professor H. K. Birnbaum
University of Illinois
Department of Metallurgy
Urbana, IL 61801

Dr. Otto Buck
Rockwell International
1049 Camino Dos Rios
P.O. Box 1085
Thousand Oaks, CA 91360

Dr. David L. Davidson
Southwest Research Institute
8500 Culebra Road
P.O. Drawer 28510
San Antonio, TX 78284

Dr. D. J. Duquette
Department of Metallurgical Engineering
Rensselaer Polytechnic Institute
Troy, NY 12181

Professor R. T. Foley
The American University
Department of Chemistry
Washington, DC 20016

Mr. G. A. Gehring
Ocean City Research Corporation
Tennessee Avenue & Beach Thorofare
Ocean City, NJ 08226

Dr. J. A. S. Green
Martin Marietta Corporation
1450 South Rolling Road
Baltimore, MD 21227

Professor R. H. Heidersbach
University of Rhode Island
Department of Ocean Engineering
Kingston, RI 02881

Professor H. Herman
State University of New York
Material Sciences Division
Stony Brook, NY 11794

Professor J. P. Hirth
Ohio State University
Metallurgical Engineering
Columbus, OH 43210

Dr. D. W. Hoeppner
University of Missouri
College of Engineering
Columbia, MO 65201

Dr. E. W. Johnson
Westinghouse Electric Corporation
Research and Development Center
1310 Beulah Road
Pittsburgh, PA 15235

Dr. F. Mansfeld
Rockwell International Science Center
1049 Camino Dos Rios
P.O. Box 1085
Thousand Oaks, CA 91360

Professor A. E. Miller
University of Notre Dame
College of Engineering
Notre Dame, IN 46556

Dr. Jeff Perkins
Naval Postgraduate School
Monterey, CA 93940

Professor H. W. Pickering
Pennsylvania State University
Department of Material Sciences
University Park, PA 16802

C
July 1977

SUPPLEMENTARY DISTRIBUTION LIST
(Continued)

Dr. William R. Prindle
National Academy of Sciences
National Research Council
2101 Constitution Avenue
Washington, DC 20418

Professor R. W. Staehle
Ohio State University
Department of Metallurgical Engineering
Columbus, OH 43210

Dr. Barry C. Syrett
Stanford Research Institute
333 Ravenswood Avenue
Menlo Park, CA 94025

Dr. R. P. Wei
Lehigh University
Institute for Fracture and
Solid Mechanics
Bethlehem, PA 18015

Professor H. G. F. Wilsdorf
University of Virginia
Department of Materials Science
Charlottesville, VA 22903

Dr. Boris Cahan
Chemical Engineering Department
Case Western Reserve University
Cleveland, Ohio 44106

BASIC DISTRIBUTION LIST (Cont'd) October 1976

Organization	No. of Copies
Naval Sea System Command Washington, D.C. 20362 Attn: Code 035	(1)
Naval Facilities Engineering Command Alexandria, Virginia 22331 Attn: Code 03	(1)
Scientific Advisor Commandant of the Marine Corps Washington, D.C. 20380 Attn: Code AX	(1)
Naval Ship Engineering Center Department of the Navy CTR BG #2 3700 East-West Highway Prince Georges Plaza Hyattsville, Maryland 20782 Attn: Engineering Materials and Services Office, Code 6101	(1)
Army Research Office Box CM, Duke Station Durham, North Carolina 27706 Attn: Metallurgy & Ceramics Div.	(1)
Army Materials and Mechanics Research Center Watertown, Massachusetts 02172 Attn: Res. Programs Office (AMXMR-P)	(1)
Air Force Office of Scientific Research Bldg. 410 Bolling Air Force Base Washington, D.C. 20332 Attn: Chemical Science Directorate Electronics and Solid State Sciences Directorate	(1) (1)
Air Force Materials Lab (LA) Wright-Patterson AFB Dayton, Ohio 45433	(1)
NASA Headquarters Washington, D.C. 20546 Attn: Code RRM	(1)
NASA Lewis Research Center 21000 Brookpark Road Cleveland, Ohio 44135 Attn: Library	(1)
National Bureau of Standards Washington, D.C. 20234 Attn: Metallurgy Division Inorganic Materials Division	(1) (1)
Defense Metals and Ceramics Information Center Battelle Memorial Institute 505 King Avenue Columbus, Ohio 43201	(1)
Director Ordnance Research Laboratory P.O. Box 30 State College, Pennsylvania 16801	(1)
Director Applied Physics Laboratory University of Washington 1013 Northeast Fortieth Street Seattle, Washington 98105	(1)
Metals and Ceramics Division Oak Ridge National Laboratory P.O. Box X Oak Ridge, Tennessee 37380	(1)
Los Alamos Scientific Laboratory P.O. Box 1663 Los Alamos, New Mexico 87544 Attn: Report Librarian	(1)
Argonne National Laboratory Metallurgy Division P.O. Box 229 Lemont, Illinois 60439	(1)

BASIC DISTRIBUTION LIST

October 1976

Technical and Summary Reports

Organization	No. of Copies
Defense Documentation Center Cameron Station Alexandria, Virginia 22314	(12)
Office of Naval Research Department of the Navy	
Attn: Code 471	(1)
Code 102	(1)
Code 470	(1)
Commanding Officer Office of Naval Research Branch Office 495 Summer Street Boston, Massachusetts 02210	(1)
Commanding Officer Office of Naval Research Branch Office 536 South Clark Street Chicago, Illinois 60605	(1)
Office of Naval Research San Francisco Area Office 760 Market Street, Room 447 San Francisco, California 94102	
Attn: Dr. P. A. Miller	(1)
Naval Research Laboratory Washington, D.C. 20390	
Attn: Code 6000	(1)
Code 6100	(1)
Code 6300	(1)
Code 6400	(1)
Code 2627	(1)
Naval Air Development Center Code 302 Warminster, Pennsylvania 18974	
Attn: Mr. F. S. Williams	(1)
Naval Air Propulsion Test Center Trenton, New Jersey 08628	
Attn: Library	(1)
Naval Construction Batallion Civil Engineering Laboratory Port Hueneme, California 93043	
Attn: Materials Division	(1)
Naval Electronics Laboratory Center San Diego, California 92152	
Attn: Electron Materials Sciences Division	(1)
Naval Missile Center Materials Consultant Code 3312-1 Point Mugu, California 93041	(1)
Commanding Officer Naval Surface Weapons Center White Oak Laboratory Silver Spring, Maryland 20910	
Attn: Library	(1)
David W. Taylor Naval Ship R&D Center Materials Department Annapolis, Maryland 21402	(1)
Naval Undersea Center San Diego, California 92132	
Attn: Library	(1)
Naval Underwater System Center Newport, Rhode Island 02840	
Attn: Library	(1)
Naval Weapons Center China Lake, California 93555	
Attn: Library	(1)
Naval Postgraduate School Monterey, California 93940	
Attn: Mechanical Engineering Dept.	(1)
Naval Air Systems Command Washington, D.C. 20360	
Attn: Code 52031	(1)
Code 52032	(1)
Code 320	(1)

BASIC DISTRIBUTION LIST (Cont'd) October 1976

Organization	No. of Copies	Organization	No. of Copies
Brookhaven National Laboratory Technical Information Division Upton, Long Island New York 11973 Attn: Research Library	(1)		
Library Building 50 Room 134 Lawrence Radiation Laboratory Berkeley, California	(1)		

August 1978

SUPPLEMENTARY DISTRIBUTION LIST

Technical and Summary Reports

People and organizations who have requested copies of reports on this research.

Dr. F.P. Mertlas
Department of Energy and Environment
Building 815
Upton, NY 11973

Dr. B. Vyas
Brookhaven National Laboratory
Building 703
Upton, NY 11973

Dr. Henry White
Physics Department
University of Missouri - Columbia
Columbia, MO 65211

Dr. M.J. Graham
National Research Council of Canada
Division of Chemistry
Ottawa, Ontario
Canada K1A OR9

Dr. B.J. Berkowitz
Corporate Research Laboratories
Exxon Research and Engineering Company
P.O. Box 45
Linden, NJ 07036

Dr. S. Gottesfeld
Bell Laboratories
600 Mountain Avenue
Murray Hill, NJ 07974

Dr. Jeff Perkins
Liason Scientist, Metallurgy
Office of Naval Research Branch Office, London
Box 39
FPO New York 09510

T.E. Evans
Inco Europe, Ltd.
European R & D Centre
Wiggin Street, Birmingham B160AJ
England

Dr. N. Sato
Faculty of Engineering
Hokkaido University
Kita-Ku, Sapporo, 060
Japan

Dr. K. Sugimoto
Department of Metallurgy
Tohoku University

C
April 1978

SUPPLEMENTARY DISTRIBUTION LIST
(Continued)

Professor H. W. Pickering
Pennsylvania State University
Department of Material Sciences
University Park, Pennsylvania 16802

Professor R. W. Staehle
Ohio State University
Department of Metallurgical Engineering
Columbus, Ohio 43210

Dr. E. A. Starke, Jr.
Georgia Institute of Technology
School of Chemical Engineering
Atlanta, Georgia 30332

Dr. Barry C. Syrett
Stanford Research Institute
333 Ravenswood Avenue
Menlo Park, California 94025

Dr. R. P. Wei
Lehigh University
Institute for Fracture and
Solid Mechanics
Bethlehem, Pennsylvania 18015

Professor H. G. F. Wilsdorf
University of Virginia
Department of Materials Science
Charlottesville, Virginia 22903

Distribution List - ONR

Martin W. Kendig
Corrosion Science Group
Department of Nuclear Energy
Brookhaven National Laboratory
Upton, NY 11973

A.S. (Bert) Krisher
Engineering Fellow
Materials Technology
Monsanto
Corporate Engineering Department
Monsanto Company
800 N. Lindbergh Boulevard
St. Louis, Missouri 63166

Tom E. Furtak
Leader, Electrochemistry Group
Solid State Physics Division
Ames Laboratory
U.S. Department of Energy
Iowa State University
Ames, Iowa 50011

Alan G. Miller, Ph.D.
Analytical Specialist Engineer
Boeing Materials Technology
Boeing Commercial Airplane Co.
P.O. Box 3707
MS 73-43
Seattle, WA 98124

J.J. Ritter
National Bureau of Standards
Washington, DC 20234